EXPLOSION GENERATED SEISMIC WAVES

M. Nafi Toksöz

Department of Earth and Planetary Sciences

Massachusetts Institute of Technology

Cambridge, Massachusetts 02139

FINAL REPORT

Period Covered: 1 October 1967 - 30 Septmeber 1971

31 December 1971

⁄DDC

RECEIVED
MAY 2 1972
C

Approved for public release; distribution unlimited.

Prepared for

AIR FORCE CAMBRIDGE,RESEARCH LABORATORIES

AIR FORCE SYSTEMS COMMAND

UNITED STATES AIR FORCE

BEDFORD, MASSACHUSETTS   01730

144

Qualified requestors may obtain additional copies from the
Defense Documentation Center. All others should apply to
the National Technical Information Service.
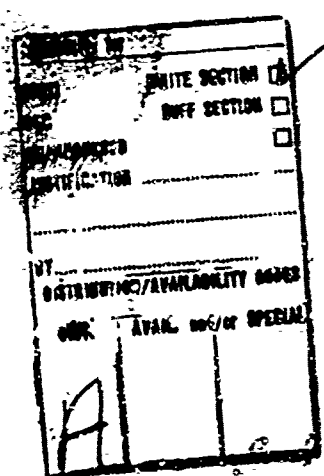
DOCUMENT CONTROL DATA - R & D

(Security classification of title, body of abstract and indexing annotation must be entered when the overall report is classified)

1. ORIGINATING ACTIVITY (Corporate author)	2a. REPORT SECURITY CLASSIFICATION
Massachsuetts Institute of Technology Department of Earth and Planetary Sciences Cambridge, Massachusetts 02139	UNCLASSIFIED
	2b. GROUP

3. REPORT TITLE

EXPLOSION GENERATED SEISMIC WAVES

4. DESCRIPTIVE NOTES (Type of report and inclusive dates)

Scientific. Final: 1 October 1967-30 September 1971   Approved: 02-18-72

5. AUTHOR(S) (First name, middle initial, last name)

M. Nafi Toksöz

6. REPORT DATE	7a. TOTAL NO. OF PAGES	7b. NO. OF REFS
31 December 1971	141	75

8a. CONTRACT OR GRANT NO.	9a. ORIGINATOR'S REPORT NUMBER(S)
F19628-68-C-0043	
b. PROJECT NO. , Task Work Unit No. 7639-08-01	
c. DoD Element 62101F	9b. OTHER REPORT NO(S) (Any other numbers that may be assigned this report)
d. DoD Subelement 681000	AFCRL-72-0012

10. DISTRIBUTION STATEMENT

A - Approved for public release; distribution unlimited.

11. SUPPLEMENTARY NOTES	12. SPONSORING MILITARY ACTIVITY
TECH, OTHER	Air Force Cambridge Research Laboratories, (LW) L. G. Hanscom Field Bedford, Massachusetts 01730

13. ABSTRACT

The mechanisms of generation of SH and Love waves by underground nuclear explosions are investigated theoretically and experimentally. An explosion in pre-stressed medium is formulated as a composite source consisting of an isotropic explosion and a double-couple representing the tectonic strain release. From the radiation patterns of Rayleigh waves and Love-to-Rayleigh wave amplitude ratios relative strength of the strain release component is determined. It is found that relative amplitudes of Love waves and tectonic strain energy release strongly depend on the medium properties in the immediate vicinity of the explosion. For "harder" media such as granite, energy release is much greater compared to "softer" media such as alluvium or salt. The strain energy release, as best as can be determined from laboratory experiments, is primarily due to the relaxation of the pre-stress field around explosion-generated and extended cracks and faults.

DD FORM 1 NOV 65 1473

14 KEY WORDS	LINK A		LINK B		LINK C	
	ROLE	WT	ROLE	WT	ROLE	WT
Underground explosions						
Source mechanisms						
Tectonic strain release						
Radiation pattern						

EXPLOSION GENERATED SEISMIC WAVES

M. Nafi Toksöz

Department of Earth and Planetary Sciences

Massachusetts Institute of Technology

Cambridge, Massachusetts 02139

FINAL REPORT

Period Covered: 1 October 1967 - 30 Septmeber 1971

31 December 1971   Details of illustrations in
                    this document may be better
                    studied on microfiche

Contract Monitor: Ker C. Thomson

Terrestrial Sciences Laboratory

Prepared for

ABSTRACT

The mechanisms of generation of SH and Love waves by underground nuclear explosions are investigated theoretically and experimentally. An explosion in pre-stressed medium is formulated as a composite source consisting of an isotropic explosion and a double-couple representing the tectonic strain release. From the radiation patterns of Rayleigh waves and Love-to-Rayleigh wave amplitude ratios relative strength of the strain release component is determined. It is found that relative amplitudes of Love waves and tectonic strain energy release strongly depend on the medium properties in the immediate vicinity of the explosion. For "harder" media such as granite, energy release is much greater compared to "softer" media such as alluvium or salt. The strain energy release, as best as can be determined from laboratory experiments, is primarily due to the relaxation of the pre-stress field around explosion-generated and extended cracks and faults.

TABLE OF CONTENTS

INTRODUCTION

The source mechanism of underground nuclear explosions has been of great interest to seismologists since it was first observed that a pure explosive source alone could not adequately account for the observed seismic radiation. The existence of prominent SH and Love waves in the seismic records from these events was a prime reason for this conclusion and indicated that the explosions were probably causing the release of some tectonic strain (Press and Archambeau, 1962). Early studies by Brune and Pomeroy (1963), Aki (1964), and Toksöz et al (1965) found that a double-couple type source combined with a pure explosion could account for the observed seismic radiation from several events.

In this report we summarize the work we have done on a number of nuclear explosions at the Nevada Test Site and in other areas. This report will consist of three parts, each of which is essentially self-contained. There is, therefore, a certain amount of repetition, such as in the theory, some of the tables, and in the references contained in the report. Part I deals with the source mechamisms determined for a large number of underground explosions and the comparison of these results to other data connected with these events. Part II consists of a detailed analysis of one nuclear event (Bilby)

and · report concerning laboratory experiments on explosive
sources. The combination of these two types of analyses
helps to clarify the problem of strain energy release in pre-
stressed media. Part III is concerned with two nuclear
events (Pile Driver and Greeley) which released a significantly
higher proportion of tectonic strain energy than other
explosions.

I. SOURCE MECHANISMS OF UNDERGROUND NUCLEAR EXPLOSIONS FROM LOVE WAVE TO RAYLEIGH WAVE RATIOS

Introduction

The source mechanisms have been determined for a number of underground explosions at the Nevada Test Site, in the Soviet Union, and in other testing sites. We have followed the method of Toksöz et al. (1965) of considering the source to be a superposition of a symmetrical explosion and a horizontal double-couple. The Love wave to vertical component Rayleigh wave amplitude ratio from such a source is then given by

$$\frac{U_L}{U_{R_Z}} = \frac{F \, k_L^{\frac{1}{2}} \, A_L \, \cos 2\theta}{(1 + F \sin 2\theta) \, k_R^{\frac{1}{2}} \, A_R \, (\overset{*}{u_o}/\overset{\cdot}{w_o})} \tag{1}$$

where assuming the source time functions for both the explosions and double-couple and the attenuation coefficients for Love and Rayleigh waves are the same, k_L and k_R are the Love and Rayleigh wave numbers, A_L and A_R are the medium responses for Love and Rayleigh waves, u_o and w_o are the components of particle velocity at the surface, F is the relative strength of the double-couple, and θ is azimuth of the fault plane. We determined the two parameters F and θ for each explosion by fitting the observed surface wave data to the above formulation.

Data

Tables Ia and Ib list the nuclear explosions we have studied. Included are seven events previously analyzed by Toksöz et al. (1965), Toksöz and Kehrer (1971), and Toksöz (1967). The surface wave data was obtained from stations throughout North America in the case of the American events. These included stations of the World Wide Standard Network (WWSS), the Long Range Measurements Network (LRSM), the Canadian Standard Seismograph Network (CSS), and two additional stations at Berkeley and Pasadena which provided long-period data. Figure 1 shows the distribution of recording stations in North America. However, not all stations provided useful data for each event. For the presumed Soviet events, data was obtained from the WWSS stations in Europe and Asia.

The film records of those events, for which the surface wave data was of sufficient quality, were manually digitized. The resulting data was then band-pass filtered to reduce noise and the two horizontal components were rotated to radial and tangential directions with respect to the epicenter. In this way essentially pure Love waves were obtained on the tangential component. Figure 2 is an example of this analysis for the explosion Boxcar at Mould Bay, Canada. The three lower traces are plotted from digital data and show the unfiltered north-south, east-west, and vertical components. The three upper

traces show the filtered data, where the horizontal components have been rotated to radial and tangential directions.

The tangential and the vertical components were then Fourier-analyzed to yield the amplitude spectra. The proper time windows for this analysis were determined by examining the filtered trace at each station individually and noting the onset and duration of the wave trains.

Love wave to Rayleigh wave amplitude ratios were determined by computing the spectral ratio of the tangential component to the vertical component over the period range 8 to 100 seconds. In general, the spectral ratios were somewhat oscillatory and thus the ratio at any one particular period could not be expected to be reliable at all stations. The period range was, therefore, divided into three bands, from 9 to 15 seconds, from 15 to 22 seconds, and from 22 to 30 seconds. The average value of the ratio in each band was then taken to represent the ratio over that band.

An automatic error scheme (Kehrer, 1969) was used to determine the best fit of Equation [1] to the observed data. In applying Equation [1], the term $k_L^{1/2} A_L / k_R^{1/2} A_R (\frac{u_o^*}{w_o})$ was taken to be a constant at all stations. An error term E was then formed between the observed and the theoretical ratios for combinations of F and θ.

$$E_j = \left[\sum_{i=1}^{N} \left(L_i/R_i - \left| \frac{S \ F_j \ \cos 2\theta_{ij}}{1 + F_j \ \sin 2\theta_{ij}} \right| \right)^2 / N \right]^{1/2} \quad [2]$$

The jth combination of F and θ which fits the data best
will be that which minimizes E. L_i/R_i is the experimentally
measured Love wave to Rayleigh wave amplitude ratio at a par
ticular station i, S is a constant, and N is the number
of stations. The values of E were contoured on a Stromberg-
Carlson 4020 grind for the three period-bands of each event.
Figure 3 shows these results for the explosion Faultless. The
minima indicate the orientation of the best fitting right-
lateral, vertical, strike-slip fault as measured clockwise
from the north at the source. A comparison of the error plots
over the three bands in Figure 3 reveals the frequency depen-
dence of F. The orientation θ of the double-couple remains
essentially unchanged over the three bands while F is greatest
at long periods and smallest at short periods. This relation
ship was observed for nearly all events and indicates that the
source of Love waves is less efficient at short periods than
the Rayleigh wave source. A similar phenomenon was noted by
Aki et al. (1969) for body waves from the Benham event. Figure
4 shows the relationship between F and the period for several
events.

Two other matrices, in addition to the one described, were
investigated to test the best fit of the data to theoretical
source configurations. The one consisted of normalizing the
difference between the observed and theoretical ratios by the
observed ratio at each station. This reduced the weights of

large observed values on the error term, with the effect that
the F value was reduced. The second method consisted of
normalizing by the theoretical ratio. This had the effect
of increasing the F value. In general, however, the
changes in F were small and the orientation remained essen-
tially unchanged. The values of F reported here are those
determined by the non-normalized matrix with the exception of
Creeley. In the case of Greeley, the absolute minimum in the
error plot for the 15 to 22 second period range occurred
for F = 0.9 and θ = 175°. However, this configuration
could not account for the consistently large values of the
ratio due north of the NTS. Over the 22 to 30 second
range, the indicated miminum occurred at the much larger F
value of 1.6. Indeed this value appeared to fit the data
best over the 15 to 22 second range as well and it was
therefore taken to represent the strength of the double-couple
for Greeley. Furthermore, an investigation of Rayleigh wave
polarity (Toksöz and Kehrer, 1971) indicated that the F value
for Greeley was greater than one.

A summary of the best fitting F and θ in the 15 to
22 second period range for each event is given in Tables Ia
and Ib. For the explosions of previous studies and for Buff,
Benham, and the presumed Soviet events of 3-20-66, 3-26-67,
and 10-21-67 for which the surface wave data was not of suf-
ficient quality to permit the calculation of spectral ratios,

the parameters F and   θ   were determined from mea-
surements of the maximum amplitudes of Love and Rayleigh
waves. Included in Table I is the ratio of the surface wave
energy of the double-couple to the energy of the explosion.
This ratio (Toksöz et al, 1965) is closely approximated by

$$E_{tect}/E_{xp} = 4/3 \ \ F^2.$$

Several conclusions can be drawn from Table I. The
close agreement in fault orientation of most of the events at
the Nevada Test Site indicates that a regional stress field
is probably controlling the strain release. The large vari-
tion within the two Soviet testing areas may be due to a lack
of data in the case of three of the events. The dependence
of F and hence the amount of stress release, on lithology
was previously noted by Toksöz (1967) and by Toksöz and Kehrer
(1971). Table I provides additional evidence that the multi-
polar source component is larger in more competent rock. Thus
strain release from a particular explosion is dependent on
the rock medium and the regional state of strain. The rela-
tively low F values for all of the presumed Soviet events
are consistent with what is known about the two Soviet testing
areas.

The north-northwest orientation of the fault planes of
most of the Nevada Test Site explosions is in good agreement

with lineaments and dominant fault patterns in the area.
Figure 5 shows the Yucca Falt portion of the Nevada Test Site
with the source mechanisms of the explosions studied there.
Included are the major natural faults and some of the fractures
produced by the events. The chief feature of Yucca Flat is
the Yucca Fault which trends northward through alluvium and is
of recent age. Although most observed displacements across
the Yucca Fault are vertical following nearby explosions,
numerous en echelon fractures along the fault were produced
in the alluvium by Corduroy (Barosh, 1968). Such an en echelon
pattern is generally related to strike-slip movement in the
underlying basement. The trend of the pattern in this case
suggests right-lateral slippage.

Figure 6 shows the Pahute Mesa portion of the Nevada
Test Site with the faults, explosion-produced fractures, and
the events studied. The main structural feature of Pahute
Mesa is the Silent Canyon Caldera, which encloses the five
events. Many normal faults, striking north-northwest, cut
the thick sequence of Tertiary volcanic rock. Recent natural
movement along some of these faults has been inferred (McKeown
et al., 1966). For Benham and Boxcar, studies of aftershock
distribution (Hamilton and Healy, 1969; Ryall and Savage, 1969)
as well as studies of faulting and fracturing caused by the
explosions (Buckman, 1969; McKeown and Dickey, 1969) have been
published. Figure 7 shows the relationships of these two sets

of data with the source mechanisms determined for the two
events. In the case of Benham, the correlation between the
orientation of the double-couple and the trend of the after-
shock pattern as well as the orientation of faults and frac-
tures is quite good. Both vertical and right-lateral move-
ments on the nearby Boxcar fault were initiated by Benham.

Hamilton and Healy (1969) found that the aftershocks of
Benham were concentrated in two patterns. Those to the north-
west of ground zero follow a northeasterly trend while those
to the west and southwest trend north-south. Fault plane
solutions from P waves of events in the first group indicate
dip-slip fault movement. Solutions for the second group in-
dicate right-lateral strike-slip motion in a northerly direction.
These two patterns were further confirmed in a study of smaller
Benham aftershocks by Stauder (1971). The solutions for the
second group of aftershocks are similar to the orientation of
the double-couple component for Benham (and other events) as
determined in this study. The Benham and Boxcar aftershocks
when considered together (see Figure 7) indicate the continuity
of the distribution pattern. Northeast-trending Benham after-
shocks overlap with those of Boxcar.

References

Aki, K. (1964). A note on surface wave generation from the
Hardhat nuclear explosion, J. Geophys. Res., 69, 1131-
1134.

Aki, K., P. Reasenberg, T. De Fazio and Y. Tsai (1969). Near-
field and far-field seismic evidence for triggering of
an earthquake, Bull. Seism. Soc. Amer., 59, 2197-2207.

Barosh, P. J. (1968). Relationship of explosion-produced
fracture patterns to geologic structure in Yucca Flat,
Nevada Test Site, Geol. Soc. Amer. Mem., 110, 199-217.

Brune, J. N. and P. W. Pomeroy (1963). Surface wave radia-
tion patterns for underground nuclear explosions and
small-magnitude earthquakes, J. Geophys. Res., 68, 5005-
5028.

Bucknam, R. C. (1969). Geologic effects of the Benham under-
ground nuclear explosion, Nevada Test Site, Bull. Seism.
Soc. Amer., 59, 2209-2220.

Fernald, A. T., G. S. Corchary, and W. P. Will.. .s (1968).
Surficial geologic map of Yucca Flat, Nye and Lincoln
Counti..s, Nevada, U. S. Geol. Geurvey Misc. Geol. Inv.
Map I-550.

Hamilton, R. M. and J. H. Healy (1969). Aftershocks of the
Benham nuclear explosion, Bull. Seism. Soc. Amer., 59,
2271-2281.

Kehrer, H. H. (1969). Radiation patterns of seismic surface
waves from nuclear explosions, M. S. Thesis, Massachusetts
Institute of Technology, Cambridge, Massachusetts.

McKeown, F. A., and D D. Dickey (1969). Fault displacements
and motion related to nuclear explosions, Bull. Seism.
Soc. Amer., 59, 2253-2269.

McKeown, F. A., P. P. Orkild, D. D. Dickey, and R. P. Snyder
(1966). Some geologic data pertinent to the seismic
characteristics of Pahute Mesa, U. S. Geol. Survey Tech.
Letter: Sp. Std. I-45.

Orkild, P. P., K. A. Sargent, and R. P. Snyder (1969). Geologic
map of Pahute Mesa, Nevada Test Site, Nye County, Nevada,
U. S. Geol. Survey Misc. Geol. Inv. Map I-567.

Press, F. and C. Archambeau (1962). Release of tectonic strain
by underground nuclear explosions, J. Geophys. Res., 67,
337-343.

Ryall, A. and W. U. Savage (1969). A comparison of seismo-
logical effects for the Nevada undergro test Boxcar
with natural earthquakes in the Nevada region, J. Geophys.

Res., 74, 4281-4289.

Stauder, W. (1971). Smaller aftershocks of the Benham nuclear explosion, Bull. Seism. Soc. Amer., 61, 417-428.

Toksöz, M. N. (1967). Radiation of seismic surface waves from underground explosions, Proceedings of the VESIAC Conference on the Current Status and Future Prognosis of Shallow Seismic Events, VESIAC Report, Willow Run Laboratories, The University of Michigan, 65-84.

Toksöz, M. N. and H. H. Kehrer (1971). Underground nuclear explosions: Tectonic utility and dangers, Science, 173, 230-233.

Toksöz, M. N., D. G. Harkrider, and A. Ben-Menham (1965). Determination of source parameters by amplitude equalization of seismic surface waves, 2. Release of tectonic strain by underground nuclear explosions and mechanisms of earthquakes, J. Geophys. Res., 70, 907-922.

TABLE Ia.
U. S. EXPLOSIONS

EVENT	DATE	REGION	MEDIUM	D.C. STRENGTH (F)	FAULT AZI.	ENERGY RATI E_{tect}/E_{exp}
Pile Driver	6-2-66	Yucca Flat (n. end)	Granite	3.20	340°	13.65
Hardhat	2-15-62	Yucca Flat (n. end)	Granite	2.00	330°	12.00
Shoal	10-26-63	Fallon, Nevada	Granite	.90	346°	1.05
Greeley	12-20-66	Pahute Mesa	Zeolite Tuff	1.60	355°	3.41
Benham	12-19-68	Pahute Mesa	Zeolite Tuff	.85	345°	.96
Chartreuse	5-6-66	Pahute Mesa	Rhyolite	.90	353°	1.05
Duryea	4-14-66	Pahute Mesa	Rhyolite	.75	355°	.75
Half Beak	6-30-66	Pahute Mesa	Rhyolite	.67	345°	.60
Boxcar	4-26-68	Pahute Mesa	Rhyolite	.59	346°	.46
Corduroy	12-3-6	Yucca Flat	Quartzite	.72	347°	.69
Rulison	9-10-69	Grand Valley Colorado	Ss. and Shale	.60	335°	.48
Faultless	1-19-68	Central Nevada	Sat. Tuff	50	344°	.33
Cup	3-26-65	Yucca Flat	Tuff	.55	200°	.40
Bilby	9-13-63	Yucca Flat	Tuff	.47	340°	.29
Tan	6-3-66	Yucca Flat	Tuff	.39	347°	.20
Bronze	7-23-65	Yucca Flat	Tuff	.33	185°	.15
Buff	12-16-65	Yucca Flat	Tuff	.31	208°	.13
Haymaker	6-27-62	Yucca Flat	Alluvium	.33	340°	.14
Sedan	7-6-62	Yucca Flat	Alluvium	0	–	0
Salmon	10-22-64	Hattiesburg, Missippi	Salt	0	–	0
Gnome	12-10-61	Carlsbad, New Mexico	Salt	0	–	0
Milrow	10-2-69	Amchitka Island	Andesite	~.6	–	<.48

TABLE Ib.

P R E S U M E D   S O V I E T   E X P L O S I O N S

EVENT	REGION	D. C. STRENGTH (F)	FAULT AZI.	ENERGY RATIO E_{tect}/E_{exp}
10-27-66	Nova Zemlya	0.90	5°	1.05
10-21-67	Nova Zemlya	0.71	43°	0.67
2-26-67	E. Kazakh	0.85	6°	0.96
3-20-67	E. Kazakh	0.81	155°	0.87
2-13-66	E. Kazakh	0.67	101°	0.60

E A R T H Q U A K E S

EVENT	REGION	D. C. STRENGTH (F)	FAULT AZI.	ENERGY RATIO E_{tect}/E_{exp}
8-31-64	E. Turkey	6.0	285°	-
7-26-67	F. Turkey	1.5	267°	

Figure   Captions

Figure 1.   Stations recording surface waves from explosions
in the continental United States.

Figure 2.   Filtered (upper three traces) and unfiltered
(lower three traces) long-period components from
the Boxcar explosions at Mould Bay, Canada (MBC)
plotted from digital data at the same gain. The
two filtered horizontal components have been
rotated to radial and tangential directions to
separate Love and Rayleigh waves.

Figure 3.   Contour plots of the deviations of combinations
of part double-couple and fault plane azimuth
from experimental Love to Rayleigh wave ratios
for three period ranges: a) 9 to 15 sec,
b) 15 to 22 sec, and c) 22 to 30 sec,
for the Faultless event.

Figure 4.   The period dependence of F, the past double-
couple, for five nuclear explosions.

Figure 5.   Map of Yucca Flat showing the fault plane orienta-
tion of the explosions studied, explosion-produced
fractures, and major natural faults in the area
(geology after Fernald et al, 1968).

Figure 6.   Map of Pahute Mesa showing the fault plane
            orientations of the explosions studied, explosion-
            produced fractures, and natural faults in the
            area (faults after Orkild et al, 1969).

Figure 7.   Source mechanisms determined for the Boxcar and
            Benham events compared to natural faults and
            explosion-produced fracturing, and aftershock
            distribution. Aftershock distribution for Benham
            (Hamilton and Healy, 1969) is that of the larger
            aftershocks (magnitude 3 to 4.2). Aftershocks
            from Boxcar (Ryall and Savage, 1969) are those
            occurring in the first two days after the event.
            The circles are of radius 5 km centered on the
   ground zero of the explosion.
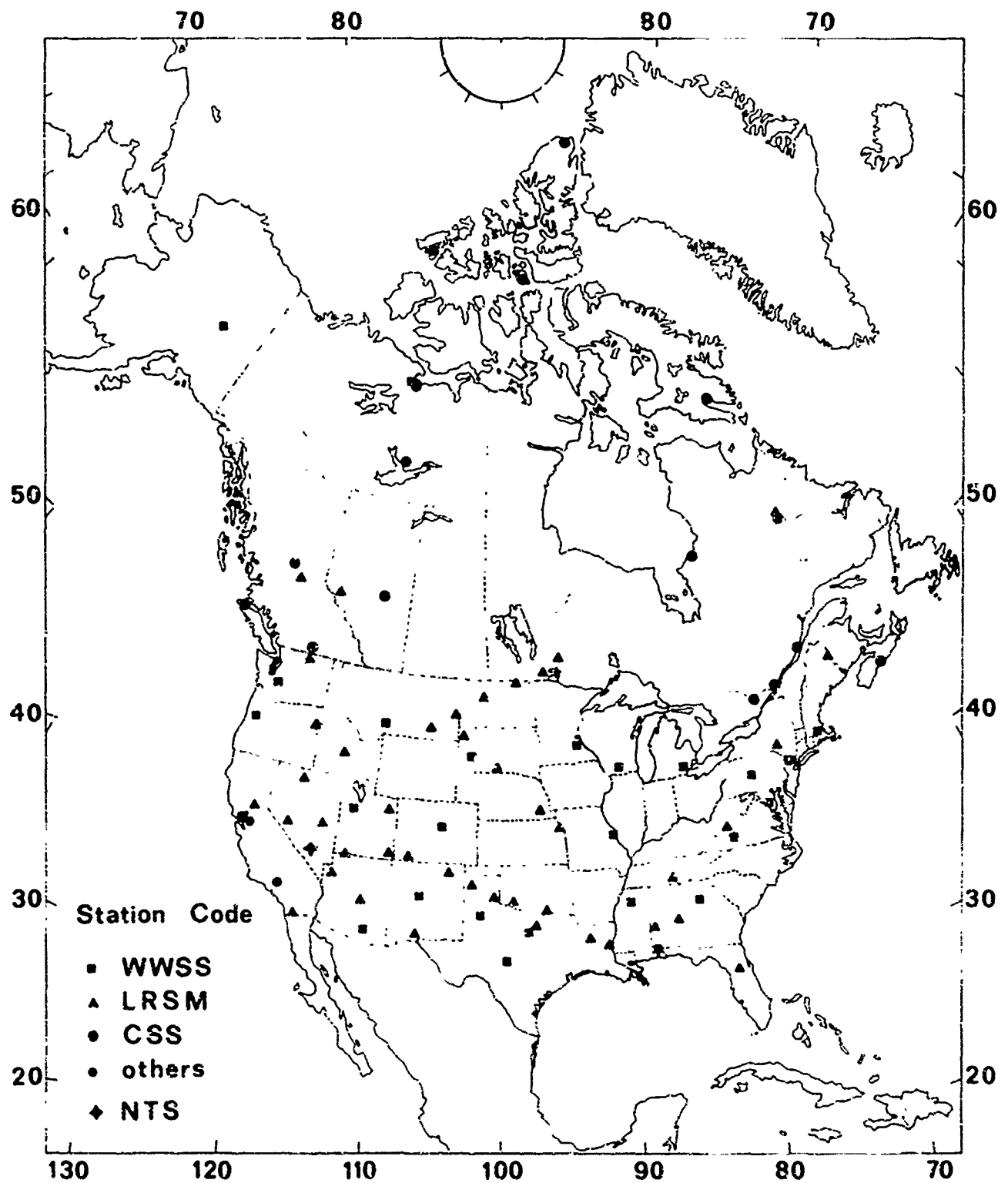
Figure 1.

BOXCAR — MBC
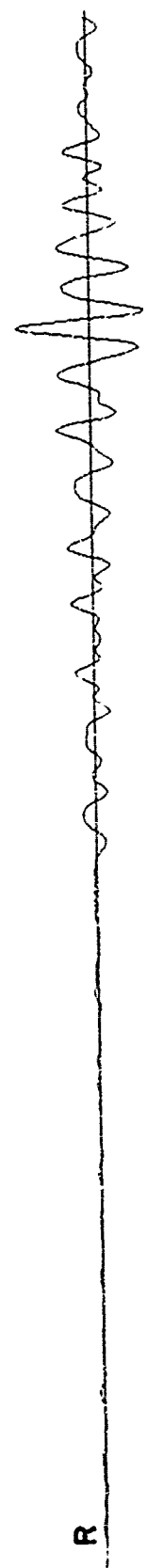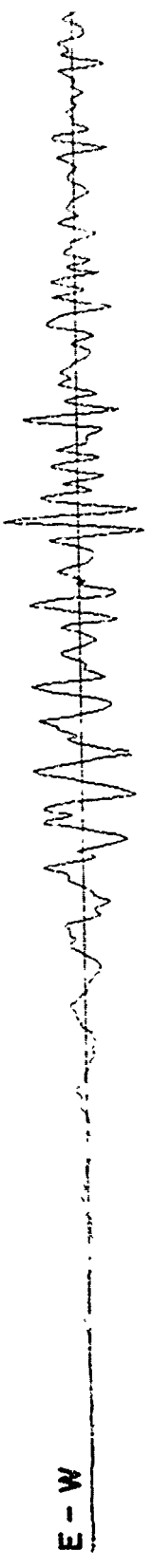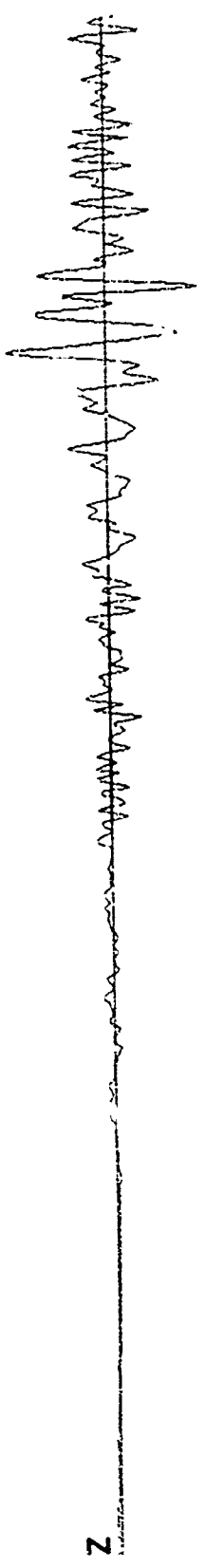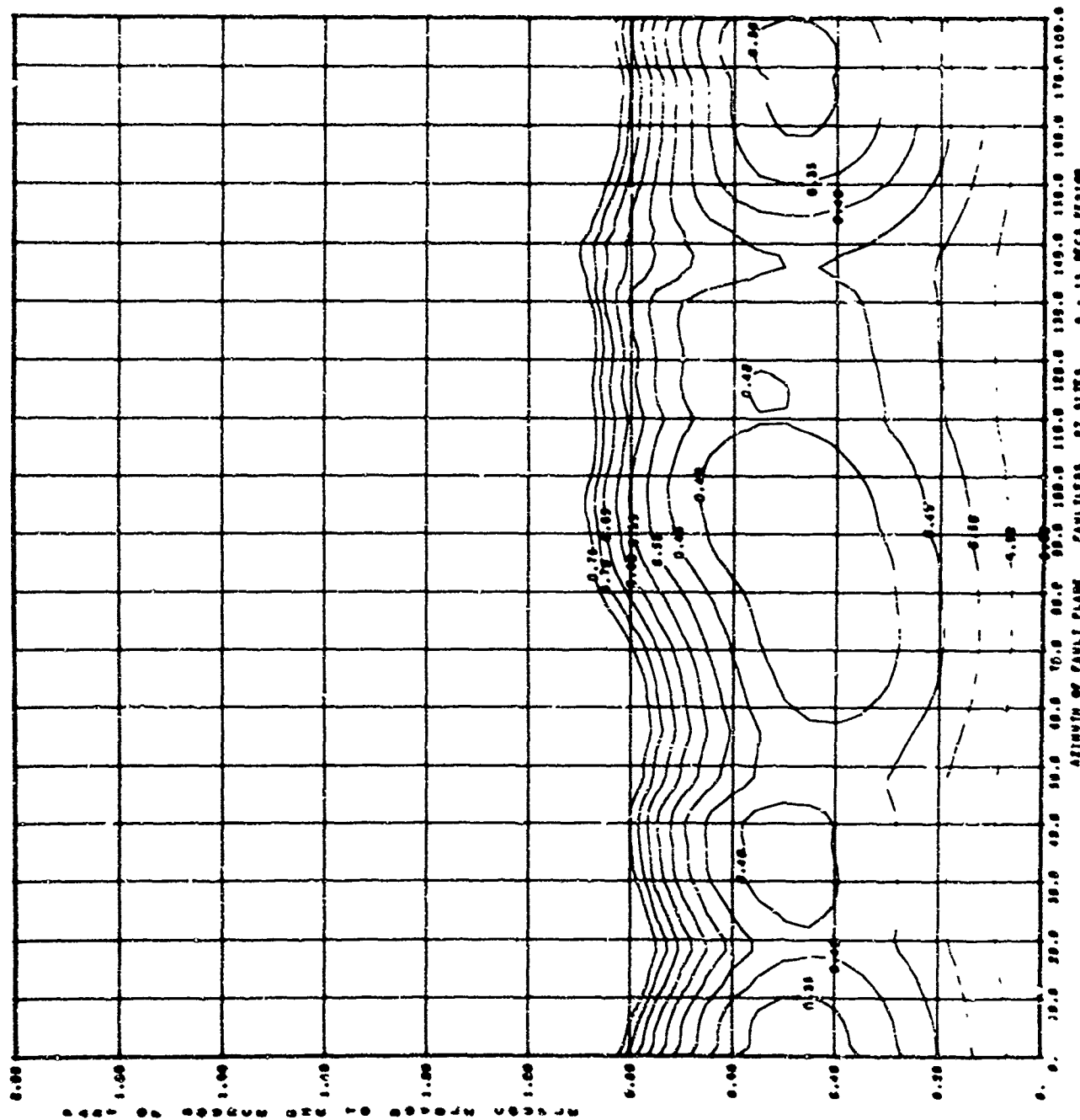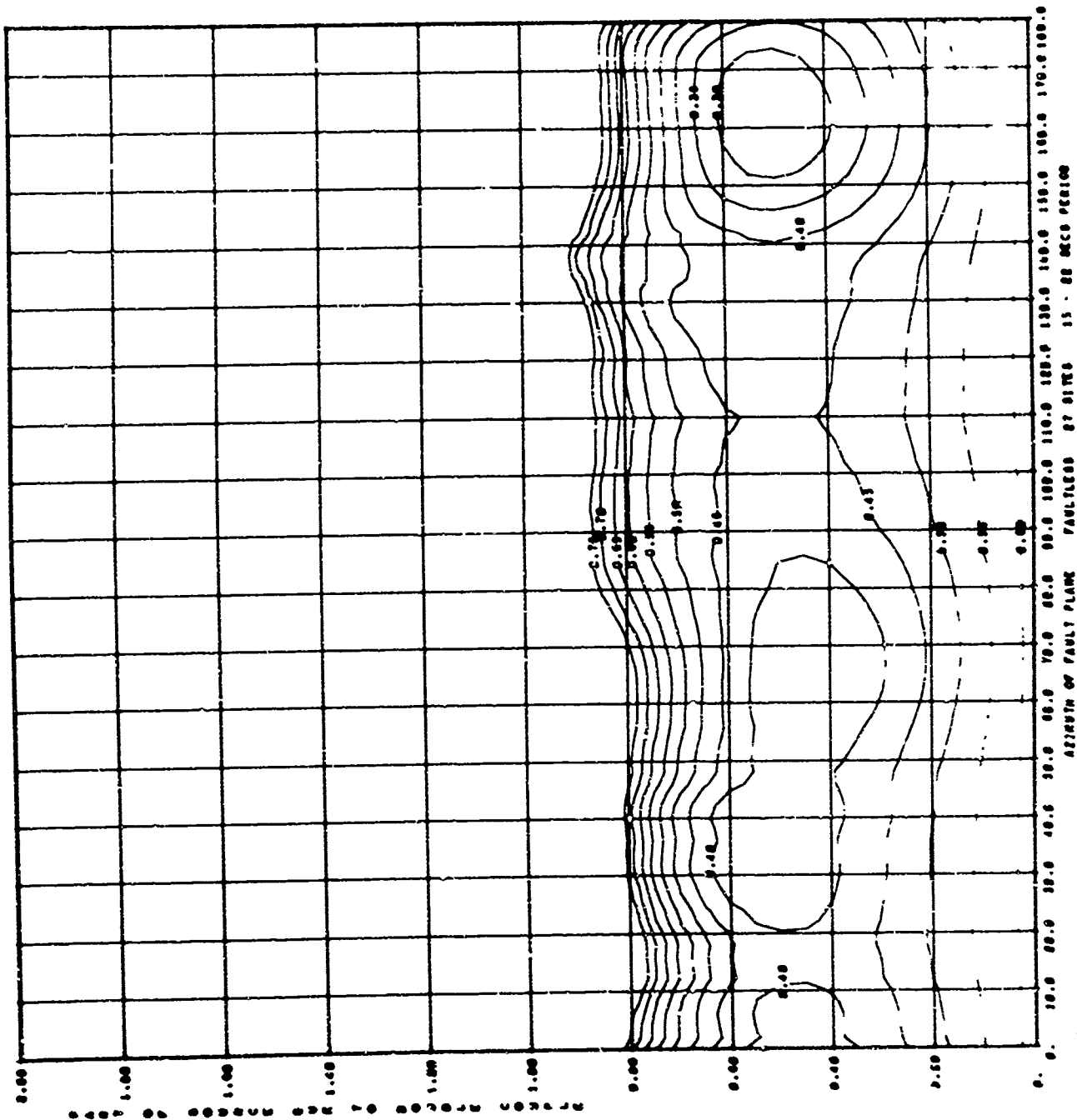
Figure 2

Figure 3a.

Figure 3b.
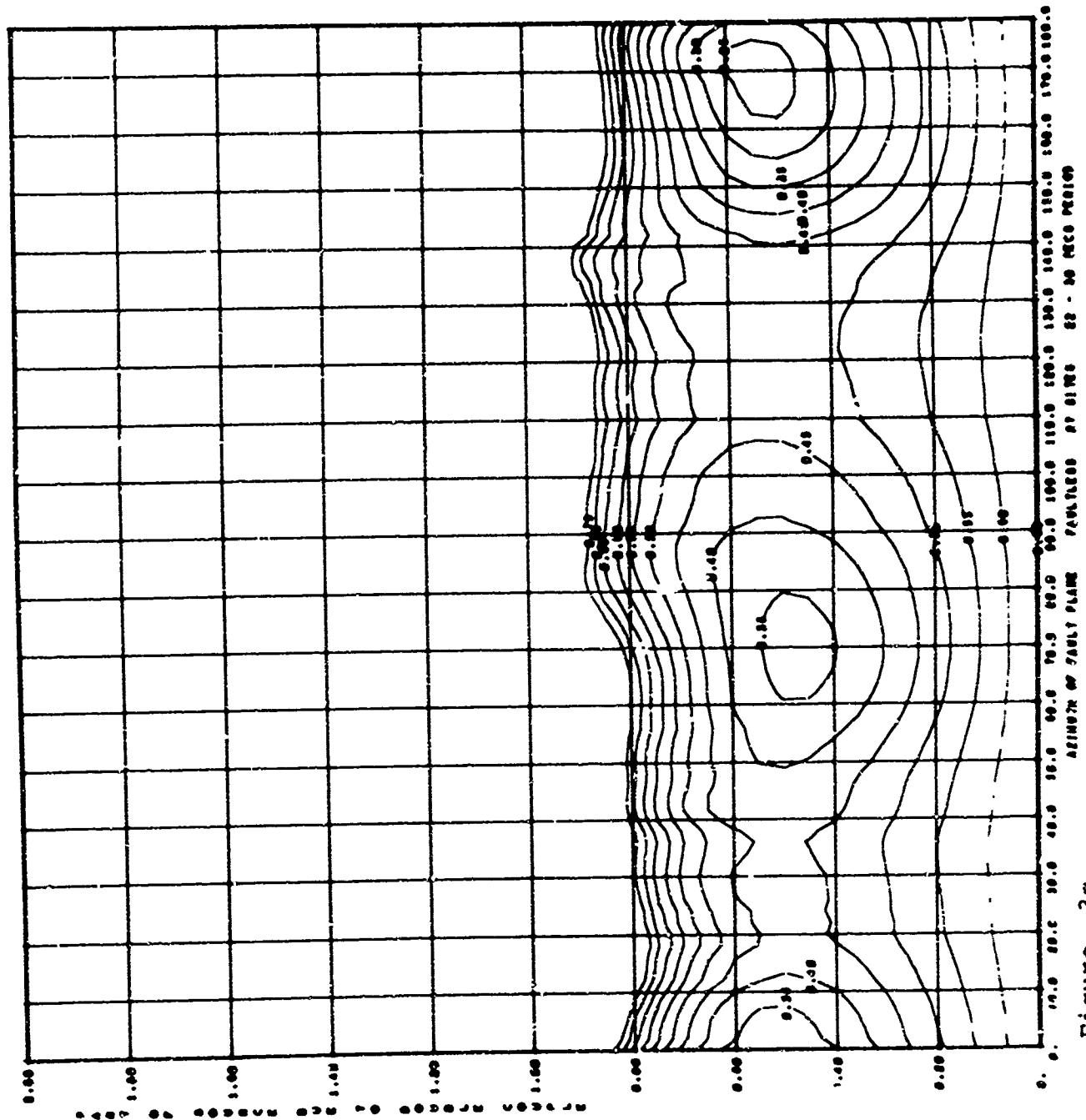
Figure 3c.
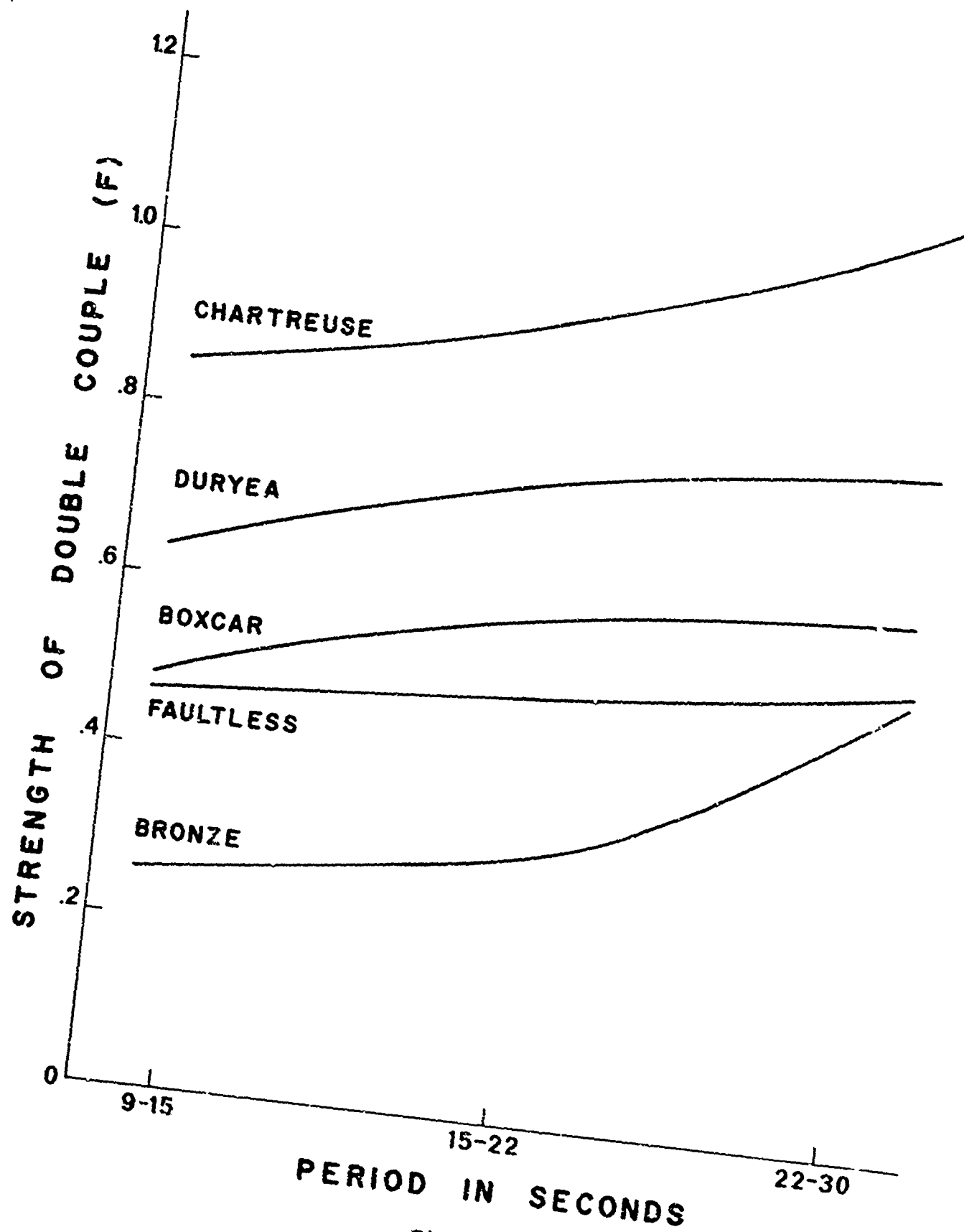
Figure 4.

Figure 5.

Figure 6.

BOXCAR

AFTERSHOCKS

BENHAM

SOURCE MECHANISM

FAULTS AND FRACTURES
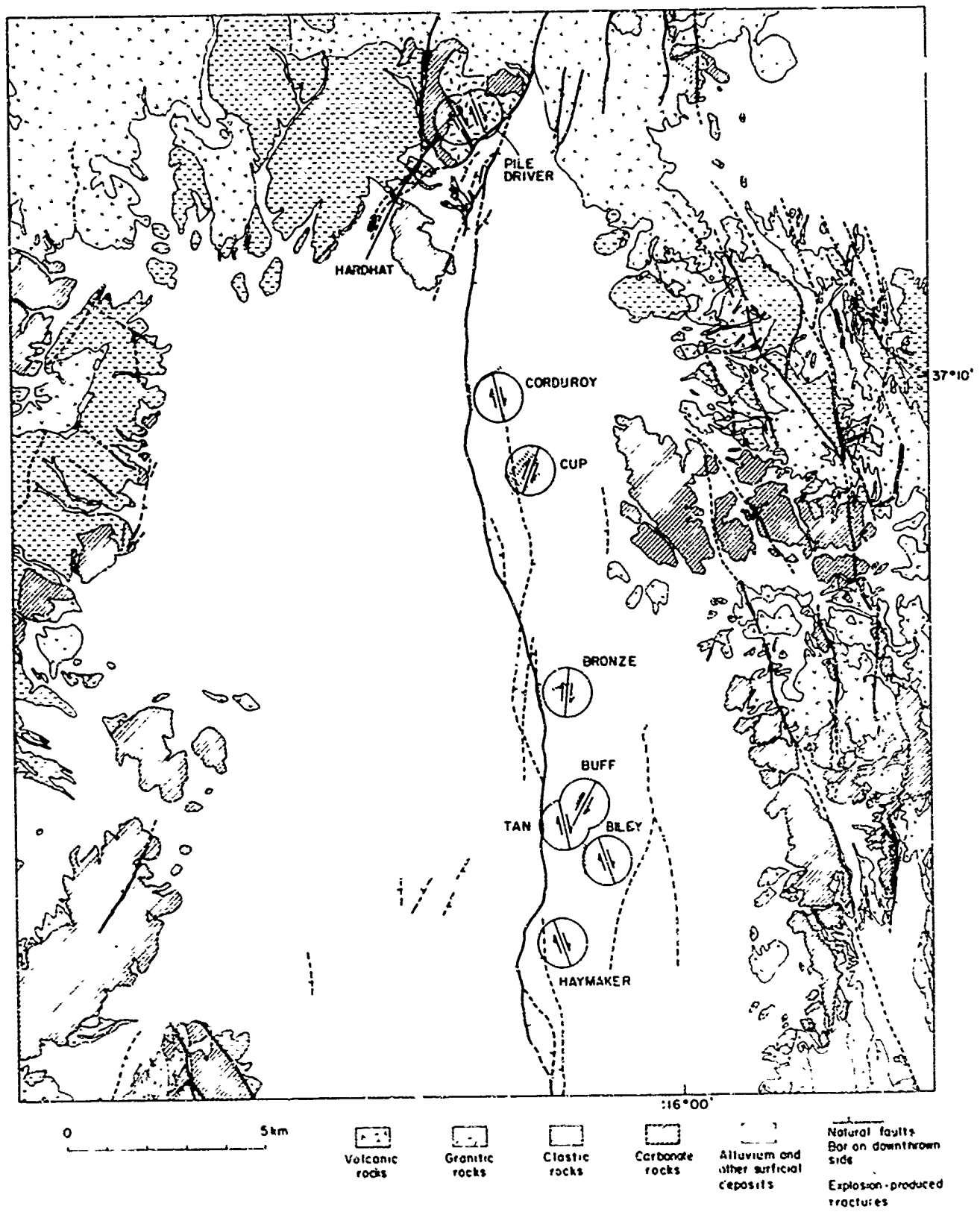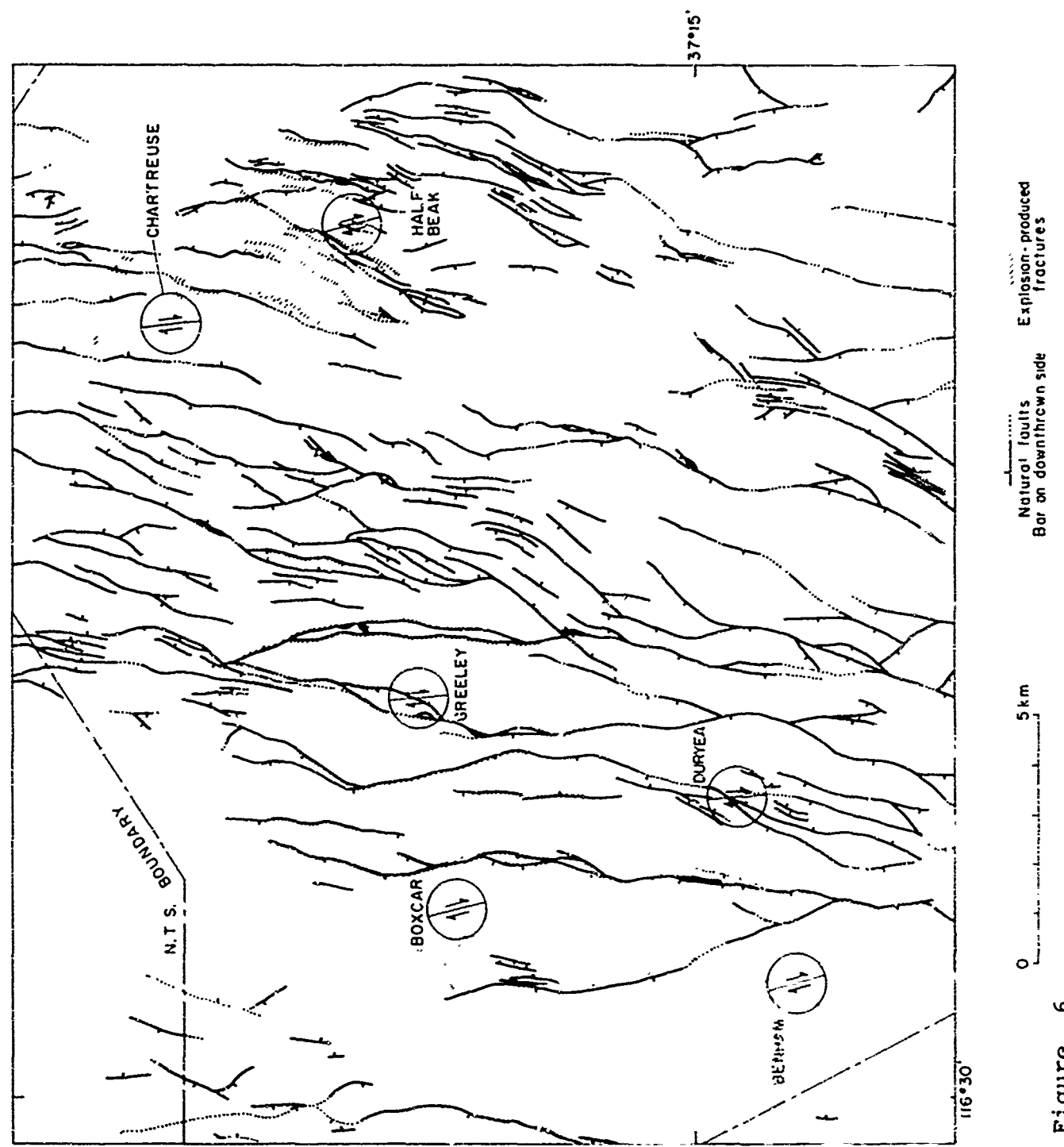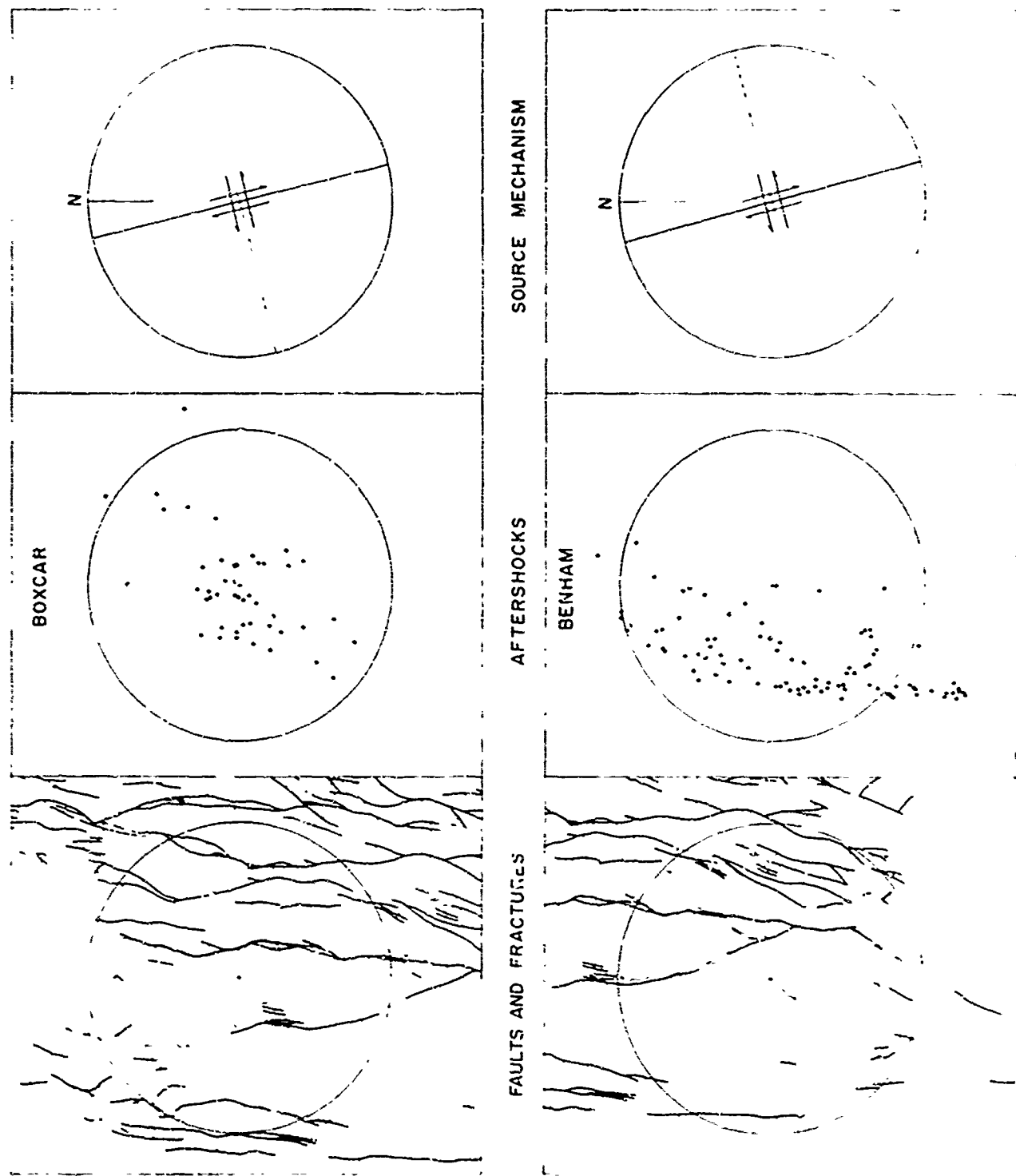
Figure 7.

II. GENERATION OF SEISMIC WAVES BY EXPLOSIONS IN PRESTRESSED
MEDIA: NUCLEAR EVENTS AND LABORATORY EXPERIMENTS

ABSTRACT

The mechanisms of generation of seismic waves by an explosion in prestressed media are studied using both field seismograms and controlled laboratory experiments. LRSM seismograms from the underground nuclear explosion Bilby are analyzed to determine the source parameters from the radiated Love and Rayleigh waves. From the normalized amplitudes of Rayleigh waves as well as the Love-Rayleigh amplitude ratios, a composite source consisting of an isotropic explosion and a double-couple is synthesized for the explosion and the associated tectonic strain release. From Bilby and other explosions studied by similar techniques, it is found that the tectonic strain energy release strongly depends on the medium properties in the immediate vicinity of the explosion. For "harder" media (such as granite) the tectonic strain energy release and the relative amplitude of Love waves are significantly higher than for softer media such as alluvium. Source time functions of Love waves associated with the explosions are closer to time functions of earthquakes than to those of explosions.

The mechanisms of the pre-existing strain energy release by explosive sources are studied in two separate laboratory experiments. In a one-dimensional experiment where an explosive source is detonated in a rod stressed in torsion, the S-wave amplitudes are found to be linearly proportional to

pre-strain. In the second experiment, radiation of seismic waves, and the near source phenomena of explosive sources in pre-stressed plates are studied by photoelastic as well as strain gauge observations. The generation of S-waves is greatly enhanced by the pre-stress condition. It is found that extended cracking (faulting) occurs along directions determined by the prestress field. The transverse (SH) waves are generated primarily by the relaxation of the stress field along these cracks. The explosion-generated cavity alone could not account for the radiated transverse seismic energy.

I. INTRODUCTION

Seismic surface and body waves generated by underground explosions and recorded at distant stations quite often show characteristics differing from those of an ideal explosive point source in a homogeneous medium. Most notable among these differences are the presence of Love waves and the azimuthal asymmetry of the Rayleigh wave radiation patterns. Through numerous studies it has been shown that the Love waves are produced at the source region, although the exact mechanism of their generation still cannot be clearly defined. The purpose of this paper is to present and interpret data, obtained from underground nuclear explosions and controlled laboratory experiments, on seismic waves generated by explosive sources in stressed media.

There have been a number of studies dealing with the radiation patterns and the generation of SH-type seismic waves by underground nuclear explosions (Press and Archambeau, 1962; Brune and Pomeroy, 1963; Aki, 1964; Toksöz et al., 1964; Toksöz et al., 1965; Toksöz, 1967; Kehrer, 1969; Molnar et al., 1969; Tsai and Aki, 1970). In addition, there are a number of previous theoretical studies on the problems of seismic wave generation by explosions (Zvolinskii, 1960; Bishop, 1963; Alverson, 1964; Cisternas, 1964; Butkovich, 1965; Archambeau, 1968). Difficulties in describing wave propagation from nuclear explosions arise because of very high stresses involved. In the im-list ...

the explosion, shock phenomena dominate, whereas in the far zone, elastic behavior prevails. The transition region is extremely important to the understanding of seismic wave generation, yet this region is extremely difficult to describe mathematically.

In the description of this complex problem, difficulties arise both in mathematical formulation and from inadequate knowledge of the behavior of geologic materials under shock loading. In the zone immediately around the explosion, a relatively small volume, hydrodynamic compressible flow equations can be used without major assumptions or approximations. In the zones where the rocks are crushed and cracked, however, neither fluid nor elastic behavior can be assumed, and a semiempirical treatment based on approximations and available data must be followed. If the explosion is placed in a medium where tectonic stresses exist, other complications arise from the stress relaxation around the cavity, the crushed zone, and the zone of numerous shock induced cracks.

Controlled laboratory experiments can provide some of the information needed for the understanding of seismic wave generation by explosions in pre-stressed media. Some experiments have been conducted in the field using explosive sources in soil (Kisslinger et al., 1961). Other model experiments have been carried out in the laboratory using explosive sources in pre-stressed plates. In these tests, the radiation patterns of seismic compressional and shear waves were observed with various transducers and oscilloscopes (Kim and Kisslinger, 1967;

Kisslinger and Gupta, 1963). Most recently, photoelastic techniques have been used to observe wave generation and propagation in pre-stressed media (Thomson et al., 1969).

In this paper we will treat, in three steps, the problem of mechanisms of seismic wave generation by explosive sources in pre-stressed media. First, we describe the radiation pattern of surface waves from a typical underground explosion at the Nevada Test Site. We determine its source mechanism by using an amplitude equalization scheme. In part two, we describe the results of laboratory experiments in which explosive sources were detonated in plates under different pre-stress conditions. Here the mechanisms of seismic wave generation, crack formation, and source complications were observed using dynamic photoelasticity and high speed photographic techniques. Finally, we interpret the field observations in light of laboratory findings.

II. FIELD OBSERVATIONS

Seismic waves from a large number of the U. S. underground explosions have been well-recorded by LRSM (Long Range Seismic Measurements), WWSS (World-Wide Seismic System) and other seismograph stations in North America. LRSM stations provide the best recordings of surface waves in the period range of 10 to 50 seconds. Most of the large explosions detonated in relatively hard geologic media (granite, tuff) generate Love

waves in addition to Rayleigh waves. Two examples of Love waves from explosions are shown in Figures 1 and 2. Explosions in loose alluvium and salt domes, and collapse events following explosions, do not generate a significant amount of Love waves. The main body of this study is devoted to the understanding of the generation of these transverse waves. Some sources that must be considered are: (1) relaxation of the pre-stressed medium around the explosion generated cavity, (2) triggering of an earthquake by the explosion, (3) radiation from explosion induced cracks in the medium, and (4) a combination of all of these.

In order to resolve this problem it is useful to first determine the radiation patterns of Rayleigh and Love waves. A group of explosions have been studied using the amplitude equalization method (Toksöz, et al., 1964, 1965; Toksöz, 1967; Kehrer, 1969). Here we illustrate the method with data from the Bilby explosion.

II.1. Radiation of Seismic Waves from the Bilby Explosion.

The nuclear explosion Bilby was detonated at the Nevada Test Site on 13 September 1963 at 17:00:00 GMT. The shot was placed at a depth of 700 m. in tuff. The computed equivalent magnitude was m_b = 5.8. A collapse event (m_b = 4.5) followed the explosion at 17:31:20.5 GMT.

Bilby generated Rayleigh and Love waves which were well

recorded at a number of LRSM stations. The station distri-
bution is shown in Figure 3. The Love waves could be iden-
tified easily since the long-period horizontal instruments
were generally oriented in radial and transverse directions
relative to the source. Furthermore, for a continental path,
Love waves have higher group velocities than Rayleigh waves
in the period range of interest.

Radiation Pattern of Rayleigh Waves. Under ideal conditions
the radiation pattern can be obtained by correcting the
observed amplitudes for instrument response, geometric spread-
ing and attenuation effects. In practice, however, the geo-
logic conditions are complicated and the absolute amplitude
method is not very effective (Toksöz and Clermont, 1967).
Thus a method of normalization must be considered. The
source and the propagation factors cannot be isolated from
each other. Therefore, we must consider methods in which
one of the variables is held constant while the effect of
the other is investigated. We used two methods for the
study of relative amplitudes to determine the radiation pat-
tern from Bilby. In the first, we normalized the amplitudes
of the Rayleigh waves generated by the explosion to those
of the collapse event that followed. In the second we used
the ratio of the Love and Rayleigh wave amplitudes to obtain
a source function.

The collapse of the cavity (formed by the explosion) seems

to provide an excellent reference for normalization. When
the amplitude ratios of the explosion-and collapse-generated
waves are taken, the propagation and instrument effects com-
pletely cancel out, and the ratio directly reflects the source
effects. In previous studies, it was found that the radia-
tion pattern from the post-explosion collapse was in general more
symmetric than the pattern from the explosion. The azimuthally
uniform amplitudes as well as the absence of prominent Love
waves were evidence of this radial symmetry (Toksöz, 1967).
If we assume that the Bilby collapse had a radially uniform
radiation pattern, then the explosion/collapse ratio would
indicate if the explosion was a symmetric source.

The ratios of peak amplitudes of the Rayleigh waves are
shown in Figure 4 as a function of azimuth. The peak ampli-
tudes were directly read from the long-period records of the
LRSM stations. In a few instances the spectral ratios were
computed, and these, on the average, showed a similar radiation
pattern as the peak amplitudes.

The azimuthal coverage in Figure 4 is far from being
complete, but in the north and northeast directions, where
there is a sufficient number of observations, the deviation
from a uniform ratio is clear. If we assume that the radial
non-uniformity of the radiation pattern from the explosion was
due to some form of tectonic complication (such as the relaxa-
tion of the medium due to the cavity or induced rupture), we
can include this effect by superimposing a multipolar term

on the explosive source. Both seismic model experiments and theoretical studies indicate that at large distances from the source, a double-couple type source function is a good representation for tectonic strain release (Honda, 1962; Burridge and Knopoff, 1964; Archambeau, 1968). Then the displacements observed at a distant station can be written as the vectorial sums of those due to an explosive source and to a double-couple.

Using the notation of Toksöz, et al. (1965), we can write the far-field expressions for the Rayleigh wave ground displacements from a near-surface explosive source.

$$W_e(\omega) = \frac{c_1}{(2\pi r)^{1/2}} \; k_R^{1/2} \left(\frac{\dot{U}_o^*}{\dot{W}_o}\right) A_R(\omega) T(\omega) \exp(-\gamma_R r) \exp[i(\omega t - k_R r - \phi_t + 3\pi/4)]$$

$$U_e(\omega) = \frac{c_1}{(2\pi r)^{1/2}} \; k_R^{1/2} \left(\frac{\dot{U}_o^*}{\dot{W}_o}\right)^2 A_R(\omega) T(\omega) \exp(-\gamma_R r) \exp[i(\omega t - k_R r - \phi_t - 3\pi/4)]$$

$$\tag{1}$$

$$V_e(\omega) = 0$$

$W_e(\omega)$, $U_e(\omega)$, $V_e(\omega)$ are the vertical, radial and tangential components of the displacement, k_R is the wave number, r is the radial distance, γ_R is the Rayleigh wave attenuation coefficient. A_R is the medium response for Rayleigh waves due to a vertical force, $\dot{U}_o$ and $\dot{W}_o$ are the components of particle velocity at the surface. $T(\omega)$ and $\phi_t(\omega)$ are the amplitude and

the phase spectra of the source time function. The displacements due to an orthogonal, horizontal double-couple source are (Ben-Menahem and Harkrider, 1964; Toksöz et al., 1965):

$$W_{dc}(\omega) = \frac{c_2}{(2\pi r)^{1/2}} \, k_R^{1/2} \left(\frac{\dot{U}_o^*}{\dot{W}_o} \right) A_R(\omega) T'(\omega) \sin 2\theta \exp(-\gamma_R r)$$

$$\cdot \exp[i(\omega t - k_R r - \phi_t' + 3\pi/4)]$$

$$U_{dc}(\omega) = \frac{c_2}{(2\pi r)^{1/2}} \, k_R^{1/2} \left(\frac{\dot{U}_o^*}{\dot{W}_o} \right)^2 A_R(\omega) T'(\omega) \sin 2\theta \exp(-\gamma_R r) \qquad (2)$$

$$\cdot \exp[i(\omega t - k_R r - \phi_t' - 3\pi/4)]$$

$$V_{dc}(\omega) = \frac{c_2}{(2\pi r)^{1/2}} \, k_L^{1/2} A_L(\omega) T'(\omega) \cos 2\theta (-\gamma_L r)$$

$$\cdot \exp[i(\omega t - k_L r - \phi_t' - 3\pi/4)]$$

The subscripts R and L refer to Rayleigh and Love waves, respectively. The angle θ is measured counter-clockwise from the principal plane (i.e. fault plane) of the double-couple.

The far-field displacements of Rayleigh and Love waves from a composite source consisting of an explosion and horizontal double-couple can be written from (1) and (2).

$$U_{Rz} = W_e(\omega) + W_{dc}(\omega)$$

$$= W_e(\omega)\{1 + F \frac{T'(\omega)}{T(\omega)} \sin 2\theta \exp[i(\delta\phi_t)]\} \qquad (3)$$

$$U_L = V_{dc}(\omega)$$

F is the relative strength of the double-couple, $\delta\phi_t = \phi_t'-\phi_t$ is the phase difference of two time functions. The term with the factor $\sin 2\theta$ gives the azimuthal dependence of the Rayleigh wave radiation.

If we assume that the source time functions are approximately the same for an explosion and the multipolar source in the period range of interest (i.e. $T = T'$), eq. (3) becomes

$$U_{Rz} = W_e (1 + F \sin 2\theta)$$

$$\qquad (4)$$

$$U_L = V_{dc}$$

The motion from the collapse of the cavity can be represented by

$$(U_{Rz})_{collapse} = C_3 W_e \exp(i\phi_c) \qquad (5)$$

where C_3 is the relative amplitude and ϕ_c is the phase of time function relative to the explosion. From previous studies, it was found that at long periods (T $\approx$ 20 sec), explosion and collapse pairs had similar spectra except for a phase term

$\phi_c \approx \pi$ (Brune and Pomeroy, 1963; Smith, 1963; Toksöz et al., 1964). With the above formulations and assumptions, the theoretical Rayleigh wave displacement ratios for a given explosion-collapse pair can be written as

$$\frac{(U_R)_{explosion}}{(U_R)_{collapse}} = C'[1 + F \sin 2\theta] \qquad (6)$$

In Figure 4 the theoretical curve is computed using (6). Choosing C', F, and the orientation of the double-couple to fit the data best, we find $C' = 12$, $F = 0.47$, and the reference direction for the double-couple principal plane (i.e. "fault plane") $\theta = 340°$. With these data the fit is good. The above figures mean that the explosion-generated surface waves were 12 times larger than those of the collapse, and that the relative strength of the double-couple force was 0.47 times that of the explosion.

Amplitude Ratios of the Love and Rayleigh Waves. The Love waves generated by the explosions can also be used to determine the nature of the source mechanism. According to our formulation, the Love waves will be generated by the tectonic component of the source. The explosion itself will not generate Love waves under ideal radially symmetric conditions.

In determining the radiation pattern, we will again use a normalization scheme to minimize the effects of propagation paths

and recorder magnifications. Since we do not have a pure
Love wave source that can be used as a reference, we will
normalize to Rayleigh waves. This scheme was successfully
applied to explosions and earthquakes by Toksöz et al. (1965).

The ratio of the Love wave amplitude to the Z compo-
nent of the Rayleigh waves generated by the explosion can
be written using equations (1), (2), (3), and (4).

$$\frac{|U_L|}{|U_{Rz}|} = \frac{F k_L^{1/2} A_L \cos 2\theta}{(1 + F \sin 2\theta) k_R^{1/2} A_R (\dot{U}_o^*/\dot{W}_o)} \exp[-r(\gamma_L - \gamma_R)] \qquad (7)$$

In writing (7), it was assumed that the source time functions.
$T(\omega)$ and $T'(\omega)$ were the same for both the explosion and the
double-couple component. Furthermore, as : the previous sec-
tion, it is assumed that the tectonic contribution can be
represented as a double-couple. Thus the Love waves are
those generated by a double-couple, and the Rayleigh waves
are the vectorial sum of those due to the explosion and due
to the double-couple.

In using (7) we must compute k_L, A_L, k_R, A_R, $(\dot{U}_o^*/\dot{W}_o)$,
γ_L, γ_R. These quantities are functions of the frequency for a
given earth structure. Fortunately, $k_L^{1/2} A_L / k_R^{1/2} A_R$ is a monotonic
and slowly varying function of frequency in the spectral
range of our interest. Thus the effect of the structure is
minimized by the normalization process, and an imprecise
knowledge of structure does not limit the applicability of

the method. We took one average structure for the Western
United States given by Alexander (1963) and computed the
amplitude response for the Rayleigh (A_R) and the Love (A_L)
waves. The method and programs of Harkrider (1964) were
used in these computations. The results are shown in
Figures 5 and 6.

In computing the Love/Rayleigh amplitude ratios from the
long period recordings on the LRSM stations we used the peak
amplitudes. In cases where spectra were computed, they peaked
at about $T = 18$ seconds. Spectral ratios are shown in Figure
7 for four stations, together with the ratio of peak ampli-
tudes. On the average the agreement is good enough to justi-
fy the use of peak amplitudes, with the understanding that
the results are valid only in the $T = 15-20$ second period
range. At longer periods U_L/U_{Rz} ratios generally tend to
increase as seen for stations CP-CL and CP02 in Figure 7.

All the available U_L/U_{Rz} data from Bilby are shown in
Figure 8, as well as the theoretical curve based on equation
(7). The reference plane for double-couple orientation
(plane of $\theta_C = 340°$) and the relative strength $F = 0.47$ are
the same values that were determined from the explosion/collapse
Rayleigh wave ratios. The agreement between the observed data
and the theoretical curve can be considered good.

The consistency of one single source model for both the
Rayleigh and the Love wave radiation patterns is encouraging.
Although this is not a definite proof, if gives support to

our method of synthesizing the source and to our assumptions.

II.2. Source Time Function of Bilby

The source time function of the explosion can be determined from the recordings of the motion at distant stations by correcting for the instrument response and the response of the propagation medium. For surface waves, we can compute both amplitude (corrected for attenuation) and phase response if the structure is known. In this study we will use an average structure and use only the amplitude spectra, since the accuracy of phase spectra depends very strongly on exact knowledge of the structure.

The Rayleigh waves recorded at three stations are first corrected for the instrument response to obtain the true ground displacement. These stations are Kanab (Utah), Campo (California) and Winnemucca (Nevada). They represent excellent azimuthal coverage at fairly close distances. The filtered Rayleigh wave pulses from two of these are shown in Figure 9 and their Fourier amplitude spectra in Figure 10. Ground displacement spectra (Figure 11) are obtained by correcting the spectra of Figure 10 for the instrument response at each station. They represent the product of the source amplitude spectrum and the response of the layered medium (i.e. propagation path) to Rayleigh waves. The medium response includes the effects of attenuation and the source depth.

To determine the source function, we must correct the

ground displacement for the propagation factor. This was
done using the impulse response of the medium (Figure 5) as
given by equation 1. The effect of attenuation was removed
using $\gamma_R = \pi f/UQ$ where U is the group velocity and Q was
assumed to be 100, independent of frequency. The corrected
spectra are shown in Figure 11. This presumably represents the spectrum
of the source pressure function.

The interpretation of amplitude spectra in terms of a
time function requires incorporating either
phase data   or some other constraint. We
assume that the pressure pulse has the form p(t) = p   t).
This formulation was discussed in an earlier study (Tu
et al., 1964). The whole problem now consists of determining the
parameter η from the spectra. A value of η = 1.5 seems to
agree well with the observations as shown in Figure 12. Dis-
crepancies at periods longer than T = 30 seconds are attributed
to the effects of lateral heterogeneities and low signal to
noise ratio. The time function is given in Figure 13.

We must note here that the p(t) we determined represents
the stress wave form not at the source but at some distance
from the point of detonation. Since we used a linear theory
based on infinitesimal strains to correct for propagation and
attenuation effects, our corrections are valid only to the
boundary of the region where these conditions are met. This
may be at a distance of several kilometers from the source
point. We must clarify one other aspect of Figure 9: the

pressure pulse was based on data in the period range of 10 to 35 seconds, so we could not see any of the fine features of the pulse that would be observable primarily in the high frequency components. Neither could we see a small residual permanent displacement or strain. Even with these limitations the shape of the time function shown in Figure 9 is similar to (although somewhat broader than) those of close-in measurements (Wistor, et al., 1963; Perrett, 1968). The source time function varies since it is dependent on the yield of the explosion, the medium, and shot depth. In gene   larger explosions have broader pulses (smaller η values)   r investigators have also proposed a step-function for the source model on the basis of surface wave data (Tsai and Aki, 1970). However, the available close-in acceleration measurements (Perrett, 1968) and near-field strain data (Smith, et al., 1969) indicate larger stresses at the beginning of the pulse than toward the tail. These emphasize the need for spectral data near the source over a broad period range for future detailed source studies.

It would be of interest to examine the source function of the Love waves generated by Bilby. Choosing four stations where Love waves are well separated from Rayleigh wave interference, we followed the same procedure as for Rayleigh waves of correcting the spectra for the instrument response, and the response of the layered medium for an orthogonal double-couple source. The resultant spectra of the source time function are shown in Figure 14, and their shapes are consistent for all four stations.

From the comparison of Figures 12 and 14 it is obvious
that the source time function of the explosion-generated
Rayleigh waves and that of the Love waves is quite different.
The Love waves seem to be richer in low frequency components.
From the available amplitude data in a relatively narrow fre-
quency band, we cannot determine the time function of Love
waves. It appears to be between a step function and a ramp,
if we assume a point source near the surface, a value of $Q = 100$,
and if we ignore the effects of source volume. With these limi-
tations, a step function with a rise time on the order of a few
seconds may be an acceptable approximation for Love waves.

The source spectra of the Rayleigh and Love waves generated
by explosions are important because they contain information
about the mechanism of the Love wave generation. The differ-
ences demonstrated above are significant. They indicate that
an explosion may trigger the Love wave radiation, but it
probably does not control its time history. The Love wave
source spectra are closer to those of earthquakes than to the
spectra of explosion generated Rayleigh waves.

II.3. Comparison with other Explosions

In determining the source properties of the Bilby explo-
sion, we followed the same procedures that were used in our
earlier studies of the Hardhat, Haymaker, Sedan and Shoal
explosions, as well as in some later events (Toksöz, et al.,

1965; Kehrer, 1969; Toksöz et al., 1971). Here we will compare
the Bilby results with those of other explosions, which are
tabulated in Table 1.

The most significant result is that Bilby, like the
Haymaker and Shoal explosions, generated Love waves. The
source mechanism in all cases can be explained in terms of an
ideal radial explosive source superimposed on a tectonic source
of double-couple form. The orientation and relative strength
of the double-couple seem to be controlled by the properties of
the medium and the orientation of the tectonic axes in the source
region. Bilby (in tuff) and Haymaker (in alluvium) were located
about 5 km apart. The radiation patterns of Rayleigh waves are
almost identical. In both cases the principal plane of the
double-couple is oriented in the direction $\theta = 340°$. Other
explosions in the same general area give similar orientation.
In the shoal explosion, which was fired in a completely differ-
ent area, the orientation of the double-couple was in very good
agreement with those of earthquakes in the area (Toksöz et al.,
1965). These facts suggest that multipolar contributions to
the radiation patterns are controlled by the general tectonic
features of the region.

The relative strength of the tectonic (double-couple)
contribution to the radiation pattern seems to be controlled
by the properties of the medium in which the explosion is de-
tonated. This is demonstrated by the observation that for ex-
plosions in salt domes (Gnome and Salmon) and loose alluvium

(Sedan), the source functions did not have multipolar compo-
nents (i.e., $F = 0$). For Haymaker, which was buried deep in
alluvium, a value $F = 0.33$ was determined. For Bilby (in
tuff) F was 0.47, and for Shoal, which was fired in granite,
F was equal to 0.9. Hardhat was another explosion in granite,
and it had an F value greater than 1.0. These and ten other
explosions recently studied (Toksöz, et al., 1971) indicate
an increase of F with increasing rock strength and, hence, strain
energy capacity of the medium.

From these examples we cannot determine conclusively
whether the multipolar component of the seismic energy radia-
tion is due to release of some of the strain energy accumu-
lated in the medium, due to fracturing or due to earthquake
triggering. Our laboratory model experiments,
described in the next section, will help to clarify some of
these points.

III. LABORATORY EXPERIMENTS

Laboratory experiments can, in principle, provide a better physical understanding of explosive seismic sources than field observations because the explosive source strength, pre-stress field and elastic properties of the medium can be varied in a known way. Two separate laboratory experiments were carried out with explosions in pre-stressed media. The first experiment utilized a rod stressed in torsion, an explosive source, and strain gauges. The second set of experiments was performed with point sources in pre-stressed two-dimensional plate model. Photoelastic techniques and high speed photography were utilized to determine the shot effects in the source region, radiation of stress waves, and the crack formation as a function of medium properties and pre-stress levels.

III.1. Stressed Rod Experiment

A simple one-dimensional laboratory experiment, giving insight into the basic physical mechanisms involved in the production of stress waves from explosive sources in pre-stressed media, is shown in Figure 15. Plexiglas rods 1.27 cm in diameter, and of varying lengths up to 2 m, were stressed in torsion. A few cm from one end, a bridge wire was inserted in a close fitting diametric hole and exploded with a 100-joule source. This was adequate energy to sever the end of the rod leaving the remainder of the rod free from the torsional restraints holding it. The resulting radiated waves were

recorded by strain gauges placed on the rod circumference
at various distances from the shot but oriented at 45° to the
rod axis. Typically four gauges were used, one recording
directly onto an oscilloscope and all four were recording on
magnetic tape. The gauges were also read statically before
firing the bridge wire source to provide a measure of the
prestrain.

Typical oscillogram tracings from four shots at dif-
ferent pre-stress levels are shown in Figure 16. Two out-
standing pulses on the oscillogram are the one-dimensional
equivalents of P and S waves. Velocities measured, using
gauges at several distances from the source, identify these
as the rod wave (P) and torsion wave (S), respectively. The
distinctive wave shapes for P and S pulses in Figure 16 in-
dicate that P-wave shape is controlled by the time function
of the explosive source. The S-wave is characterized by a
step-function input, and corresponding to the permanent re-
laxation of the torsional strain in the medium.

A number of oscillograms were obtained at various pre-
strain levels but with the same explosive source. The ampli-
tudes of the P and S waves are plotted as a function of the
pre-strain level in Figure 17. It is quite apparent that the
amplitude of the S-wave due to strain release increases
linearly with an increase in the prestressing field while
the P-wave amplitude remains constant. From the zero inter-
cept times for both P and S waves in time-distance plots, it
can be concluded that at the precision level of this experiment,

there was no evidence of a different origin time for P than for S. Furthermore, the observed time function of radiated S-waves (Fig. 16) can be characterized as a Heaviside step function, as seen through response of strain gauges. This is consistent with the source time functions observations for the Rayleigh waves and the Love waves from the Bilby explosion, as determined in the previous section.

III.2. Two-dimensional Photoelastic Experiments

The one-dimensional experiment cannot be used to model the spatial variation of radiation pattern from explosive sources in pre-stressed media. However, a close simulation of the underground explosions can be achieved by using two-dimensional modeling techniques.

The experimental procedure used in this study involves glass and plexiglas plates stressed in tension or shear. The explosive source is simulated by a small radial shot and the source and radiation fields are observed by dynamic photo-elastic techniques. This experiment differs from previous studies by Kim and Kisslinger (1967) utilizing aluminum and plexiglass

plates and strain gauge techniques. The main differences are
that in the current study: 1. A pre-stressing frame
capable of synthesizing a variety of static stress fields
including tension, compression, and shear was used. 2. The details
of the explosion, dynamic cracking, and wave generation in
the near source region were continuously observed through
the use of dynamic photoelastic techniques. 3. Glass was
included among the model material used. The shock loading
properties of glass are closer to those of rock-forming
silicates, and its more brittle character simulates near
surface rocks somewhat better than the more ductile, but
experimentally more convenient, plastics or metals. In the
experiment, glass turned out to be more important than
Plexiglas for studying cracking phenomena because the crack
velocity in glass was higher than the expansion velocity of
explosion gases, whereas in the Plexiglas it was lower. There-
fore, only in the case of glass did we obtain adequate de-
tailed photographic evidence of the dynamic cracking phenomena.

Figure 18 shows in outline the apparatus used in our two-
dimensional work. Referring to this figure, explosive excita-
tion of the model was provided by a closed loop of mild detonating
fuse (MDF). This induced a radial shock source in the plate
as the shock wave from the detonation in the MDF enetered the plate
model simultaneously from both sides. The model was surrounded by
polarizing optics so that the explosion process, cracking,
wave generation and propagation could be made visible to the

high speed framing camera by means of the photoelastic effect.
Suitably conditioned intense paraxial illumination was pro-
vided by the Argon bomb, a   front surface mirror, and the
Fresnel lens.

A much more detailed discussion of the experimental
technique, the methods of using dynamic photoelastic obser-
vations (isochromatics and isoclinics) to identify seismi-
cally interesting features, is given in our earlier paper
(Thomson et al., 1969) and will not be further elaborated
on here.

In addition to photoelastic observations, strain gauges
were used to record the dynamic field at points too far
distant from the source for the optical techniques to be
completely adequate. These gauges were set out so as to
instrument one quadrant surrounding the source.

In the following section we will investigate in detail
both the propagation of the stress waves from the shot and
the characteristics of the cracking phenomena.

III.2.1. Stress-Wave Propagation in a Stressed Plate

To understand the fringe patterns shown in Figures 19
to 24, it is necessary to introduce some basic definitions
and results of some calculations.

Upon passage through a stressed plate model, monochro-
matic circularly polarized light becomes polarized in two
orthogonal directions. These are parallel to the principal

stress directions in the plane of the plate. Since the light
polarized in each direction experiences a different velocity
in traversing the model, an interference effect due to the
resulting phase difference is observed when the two compo-
nents of the incident beams are combined upon passage through
the analyzer. The fringes so produced are called isochroma-
tics and are proportional to the difference in the principal
stresses $(\sigma_1 - \sigma_2)$ and hence the maximum shearing stress.
The fringe order is thus given by:

$$n = h \ (\sigma_1 - \sigma_2)/f$$

$$n = \frac{2h}{f} \ |\tau_m|$$

(8)

where τ_m is the maximum shear stress, h is the plate thickness
and f is the constant of proportionality which is wavelength
dependent. Therefore, if white light is used to illuminate
the model the isochromatic effect is a multicolored inter-
ference pattern. Knowing the stress field $(\sigma_r, \sigma_\theta, \sigma_{r\theta})$ one
can calculate the isochromatics from equation (8) and to
within a numerical constant factor (for a particular material
and thickness). This factor must be determined experimentally.

In plane polarized light not only are the isochromatics
observed but an additional set of extinctions, called the
isoclinics, are seen wherever the principal stress directions
are parallel or perpendicular to the pass directions of the
polarizer and analyzer. In this experiment, polarizer and

analyzer were oriented at 45° and 135°. Thus in the unstressed plate case, shot generated P waves will have isoclinics in directions θ = 45, 135, 225, 315°. The S-waves from the same source will have isoclinics at θ = 0, 90, 180 and 270°. The isoclinics are used to identify the wave types (P or S) in these experiments.

In the case of the stressed plate the isoclinics will shift due to the static stress field. In this case the loci of isoclinics can be calculated from the vectorial summation of principal static and dynamic stresses.

Examples of isochromatics and isoclinics from a shot in an unstressed plexiglas plate are shown in Figure 19. Note that these patterns are very clear for P-waves, but less clear for S-waves which were much smaller in amplitude. In fact, S-waves can be identified in this case on the basis of the isoclinics. The theoretical isochromatic and isoclinic pattern for a radial transient source in a plate is given in Figure 20.

In performing the calculations on which Figure 20 (and also Figure 23) were based, it was assumed that the dynamic stress components displayed geometric attenuation inversely proportional to the square root of the distance from the source and that the wave form propagated without shape change. These assumptions are only approximations and in order to better understand the effect on the isochromatics we have made a few precise theoretical calculations for the cylindrical source in a plate. The analytic formulations of

this problem have been given by Kromm (1948). The numerical solution of the integral equation has been discussed by Barker, Toksöz, and Ward (1969). The results for a particular transient cavity pressure are shown in Figure 21, where the radial stress, displacement, and maximum shear stress have been computed as a function of normalized distance r = distance/hole radius from the source for glass and plexiglas. Looking at the maximum shear stress in Fig. 21, it is clear that fringes would separate better in the case of plexiglas than in the case of glass.

The principal features of Figure 19 were identified by comparing them to the theoretical isochromatics and isoclinics of Fig. 20 and by the use of time-distance plots to obtain velocity. Fractional fringe orders only $(n < 1)$ are visible in this framing camera sequence. The compressive and dilatational portions of P, the zero order isochromatic separating them and a weak S waves are all visible in this photograph. The spreading effect on the isoclinics caused by superposition of P and S waves indicated theoretically in Fig. 20 can be seen in fact by close inspection of Fig. 19.

Using black and white photography, the actual stress level is determined from the observed fringe order n and equation (8). Color photography was used to compute stress levels from the retardation of one wavelength with respect to another wavelength and the resulting chromatic effects.

The main emphasis of this work is to determine the effect of pre-stress on the generation and radiation of seismic waves. For this reason, photoelastic experiments with explosive sources were repeated with prestressed plates. The plexiglas and glass plates were stressed in pure tension or pure shear using the stress frame. The shear was generated by applying equal amounts of tension and compression in the y and x directions, respectively. The maximum amount of stress was limited to about 100 bars per axis.

The static stress field is somewhat complicated by the presence of a small hole (drilled to place the explosive source) in the center of the plate. The radial, σ_r, tangential, σ_θ, and shear, $\tau_{r\theta}$, components of the stress around the hole of radius, a, can be computed from Muskhelishvili's solution (Savin, 1966).

In our experiments the hole radius is a = 0.185 cm. Thus in most of the plate where fringe patterns are observed, $\frac{a}{r} \ll 1$. Neglecting the higher order terms of $\frac{a}{r}$, the static stress field can be expressed as (Thomson, et al., 1969)

$$\sigma_r = \frac{\bar{\sigma}}{2} (1 + \cos 2\theta)$$

$$\sigma_\theta = \frac{\bar{\sigma}}{2} (1 - \cos 2\theta) \tag{9}$$

$$\tau_{r\theta} = - \frac{\bar{\sigma}}{2} \sin 2\theta$$

for tension, and as

$$\sigma_r = \bar{\sigma} \cos 2\theta$$

$$\sigma_\theta = -\bar{\sigma} \cos 2\theta \hspace{3cm} (10)$$

$$\tau_{r\theta} = -\bar{\sigma} \sin 2\theta$$

for simple shear stress, where θ is measured counter-clockwise
from tensile axis.

When an explosive source is fired in the pre-stressed
plate, the dynamic stress components are superimposed over
the static field given above, producing a complicated iso-
chromatic and isoclinic pattern (Thomson, et al., 1969).
These complications make it difficult to extract the dynamic
radiation patterns from the framing camera photographs, and
therefore strain gauge observations were used for this purpose.
The radiation pattern of seismic waves from an explosive source
in a glass plate under tensile stress is shown in Fig. 22.
In this figure, in addition to a complicated S-wave radiation
pattern, we also see the development and growth of cracking
and radiation from crack tips. These experiments were repeated
both with plexiglas and glass plates under shear pre-stress
conditions. The radiation patterns were similar to the above
cases. In the case of pre-stressed plates, the shear waves
were more abundant than in the unstressed plate experiments.

The maximum stress level was determined by the static
breaking strength of the plate, which was lowered considerably
because of the presence of the shot hole. Furthermore, in the

case of glass plates static flexural failure occurred before a tensile or shear failure. In the dynamic experiments, the maximum static stress level achieved was 167 bars.

III.2.2. Strain Guage Measurements of P-S Wave Radiation Patterns.

A set of four BLH foil strain gauges were used to determine the azimuthal variations of P and S wave radiation patterns under different pre-stress conditions. Gauge outputs were recorded on oscilloscopes writing in the single-sweep mode. Each gauge had an active area of 8×10 mm, and this limited its response to periods greater than 4 microseconds. In most of the experiments strain gauges were oriented at 45° to the radial direction and placed at 5 azimuths, at $\theta = 0$, 30, 60, and 90°, at a distance of 16 cm from the source. Since the presence of symmetry was shown from framing camera pictures, instrumenting only one quadrant with strain gauges was sufficient for determining the radiation pattern.

The strain gauge experiments were carried out with shots in both unstressed and stressed plates. In the case of un-stressed plates, no significant S-waves were detected above the noise level. In the case of pre-stressed plexiglas and glass plates, however, well-defined S-waves were recorded. The radiation patterns of P and S-waves for plexiglas and glass plates, stressed under tension to 163 bars and 114 bars, respectively, are shown in Figure 23.

Utilizing the local plane wave formulation, strain energy can be estimated from the observed compressional and shear

wave strains radiated.

$$W = \sum_{i=1}^{3} p_i \epsilon_i \tag{11}$$

where $W = \langle \quad \rangle$ energy density and p_i and ϵ_i are principal

stresses and strains respectively. For compressional waves

the strain measured with a gauge oriented at 45° to the

radial direction (ϵ) is related as $\epsilon_1 = 2\epsilon$ and for shear

waves $\epsilon = \epsilon_1 = -\epsilon_2$. Thus the compressional and shear wave

potential energy density fluxes, W_p and W_s, can be expressed

as

$$W_p = V_p \frac{8\nu\ (\lambda+\mu)}{\lambda+2\mu} \epsilon^2 = M \epsilon^2 V_p$$

$$\tag{12}$$

$$W_s = 2\mu \epsilon^2 V_s$$

where V_p and V_s are plate and shear velocities, respectively.

For plexiglas and glass used in this experiment, $M = 0.95 \times 10^{11}$

and 13.2×10^{11} dynes/cm^2, respectively. The corresponding

rigidities for plexiglas and glass are $\mu = 0.143 \times 10^{11}$ and

2.5×10^{11} dynes/cm^2. The shear-to-compressional potential

energy density ratios are shown in Figure 24 for peak values

of ϵ.

From the radiation patterns of both the peak energy

density ratios and the strain amplitudes themselves (Figures

23 and 24), it is clear that the S wave radiation can be

explained by either a dipole or double couple type source

having approximately a sin 2θ azimuthal dependence. The P

wave radiation is less clear since the contribution from the explosion as well as radiation due to pre-stress are super-imposed. It is apparent that the radiation pattern for P would be approximated by a function of θ of the form $(A + B \cos^2\theta)$ where A and B are constants, suggesting again the dipole source with the addition of an isotropic component.

Inspecting the radiation patterns and energy ratios displayed in Figures 23 and 24, we are faced with two questions: (1) where does the S wave energy come from, and (2) what is the reason for the skewness in the P wave radiation patterns? Let us first consider the energy question. The total energy of an elastic wave is equal to twice the potential strain energy integrated over a cycle. Thus we can compute the P and S wave energies by integrating the energy fluxes given in (12) for the duration of the pulse first, and then integrating over the radiation pattern.

At the level of approximation being used here we can evaluate these integrals by fitting each of the compressional and dilatational half-cycles of strain wave forms with a half sine wave. Integrating the flux azimuthally, allowing for the radiation pattern, we obtain approximate expressions for the total energy E_P and E_S in P and S waves for each half-cycle of duration t_0:

$$E_P = \pi h \rho V_P^3 A_{45}^2 t_0 r$$

$$E_S = \pi h \rho V_S^3 B_{45}^2 t_0 r$$

(13)

where h is the model thickness, r is the distance of the strain gauge from the source and A_{45} and B_{45} are peak strain gauge readings for the P and S waves respectively in the record interval under study, and the gauges are assumed located at the peak of the radiation pattern and oriented at $\pi/4$ to the radius vector from the source. For gauges not located at the peak of the radiation pattern an additional correction was applied in obtaining total energy values as discussed subsequently in connection with the radiation patterns. For three shots shown in Figures 23 and 24 (shots No. 13028, 13029, 13030), the corresponding P wave energies (averaged from the observations at each gauge) are: 313, 231 and 143×10^5 ergs. The S-wave energies are 49.3, 3.72 and 0.73×10^5 ergs. The corresponding tensile prestress figures in bars are 163, 163, and 114. Note that the first two shots are in plexiglas and the third in pyrex glass.

The S-wave energies cannot come from the conversion of the explosive energy into S waves since very little if any S waves are generated by the explosions in unstressed plates. Thus, we must look into the energy release from the stressed plate. The explosion crushes a small circular region of the plate around the shot point. This normally does not exceed a radius of 1 cm. Beyond this region some radial cracks extend to greater distances. If all the strain energy in a zone of radius a_1 is radiated as seismic energy, the total amount

will be

$$E_{ST} = [\pi a_1^2 h] \; \frac{1}{2} \sum_{i=1}^{3} \sigma_i \, \epsilon_i \;\; = \;\; \pi a_1^2 h \; \frac{2\bar{\sigma}^2}{E} \qquad (14)$$

where E is Youngs modulus and was determined from observed

plate wave velocities and h is the plate thickness. Equation

(14) gives a good approximation to the upper limit of the

available seismic energy if a_1 is taken to be the radius of

the "quasi-elastic" cracked zone (Archambeau and Sammis,

1970). The problem that arises in estimating the energy

from (14) is that of the definition of the cracked zone

radius. In our experiments, the approximate values for the

radius of the totally crushed and extensively cracked zone

were about 0.4 cm and 1 cm, respectively. The values of E_{ST}

for the strain levels of shots 13028, 13029 and 13030 are

tabulated in Table 2 for the larger value of a. Comparing

these figures with the previously given wave energies, it

will be apparent that the available strain energy is smaller

than the total energy radiated as S waves for a = 1 cm.

We should further consider that not all the available

strain energy is radiated as seismic energy. In fact, only

a small fraction is likely to be radiated in the spectral

range of our measurements, and this too must be divided into

P and S waves. Thus it is clear that a source region much larger than the crushed zone must be considered. This leads us to consider relaxation of the medium along the cracks that radiate to greater distances from the source than those considered in Table 2. The cracking phenomenon will be discussed in the next section.

The second problem we must consider is the skewness of the P wave radiation pattern. This phenomenon, apparent on our radiation patterns, can also be seen on the data of Kim and Kisslinger (1967). It cannot be attributed to asymmetry of the shot since it occurs only in the pre-stressed experiments. Since there is a contribution to P waves from the radiation of the strain energy due to the relaxation of the plate, then the mechanism of this relaxation must be taken into account. From the above discussion as well as from the description of the cracking in the next section, the growth of the cracks does affect the radiation pattern. Furthermore, where cracks extend close to the observation position, the growth can be characterized as a unilateral tensile fault. This presumably is due to the scattering effect of the shattered region behind the crack tips, on radiation not projected broadly in the direction of crack propagation. We have computed the radiation pattern of a unilateral tensile fault propagating perpendicular to the tension axis, utilizing Ang and Williams' (1959) formulation as given by Savage and Hansinha (1963). The radiation patterns for P and S waves are

proportional to:

$$c \ (1-2V_S^2 \cos^2 \theta / V_p^2) \ / \ (V_p - c \cos \theta)$$

and   (15)

$$c \sin 2\theta \ / \ (V_S - c \cos \theta)$$

respectively, where c is the crack velocity. In our experi-
ments, the observed radiation patterns of Figure 23 and 24
have an additional isotropic component due to the explosive
source affecting the P-wave radiation patterns. A set of
theoretical radiation patterns were calculated using (15)
with the addition of various isotropic components. These are
shown in Figure 25. The data of Figure 25 apply to plexi-
glas.

Two aspects of Figure 25 are noteworthy. (a) Increasing
crack propagation velocity produces a shift of the radiation
pattern maximum in the direction of crack propagation and
(b) increasing the isotropic component, while broadening
the radiation pattern, does not change the position of the
maximum. The radiation pattern maxima for P and S and for
glass and plexiglas were calculated as a function of crack
velocity. The results are shown in Figure 26.

Inspecting the shift in the radiation pattern of P waves
from the observations of Figure 23 and comparing this to the
theoretical shift of Figure 26, it is apparent that only a
crude estimate of the crack velocity can be obtained, because
of the limited number of data points available. A crack
velocity of six tenths the shear wave speed is consistent with

observations for both materials. The crack speed was, however,
measured accurately from the optical observations, and the
subject of crack propagation will be dealt with separately in
the next section. In reducing the strain gauge observations
to wave energy, as listed in Table 2, gauge observations
were corrected for the radiation pattern effects using a
crack velocity $0.6 V_s$.

II.2.3. Near Source Phenomenon and Crack Propagation

The stresses in the immediate vicinity of the explosion
are very high and may reach hundreds of kilobars. This easily
exceeds the compressive strength of the material, and a crushed
zone which extends from a few millimeters to a centimeter or
more, depending on the shot size and the medium, is developed.
As the stress wave propagates outward from the shot point,
the pressure falls gradually until the elastic limit of the
material is reached. Between the crushed and elastic zones,
there is a region of radial cracking produced by the tensile
failure during the unloading (dilatational) phase of the stress
waves. Because of the importance of this region for the
radiation patterns of seismic waves, great emphasis was
placed on understanding its properties in our dynamic photo-
elastic experiments.

The immediate source region of an explosion in $\frac{1}{8}$ " thick
glass plate is shown in Figure 27. The evaporated zone (totally
dark) and the crushed zone are indicated very clearly. The

initial radial cracks are visible along the inner edges of the isochromatics.

In unstressed plate experiments the radial cracks are distributed isotropically and grow in radial directions. In the case of pre-stressed plates, initially the cracks do start radially. However, after some time the cracks either stop growing or turn in the direction dictated by the stress axes. In the case of plates under tension, the favored direction of growth is perpendicular to the tension axis.

The propagation of explosion-induced cracks in glass plate under tension is shown in Figure 28. The preferred growth (in direction perpendicular to stress axis) and the radiation of seismic energy from the cracks (light zones) are indicated clearly. The stress concentration at crack tips is visible. The dark areas are the stress-free (relaxed) regions.

In addition to the above observations we have been able to determine the velocity of the crack propagation by following the progress of crack tips in successive frames. By repeating this for shots at different stress levels, we have also been able to obtain the pre-stress dependence of the terminal velocity. The results for a glass plate are shown in Figure 29. First of all, the velocities indicated are terminal velocities. We could not determine the acceleration phase of the crack growth since our measurements could not

begin before 2 cm radial distance. Secondly, there were
variations in velocities between c = 0.7 and 1.7 km/sec,
when short as well as long cracks were measured. This range
is indicated in Fig. 29.

The highest crack velocity in unstressed glass plate is
c = 1.70 ± .03 km/sec. The ratios of this velocity to plate-
compressional and shear velocities are c/V_p = 0.32 and
c/V_s = 0.51 respectively. For the glass plate stressed to
114 bars tension, the dynamic crack velocity was c = 1.84 ± 0.02
km/sec and the ratios were c/V_p = 0.35 and c/V_s = 0.55. The
intermediate (45 bar) tension pre-stress case gave values the
same as the unstressed case within the experimental error.

It would be useful to compare our values of crack velo-
cities with theoretical prediction as well as other experi-
mental results. There have been extensive theoretical studies
of crack propagation. Most recent reviews can be found in
Liebowitz (Vol. I and II, 1968), Tetelman and McEvilly (1967)
and Cottrell (1970). Very briefly, a necessary condition for
the propagation of an elliptical elastic tensile crack is
that the maximum tensile stress at its tip reach the theore-
tical cohesive strength. For completely brittle and elastic
solids where the elastic limit is much greater than the cohe-
sive stress, the Griffith relationship can be applied. Con-
sidering the crack to be a thin ellipsoid with semi-major and
minor axes 1 and h, the incremental release of the stored
elastic strain energy (W_E) is equal to the incremental increase

of surface energy (W_s) as new surface is created. At the tip
of the crack there is a strong stress concentration. The
transfer of this elastic energy to moving the adjacent
points apart at the crack tip limits the velocity of the crack
growth. With these physical models, an expression can be de-
rived for the propagation velocity of the crack (Tetelman and
McEvilly, 1967):

$$c = 0.38 \, V_p \left[1 - \frac{W_s}{W_E} \right]^{1/2} = 0.38 \, V_p \left[\frac{1 - 8\mu(1+\nu)\gamma_s}{\pi \Sigma^2 \ell} \right]^{1/2} \qquad (16)$$

where c = crack velocity, V_p = compressional velocity (plate
velocity in our case) and W_s = surface energy of crack.
W_E = strain energy in the crack, γ_s = unit surface energy and
Σ = theoretical strength, ℓ = half crack length and ν = Poisson's
ratio. For soda-lime glasses, for example, approximate values
are $\gamma_s \simeq 10^3$ ergs/cm^{2}m and $\Sigma \simeq 10^9$ dynes/cm^2 (Shand, 1961).
From these it is clear that the second term in the brackets
is fairly small and the maximum theoretical crack velocity is
$c = 0.38 \, V_p$. This theoretical value is in agreement with some
other predictions for tensile fractures in brittle material
where a value of about $c = 0.63 \, V_s$ is obtained (Yoffe, 1951;
Mansinha, 1964). There have been other theoretical derivations
relating the terminal crack velocity to Rayleigh velocity
(Baker, 1962; Broberg, 1960; Craggs, 1960; Kachanov, 1961;
Stroh, 1957). In these cases where crack velocity coincides
with Rayleigh velocity, the theoretical values differ from

others, unless the Rayleigh velocity is taken to be lower at the crack tip.

The effect of pre-stress in the material is to increase stress concentration and the strain energy W_E, while reducing the bonding energy W_s. Thus as the pre-stress level increases, W_s/W_E approaches zero, and the crack velocity reaches its asymptotic value of $c \to 0.38 \, V_p$.

The agreement between our measured values of crack velocity and the theoretical values of eq. 16 is very good, both in absolute value and pre-stress dependence. The observed values are slightly lower than the theoretical values based on perfectly brittle behavior. This is expected since there is always some plastic deformation in the fracture process, and soft glasses always fail to reach the predicted terminal velocities.

There have been other measurements of crack velocities in glass (Schardin, 1959), and these are in excellent agreement with ours. The crack velocities have also been measured in rock by a high speed photographic technique similar to ours (Bieniawski, 1966). In gabbro plates, Bieniawski's value for terminal fracture velocity was $c = 1875$ m/sec. In terms of plate velocity V_p, this value is equivalent to $c = 0.31 \, V_p$, in excellent agreement with our value under zero stress.

The implications of the explosion-induced crack growth in terms of the radiation pattern of seismic waves from underground explosions are significant. First of all, the cracking

extends the source region, and also provides the means of
converting some explosion energy into seismic waves of compli-
cated radiation pattern. This radiation, however, is iso-
tropic in the case of unstressed media. In the presence of
a stress field or tectonic lineations, the cracks grow in a
preferred direction and to greater lengths, resulting in
coherent radiation of tectonic strain energy as well as some
converted explosion energy. Even under ideal experimental
conditions, however, some complexities are introduced into
the radiation patterns due to the presence of several cracks,
and irregularities in growth. These may explain the devia-
tions of some data points from the idealized composite radia-
tion patterns, in the case of field observations such as
those of Figs. 4 and 8.

IV.   DISCUSSION AND CONCLUSIONS

So far in this paper we have described separately:
(1) the source properties of several underground explosions
as derived from the analysis of seismograms, and (2) the re-
sults of a series of laboratory experiments dealing with ex-
plosive sources in prestressed media.   In this section we will
combine the results of both studies to explain the mechanisms
of Love wave generation and tectonic strain release by
explosions.

The main results of field data analysis and the associated
laboratory experiments are the following:

1.   All explosions detonated in hard media (granite,
rhyolite, tuff) generate some Love waves at or in the immediate
vicinity of the source (see Table 1).   Laboratory experiments
indicate that the transverse waves are generated primarily
because of the existence of a stress field.   Even in brittle
materials such as glass, under unstressed conditions, few
transverse waves are generated by an explosive source compared
to the prestressed case.

2.   The Love and Rayleigh wave radiation patterns can be
explained by a composite source consisting of an isotropic
explosive source plus a double-couple source.   It was assumed
that the double-couple component was horizontal (pure strike
slip, vertical fault plane).   With the available scattered
data, it is not possible to determine uniquely and reliably

more definite source models specifying all the parameters (strike, dip angle, slip direction, magnitude) of the source function.

3. The strength of the double-couple source relative to the explosion (F value) increases with increasing strength of the medium as shown in Table 1. It should be remembered that (a) F is period dependent, and the value listed in the Table is applicable at $T \approx 15-20$ seconds, and (b) in general the F value listed is a lower bound since we assumed a vertical strike slip source function for Love wave generation. This is the most efficient radiator of Love waves, relative to Rayleigh waves. Any other double-couple source model that may fit the observed data would have a larger F value.

4. The orientation of the strike of the double couple in general is in agreement with the strike of the tectonic fiber as determined from the existing faults, strikes of earthquakes and the aftershocks following the large explosions such as Benham (Hamilton and Healy, 1969; Kehrer, 1969; McKeown and Dickey, 1969; Toksöz, et al., 1965). This phenomenon is in agreement with what was observed in the experiments with an explosive point source in prestressed plates, where growth of the cracks and the radiation pattern of S-waves were governed by the principal stresses.

5. The corrected spectra and the resulting time functions for the Love and Rayleigh waves showed that the Love wave spectra were relatively richer at longer periods than Rayleigh

wave spectra. In fact, Bilby data as well as others indicate
that the spectra of Love waves generated by the explosions
are similar to those of comparable magnitude earthquakes.
Explosion generated Rayleigh waves, on the other hand, have
spectra shifted to shorter periods (Toksöz, et al., 1965;
Molnar, et al., 1969; Toksöz, et al., 1970). Our one-
dimensional laboratory experiments also show that the time
function of stress relaxation, generated in a pre-stressed rod, is
of much lower frequency compared to those of the explosions (see
Figure 16).

6. The energy of the double-couple component of the
source holds the main clue to the source of this energy and
the mechanism of its release. Although it is difficult to
compute the total energy, at all frequencies, the power of
the double-couple source relative to the explosion at $T \simeq 20$
seconds is proportional to F^2 .(Table 1). The theoretical
estimations of the strain energy release due to the introduc-
tion of a cavity in the pre-stressed medium are hampered by
the lack of direct knowledge of pre-stress (Press and Archambeau,
1962; Toksöz, et al., 1965; Archambeau and Sammis, 1970; Smith,
et al., 1969). The laboratory experiments provide some answers.
From the strained rod experiments we see that the S-wave strain
amplitude increases linearly with pre-stress (Figure 17) as ex-
pected theoretically. The calculations carried out using data
from unstressed plate experiments show that relaxation around
the cavity alone cannot account for the radiated strain energy.

This combined with the observed S-wave radiation patterns, requiring a growing crack, suggest that relaxation associated with extended cracking contributes significantly to the radiation of strain energy in pre-stressed media. In the case of field testing, relaxation of the medium occurs both along the newly-formed extended cracks (faults) and as movement along pre-existing fault zones. Strain measurements around the Nevada Test Site show this (Dickey, 1969).

8. Based on field studies as well as our laboratory experiments we can state that explosions in pre-stressed media release some of the strain energy, and the mechanism of the release of this energy is similar to that of an earthquake. The amount of tectonic strain energy released depends strongly on the pre-existing stress level. Explosion induced cracking controls the radiation pattern and the extent of tectonic strain energy release. The explosion cavity alone cannot account for all the energy release. The radiation patterns of seismic waves are frequently complicated by the growth of cracks with finite velocities, and relaxations along different faults and cracks.

Acknowledgements

REFERENCES

Aki, K. (1964). A note on surface wave generation from the Hardhat nuclear explosion, J. Geophys. Res., 69, 1131-1134.

Alexander, S.S. (1963). Surface wave propagation in the Western United States, Ph.D. thesis, California Institute of Technology, Pasadena, California.

Alverson, R.C. (1964). Spherical waves in elastic-plastic media, Final Rept. on SRI Project No. GTU-3731, Stanford Research Institute, Menlo Park, California, 35-155.

Ang, D.D. and M.L. Williams (1959). Dynamic stress field due to an extensional dislocation, Proc. Ann. Conf. on Solid Mech., 4th, U. Texas, 36-52.

Archambeau, C.B. (1968). General theory of elastodynamic source fields, Rev. Geophys., 6, 241-288.

Archambeau, C.B. and C. Sammis (1970). Seismic radiation from explosions in prestressed media and the measurement of tectonic stress in the earth, Rev. Geophys., 8, 473-499.

Baker, B.R. (1962). Dynamic stresses created by a moving crack, J. Appl. Mech., 29, 449-458.

Barker, T.G., M.N. Toksöz, and R.W. Ward (1969). Explosion generated seismic waves, AFCRL Rept. 69-0130.

Ben-Menahem, A. and D. Harkrider, (1964). Radiation patterns of seismic surface waves from buried dipolar point sources in a flat stratified earth, J. Geophys. Res., 69, 2605-2620.

Bieniawski, Z.T. (1966). Fracture velocity of rock. South Africa CSIR Rept. MEG 517.

Bishop, R.H. (1963). Spherical shock waves from underground
    explosions: close-in phenomena of buried explosions, Final
    Rept., SC-4907(RR), Sandia Corp., Albuquerque, 115-158.

Broberg, K.B. (1960). The propagation of a brittle crack,
    Arkiv Fysik, 18, 159-192.

Brune, J.N. and P.W. Pomeroy (1963). Surface wave radiation
    patterns for underground nuclear explosions and small-
    magnitude earthquakes, J. Geophys. Res., 68, 5005-5028.

Burridge, R. and L. Knopoff (1964). Body force equivalents
    for seismic dislocations, Bull. Seism. Soc. Am., 54,
    1875-1888.

Butkovich, T.R. (1965). Calculation of the shock wave from
    an underground nuclear explosion in granite, J. Geophys.
    Res., 70, 885-892.

Cisternas, A. (1964). The radiation of elastic waves from
    a spherical cavity in a half-space, Ph.D. thesis, California
    Institute of Technology, Pasadena, California.

Cottrell, A.H. (1970). The structure of a crack, in Physics
    of Strength, Ed. A. Argon, MIT Press, Cambridge (in press).

Craggs, J.W. (1960). On the propagation of a crack in an
    elastic-brittle material, J. Mech. Phys. Solids, 8, 66.

Dickey, D.D., Strain associated with the Benham underground
    nuclear explosion, Bull. Seism. Soc. Am., 59, 2221-2230, 1969.

Hamilton, R.M. and J.H. Healy (1969). Aftershocks of the
    Benham nuclear explosion, Bull. Seism. Soc. Am., 59, 2271-
    2281.

Harkrider, D.G. (1964). Surface waves in multilayered elastic
    media, 1, Rayleigh and Love waves from buried sources in
    a multilayered elastic halfspace, Bull. Seism. Soc. Am.,
    54, 627-680.

Honda, H. (1962). Earthquake mechanism and seismic waves,
    Geophys. Notes, 15, 1-97 (supplement).

Kachanov, L.M. (1961). On kinetics of crack growth, PMM,
    Zhurnal Prikladnoi Matematiki i Mekhaniki, Moskow, 25,
    498-502, (in Russian).

Kehrer, H.H. (1969). Radiation patterns of seismic surface
    waves from nuclear explosions, M.S. thesis, Massachusetts
    Institute of Technology, Cambridge, Massachusetts.

Kim, W.H. and C. Kisslinger (1967). Model investigations of
    explosions in prestressed media, Geophysics, 32, 633-651.

Kisslinger, C., E.J. Mateker, and T.V. McEvilly (1961). SH
    motion from explosions in soil, J. Geophys. Res., 66,
    3487-3496.

Kisslinger, C. and I.N. Gupta (1963). Studies of explosion-
    generated dilatational waves in two dimensional models,
    J. Geophys. Res., 68, 5197-5206.

Kromm, A. (1948). The propagation of elastic waves in plane
    discs with a curcular hole, Zeitschrift für angewandte
    Mathematik und Mechanik, 28, 104-114.

Liebowitz, H. (Ed.) (1968). Fracture, an advanced treatise,
    Vol. 1 and 2, Academic Press, New York.

Mansinha, L. (1964). The velocity of shear fracture, Bull.
Seism. Soc. Am., 54, 369-376.

McKeown, F.A. and D.D. Dickey (1969). Fault displacements
and motion related to nuclear explosions, Bull. Seism.
Soc. Am., 59, 2253-2269.

Molnar, P., K. Jocob, and L.R. Sykes (1969). Microearthquake
activity in eastern Nevada and Death Valley, California,
before and after the nuclear explosion Benham, Bull. Seism.
Soc. Am., 59, 2177-2184.

Perret, William R. (1968). Free field particle motion from a
nuclear explosion in slat, Part I, 257 p., VUF 3012, Sandia
Laboratory.

Press, F. and C.B. Archambeau (1962). Release of tectonic
strain by underground nuclear explosions, J. Geophys.
Res., 67, 337-343.

Savage, J.C. and L. Mansinha (1963). Radiation from a
tensile fracture, J. Geophys. Res., 68, 6345-6358.

Savin, G.N. (1966). Stress concentration around holes,
Pergamon Press, New York.

Schardin, H. (1959). Fracture (L. Auerbach, D.K. Fellbeck,
G.T. Hahn, and D.A. Thomas, Eds.), Wiley, New York.

Shand, E.B. (1961). Fracture velocity and fracture energy
of glass in the fatigue range, J. Am Ceram. Soc., 44,
21-26.

Smith, S.W. (1963). Generation of seismic waves by underground explosions and the collapse of cavities, J. Geophys. Res., 68, 1477-1483.

Smith, S.W., C.B. Archambeau, and W. Gile (1969). Transient and residual strains from large underground explosions, Bull. Seism. Soc. Am., 59, 2185-2196.

Stroh, A.N. (1957). A theory of the fracture of metals, Advan. Phys., 6, 418-465.

Tetelman, A.S. and A.J. McEvilly, Jr. (1967). Fracture of structural materials, Wiley, New York.

Thomson, K.C., T.J. Ahrens, and M.N. Toksöz (1969). Dynamic Photoelastic studies of P and S wave propagation in pre-stressed media, Geophysics, 34, 696-712.

Toksöz, M.N. (1967). Radiation of seismic surface waves from underground explosions, Proceedings of the Vesiac Conference on the current status and future prognosis of shallow seismic events, VESIAC Rept., Willow Run Laboratories, The University of Michigan, 65-84.

Toksöz, M.N. and K. Clermont (1967). Radiation of seismic waves from the Bilby explosion, Teledyne, SDL technical report 183, prepared for AFTAC.

Toksöz, M.N., A. Ben-Menahem, and D.G. Harkrider (1964). Determination of source parameters by amplitude equalization of seismic surface waves, 1. Underground nuclear explosions, J. Geophys. Res., 69, 4355-4366.

Toksöz, M.N., D.G. Harkrider, and A. Ben-Menahem (1965).
Determination of source parameters by amplitude equali-
zation of seismic surface waves, 2. Release of tectonic
strain by underground nuclear explosions and mechanisms
of earthquakes, J. Geophys. Res., 70, 907-922.

Toksöz, M.N., H. Kehrer, and R. Ward (1971). Source pro-
perties of NTS explosions (in preparation).

Wistor, J.W., J.A. Beeler, and G.J. Hansen (1963). Long-
period displacement gages: close-in phenomena of buried
explosions, Final Rept. SC-4907(RR), Sandia Corp.,
Albuquerque, 57-82.

Yoffe, E.H. (1951). The moving Griffith crack, Phil. Mag.,
42, 739-750.

Zvolinskii, N.V. (1960). On the emission of an elastic wave
from a spherical explosion in the ground, Soviet J. App.
Math. Mech., 24, 166-176.

FIGURE CAPTIONS

Fig. 1. Long period seismograms of the Bilby explosion at two
LRSM stations: CP-CL (Campo, California, Δ=482 km) and
FR-MA (Forsyth, Montana, Δ=1282 km). Time marks are
10 seconds apart. Z indicates vertical, R and T the
horizontal components, respectively. Numbers are
relative magnification of each component. Note the
absence of Love waves at FR-MA.

Fig. 2. Love and Rayleigh waves from the explosion Greeley,
recorded at Kansas City, Missouri. Z, H are vertical
and horizontal components, respectively.

Fig. 3. Distribution of LRSM stations which recorded waves from
Bilby in North America. "Star" indicates shot location.

Fig. 4. The radiation pattern of normalized Rayleigh waves for
Bilby. The points are the ratio of the amplitudes of
explosion-generated to collapse-generated Rayleigh
waves. The curve is the theoretical radiation pattern
for a composite source consisting of an explosion and
an orthogonal double-couple.

Fig. 5. Rayleigh wave amplitude response of the layered medium
to an explosive source near the surface, with impulsive
time function.

Fig. 6. Love wave amplitude response of the medium to a double-
couple source near the surface.

Fig. 7. Love wave to Rayleigh wave vertical component Fourier
amplitude spectral ratio at four stations. Dashed lines
are the ratios of peak amplitudes measured in time domain.

Fig. 8. Amplitude ratios of the explosion-generated Love and Rayleigh waves (U_θ/U_{Rz}) as a function of azimuth. The theoretical curve is for the composite source described in Fig. 4.

Fig. 9. Rayleigh wave pulses at two stations plotted from digitized data.

Fig. 10. Fourier amplitude spectra of the Rayleigh wave pulses shown in Fig. 9.

Fig. 11. Ground displacement spectra obtained from those of Fig. 10 after correction for instrument response.

Fig. 12. Amplitude spectra of source time function after correction for propagation effects. Circles indicate data uncorrected for attenuation; triangles indicate the data corrected taking $Q = 100$.

Fig. 13. The Rayleigh wave source time function for Bilby at the boundary of the seismic zone where strains are infinitesimal.

Fig. 14. Amplitude spectra of source time function for Love waves after correction for propagation effects. Circles are uncorrected; triangles are corrected for attenuation taking $Q = 100$.

Fig. 15. Laboratory set-up for one-dimensional experiment. Stress waves from an explosive source in a rod under torsion are recorded by strain gauges.

Fig. 16. Strain gauge seismograms from one-dimensional experiment at different pre-stress values.

Fig. 17. Amplitudes of P and S waves as a function of pre-strain.

Fig. 18. Experimental set-up for the two-dimensional dynamic photoelastic studies of explosive sources in pre-stressed media.

Fig. 19. Isochromatics and isoclinics from a shot in unstressed $\frac{1}{16}$" thick plexiglas. Interframe time 4.16 μsec.

Fig. 20. Theoretical isochromatics and isoclinics for P and S waves.

Fig. 21. Theoretical pulse shapes as a function of distance for radial stress and displacement and maximum shear stress, from a cylindrical source in a plate. r is distance in units of source radius.

Fig. 22. Isochromatics and isoclinics from a shot in a $\frac{1}{3}$" thick glass plate stressed under tension (45 bars). Interframe time 2.08 μsec. Note the growth of cracking.

Fig. 23. Dynamic radiation patterns of P and S waves from explosive sources in pre-stressed plexiglas and glass plates under tension, as measured by strain gauges.

Fig. 24. Maximum strain energy ratios of P and S waves versus azimuth from tensile axis.

Fig. 25. Theoretical P and S wave radiation patterns from a tensile fault plus explosion in glass. Each curve individually normalized to its extreme value. α, β are compressional and shear velocities in the plate. c = crack propagation velocity. U_p/U_{pc} is the ratio of the strength of the isotropic component to tensile crack component.

Fig. 26. Shift of the maxima of theoretical radiation patterns of P and S waves as a function of crack velocity for a tensile crack.

Fig. 27. Immediate source region of an explosive source in $\frac{1}{8}''$ thick pyrex plate glass, showing dynamic cracking and isochromatic fringe pattern. Picture taken 12 μsec after detonation. Exposure time is 0.1 μsec.

Fig. 28. Dynamic photoelastic isoclinic and isochromatic patterns produced by radial explosive source in $\frac{1}{8}''$ thick pyrex glass plate. Tensional prestress in vertical direction of 45 bars is applied to plate. Polarizer and analyzer polarization axes are at 45° and 135° with respect to horizontal. Effective exposure time for each frame, 0.25 μsec. a,b,c, and d frames taken at 26.0, 42.7, 53.1, and 55.2 μsec after expansion of explosive source.

TABLE 1

List of explosions and relative strength
of double couple components.

EXPLOSION	DATE	REGION	MEDIUM	D.C. STRENGTH (T=20 sec).	FAULT AZI.
HARDHAT	2-15-62	Yucca Flat (n. end)	Granite	3.00	330°
SHOAL	12-26-63	Fallon, Nevada	Granite	.90	346°
CHARTREUSE	5- 6-66	Pahute Mesa	Rhyolite	.94	353°
HALF BEAK	6-30-66	Pahute Mesa	Rhyolite Zeolitized	.67	345°
BENHAM	12-19-68	Pahute Mesa	Tuff	.85	345°
CORDUROY	12- 3-65	Yucca Flat	Quarzite	.72	347°
CUP	3-26-65	Yucca Flat	Tuff	.55	200°
BILBY	9-13-63	Yucca Flat	Tuff	.47	340°
TAN	6- 3-66	Yucca Flat	Tuff	.39	340°
HAYMAKER	6-27-62	Yucca Flat	Alluvium	.33	340°
SEDAN	7- 6-62	Yucca Flat	Alluvium	0	--
SALMON	10-22-64	Hattiesburg, Miss.	Salt	0	--
GNOME	12-10-61	Carlsbad, New Mexico	Salt	0	--

TABLE 2

Observed S-wave and calculated maximum available energies
for explosions in pre-stressed plexiglas and glass plates.

Shot No.	Medium	Tensile pre-stress (bars)	Observed S-wave energy	Maximum available strain energy a = 1 cm
13028	Plexiglas	163	49.3×10^5	2.84×10^5
13029	Plexiglas	163 (?)	3.72×10^5	2.84×10^5
13030	Glass	114	0.73×10^5	0.16×10^5
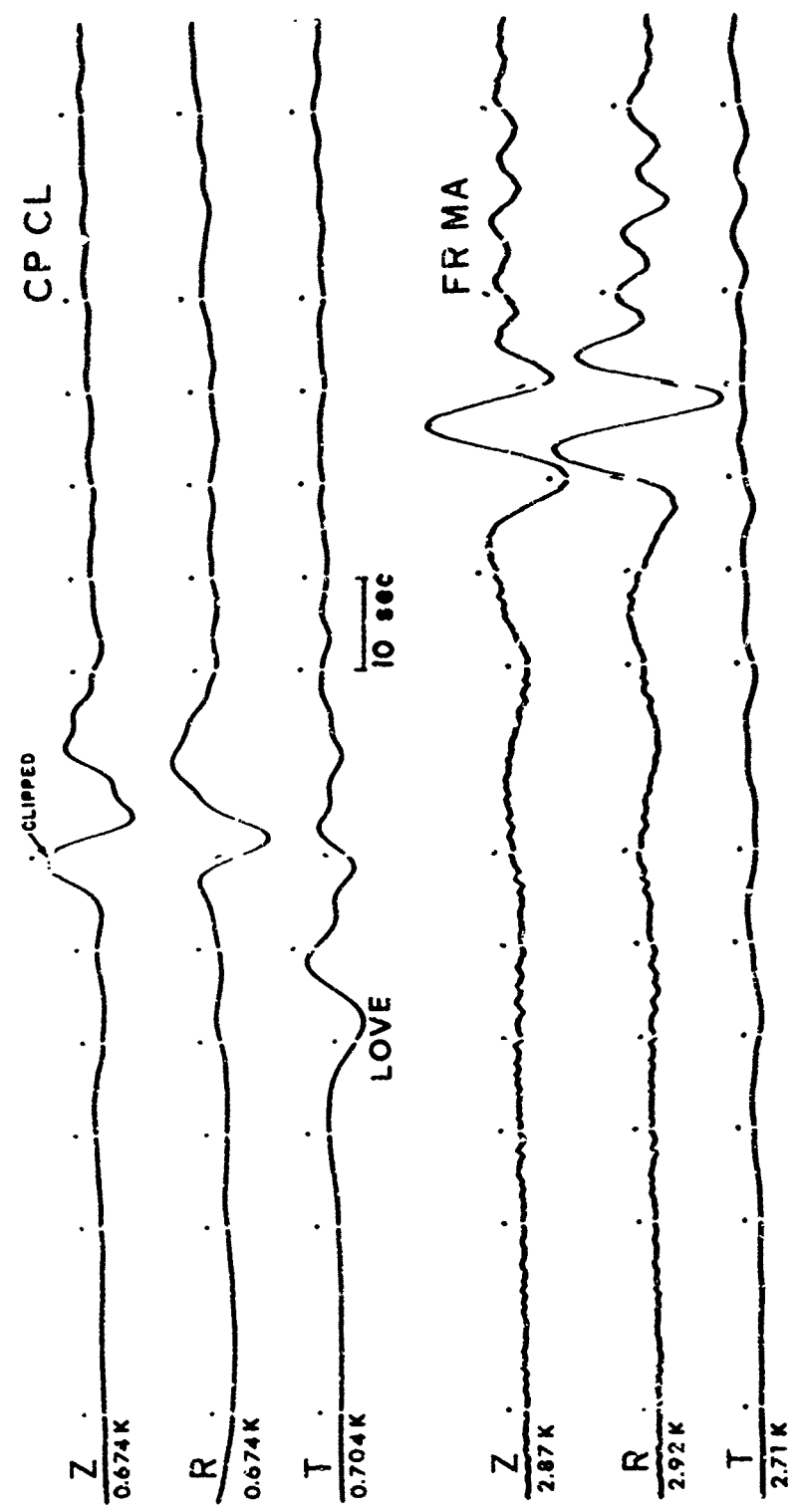
Fig. 1
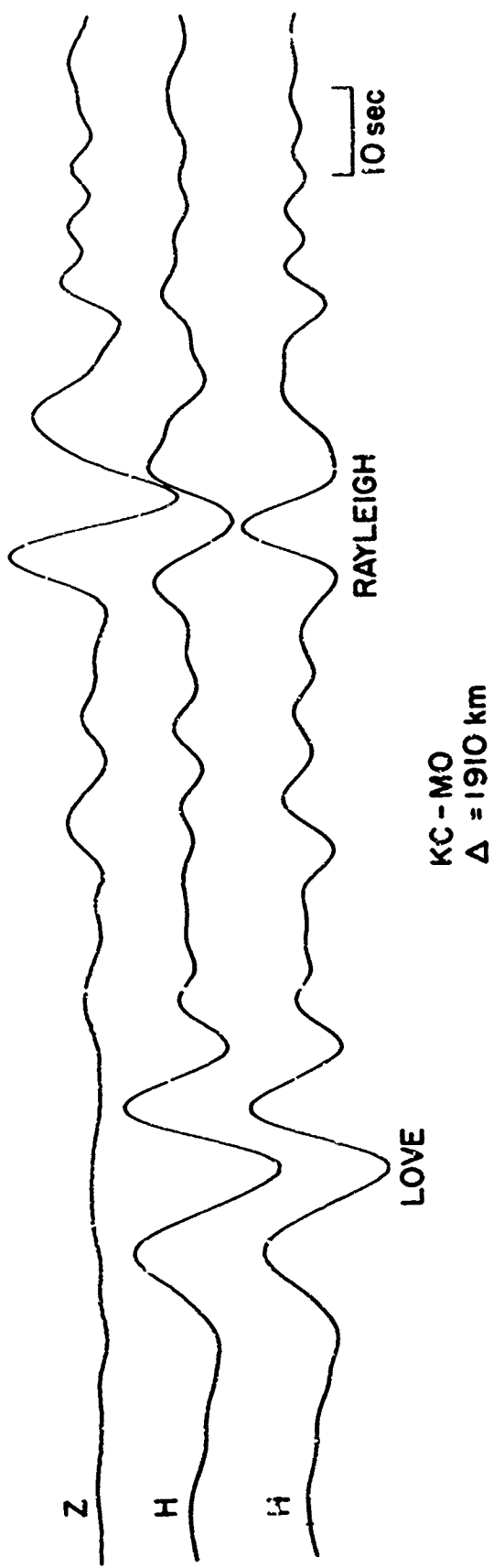
Fig. 2
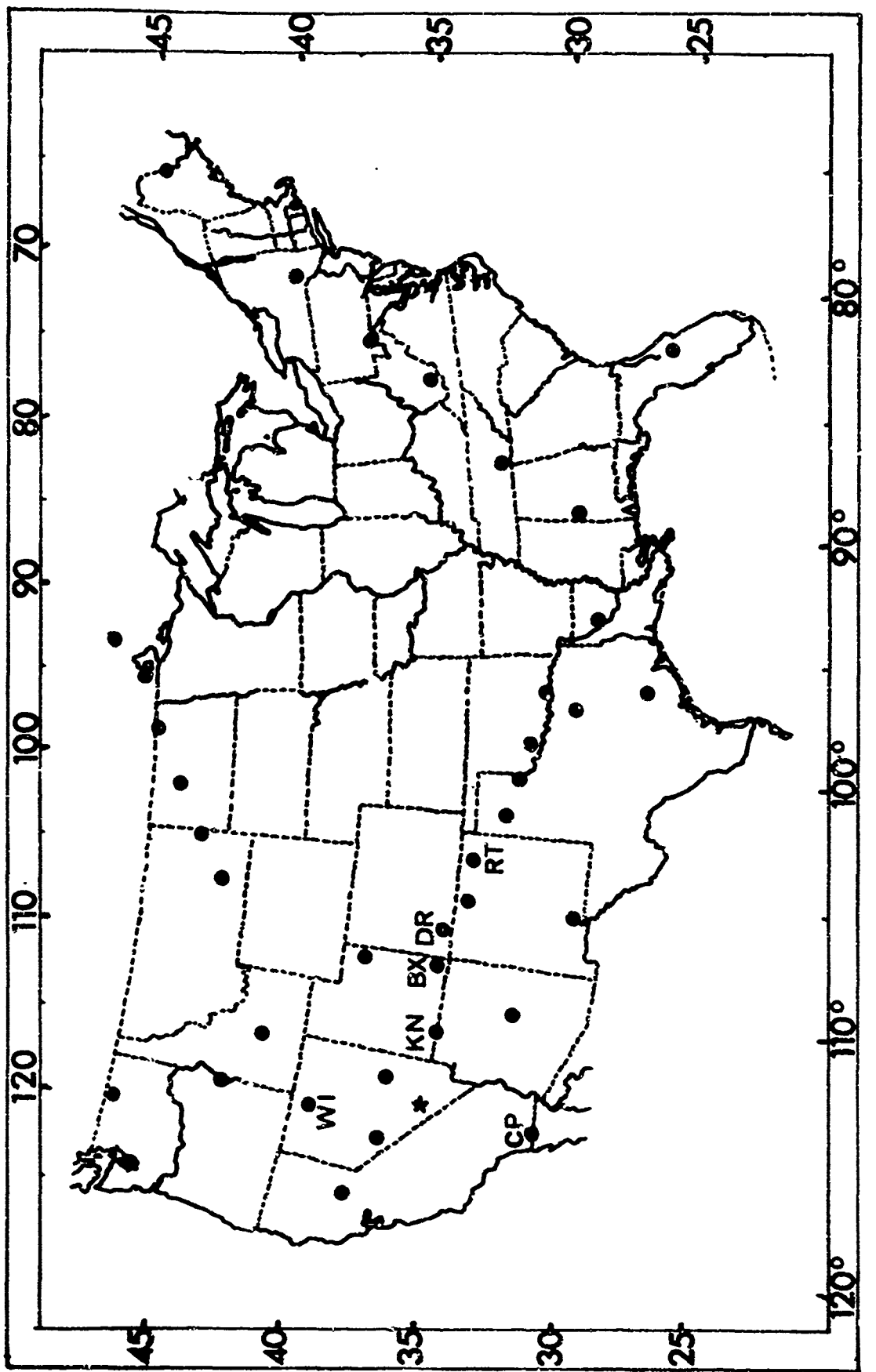
Fig. 3
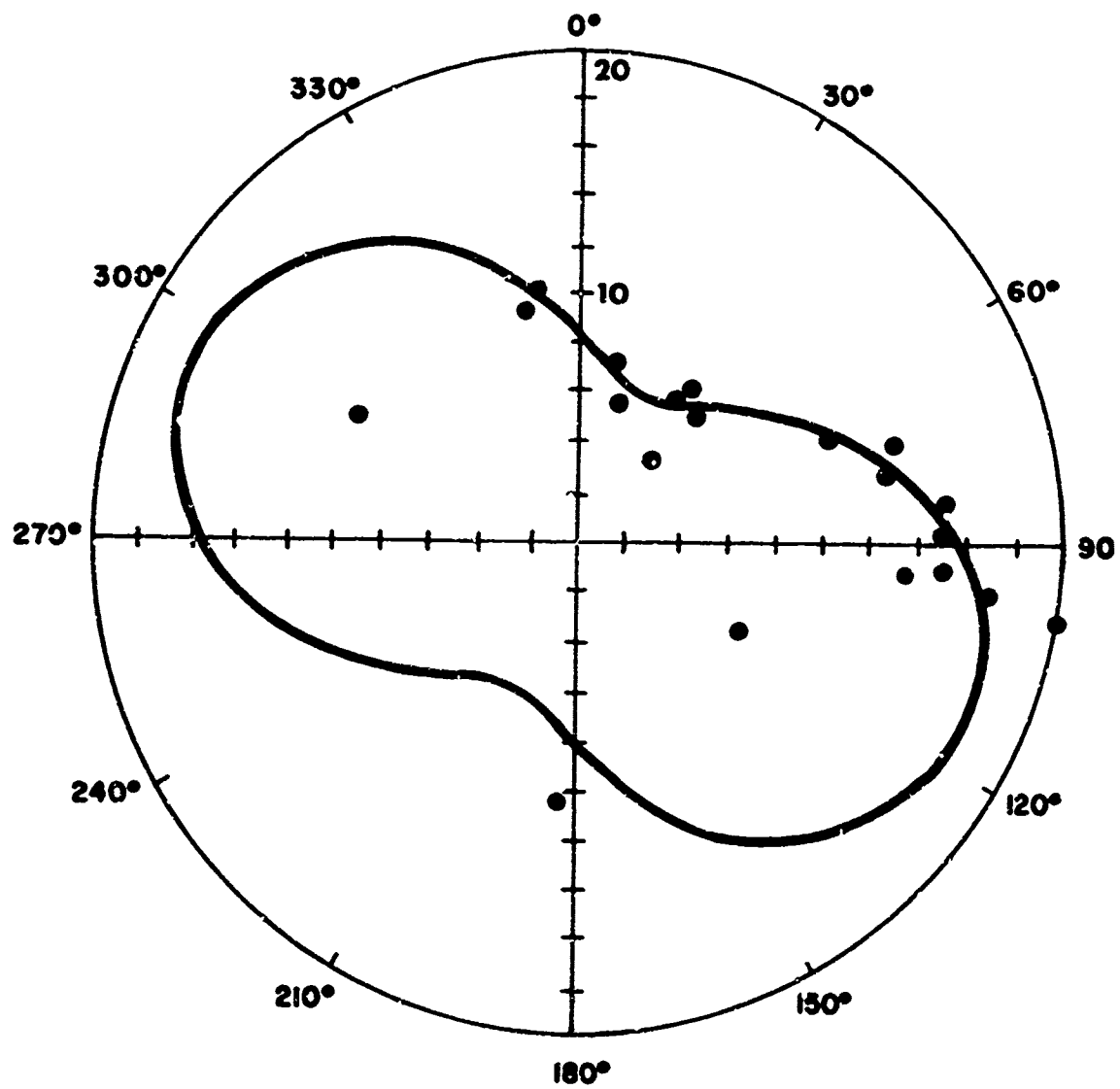
Fig. 4
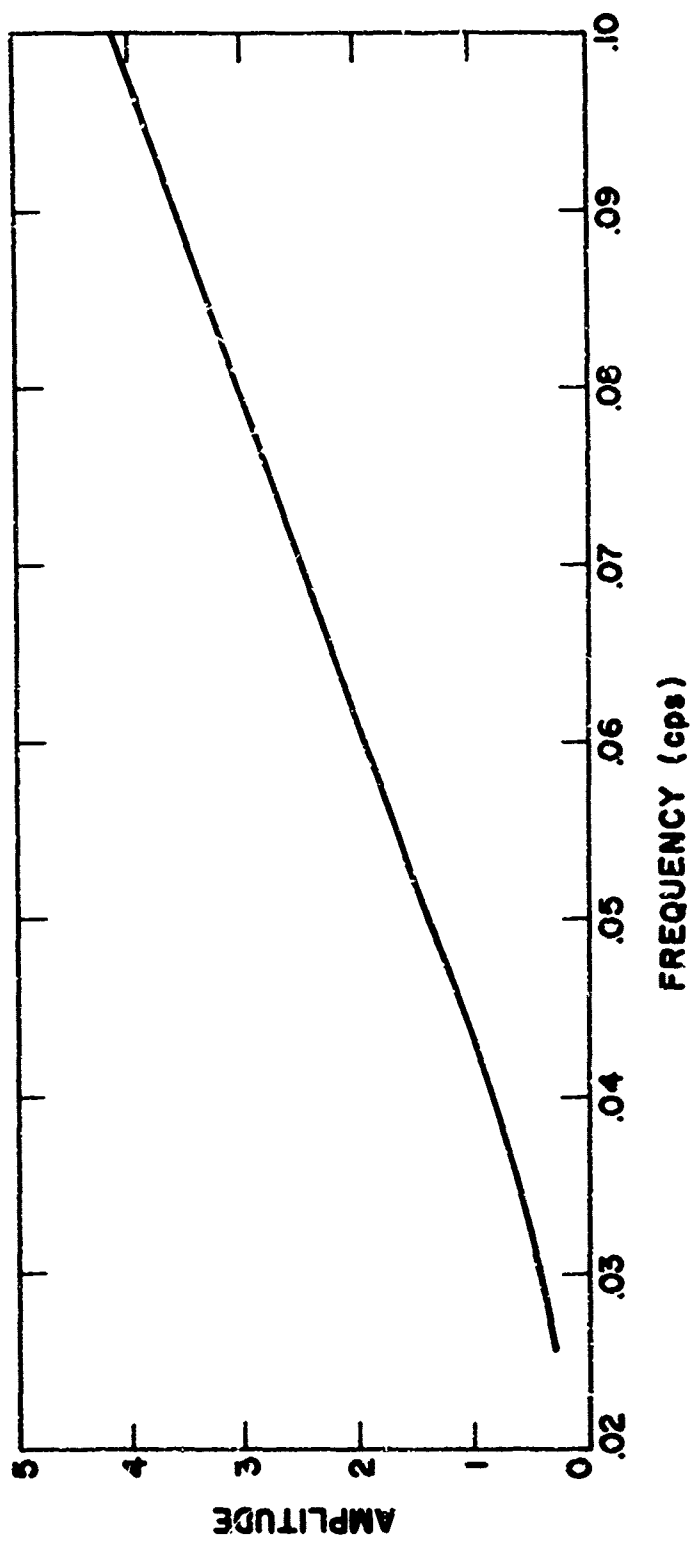
Fig. 5
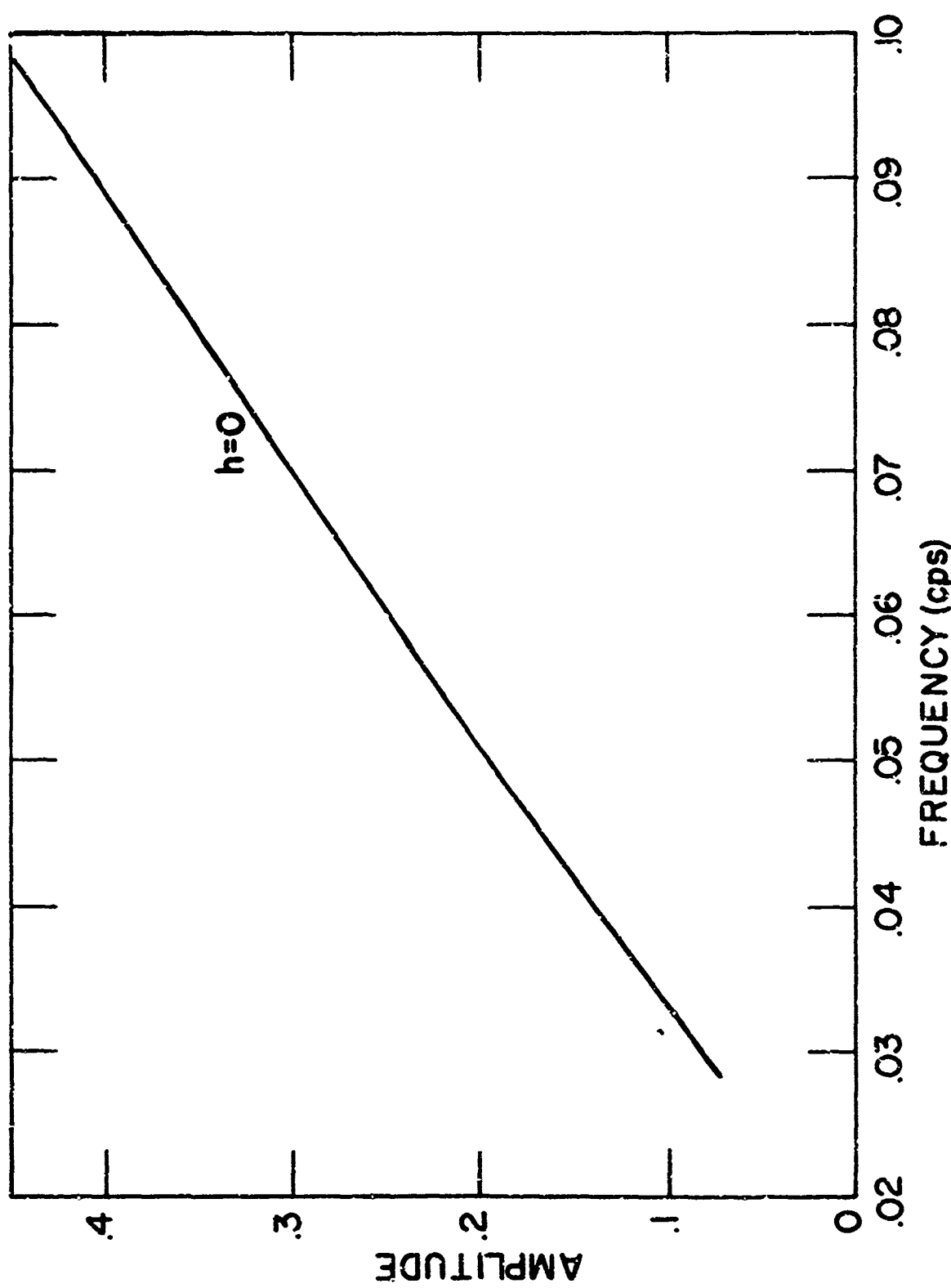
Fig. 6
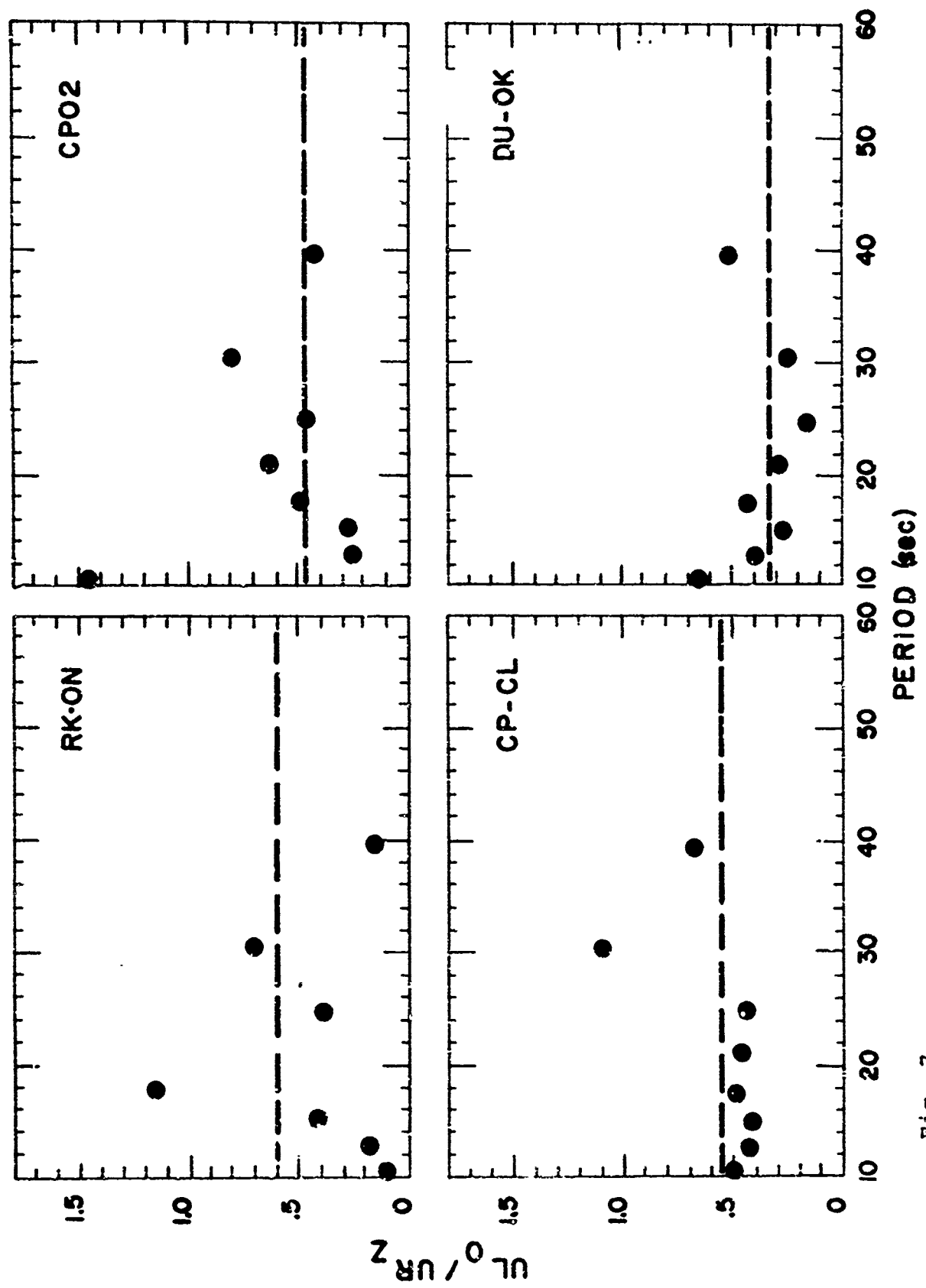
Fig. 7

Fig. 8

Fig. 9

Fig. 11

Fig. 12

Fig. 13

Fig. 14

Fig. 15

Prestrain: zero
Gain: 40 db
P   S
Δ = 55 cm

Prestrain: 0.0004
Gain: 40 db
P   S
Δ = 60 cm

Prestrain: 0.002
Gain: 50 db
S
P
Δ = 60 cm

Prestrain: 0.005
Gain: 45 db
S
P
Δ = 45 cm

100 μ sec

Fig. 16

89-248

Fig. 27

89 - 245

Fig. 18

SMOKE

COMPRESSIVE P PHASE

DILATIONAL P PHASE

P WAVE
ISOCLINIC

ZERO ORDER ISOCHROMATICS

S WAVE
ISOCLINIC

Fig. 19

T = 0.5   T = 2.0
T = 1.0   T = 2.5
T = 1.5   T = 3.0
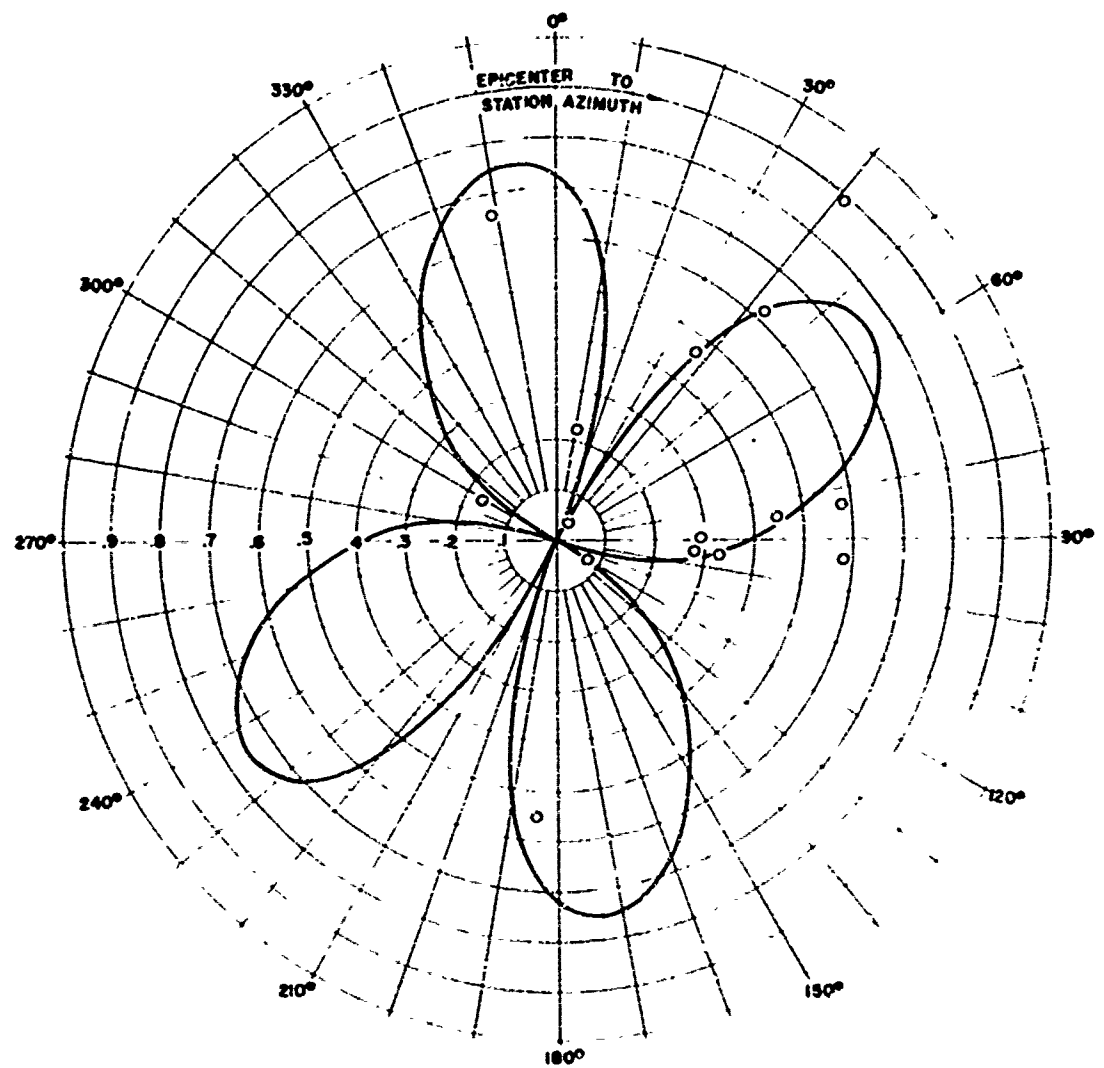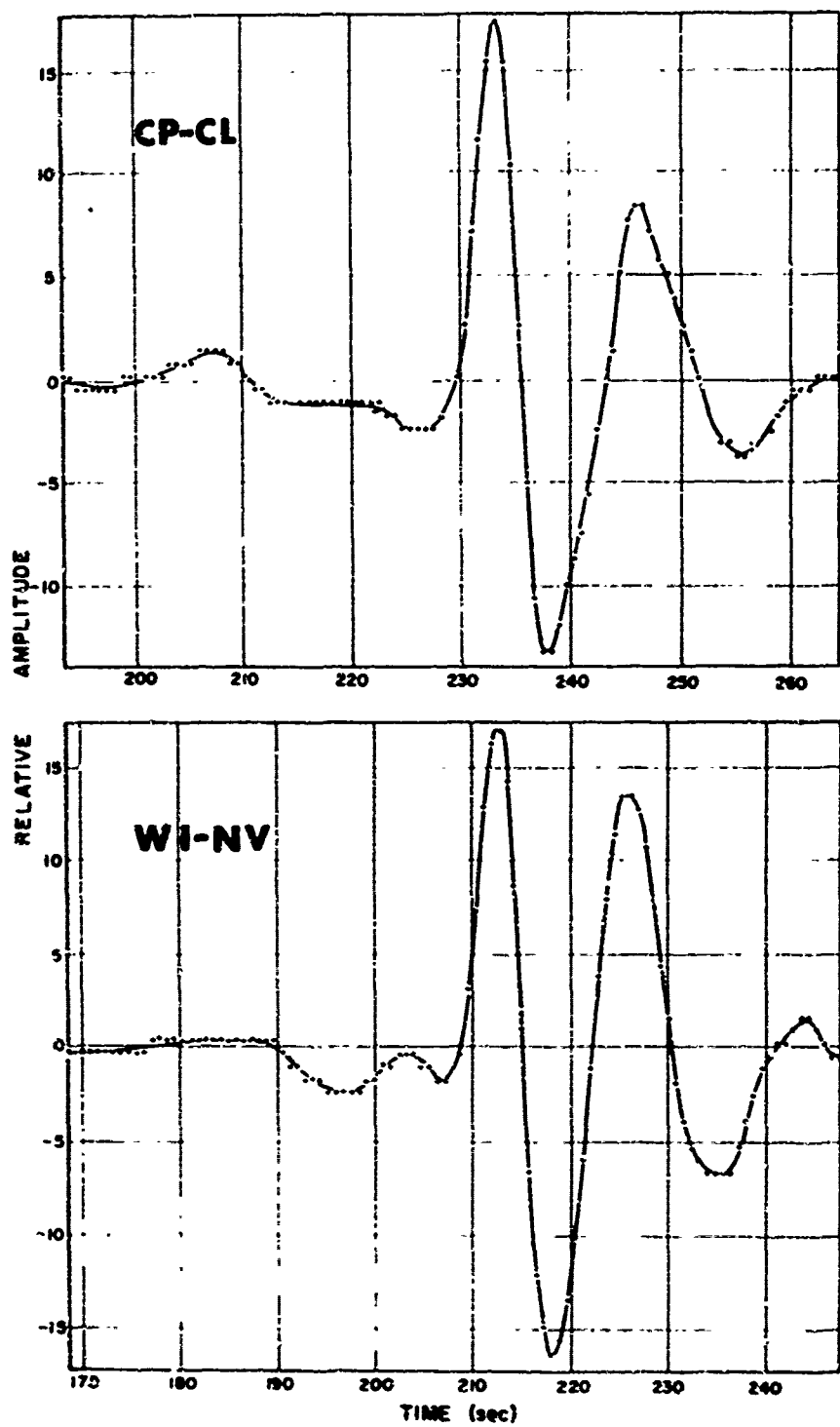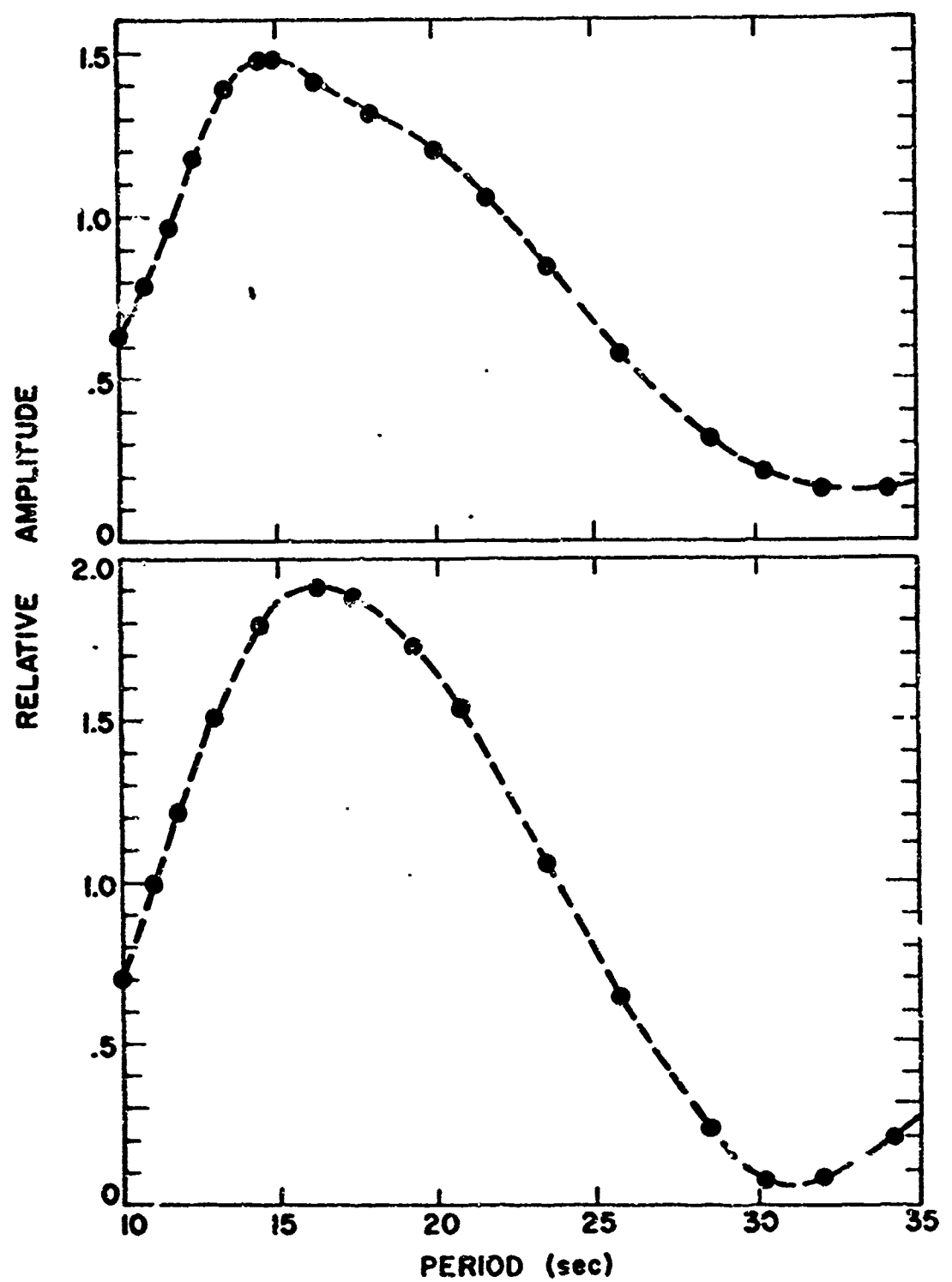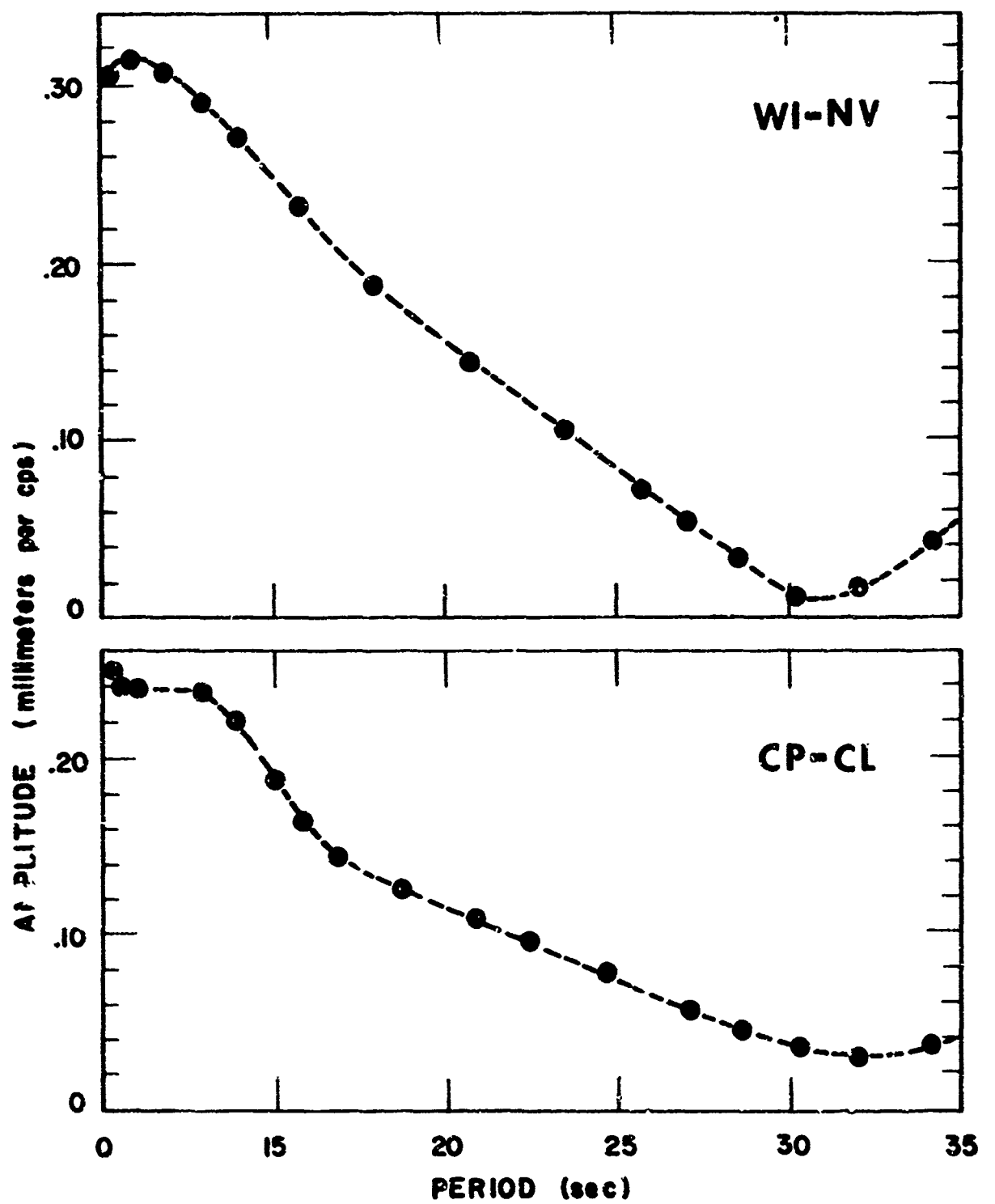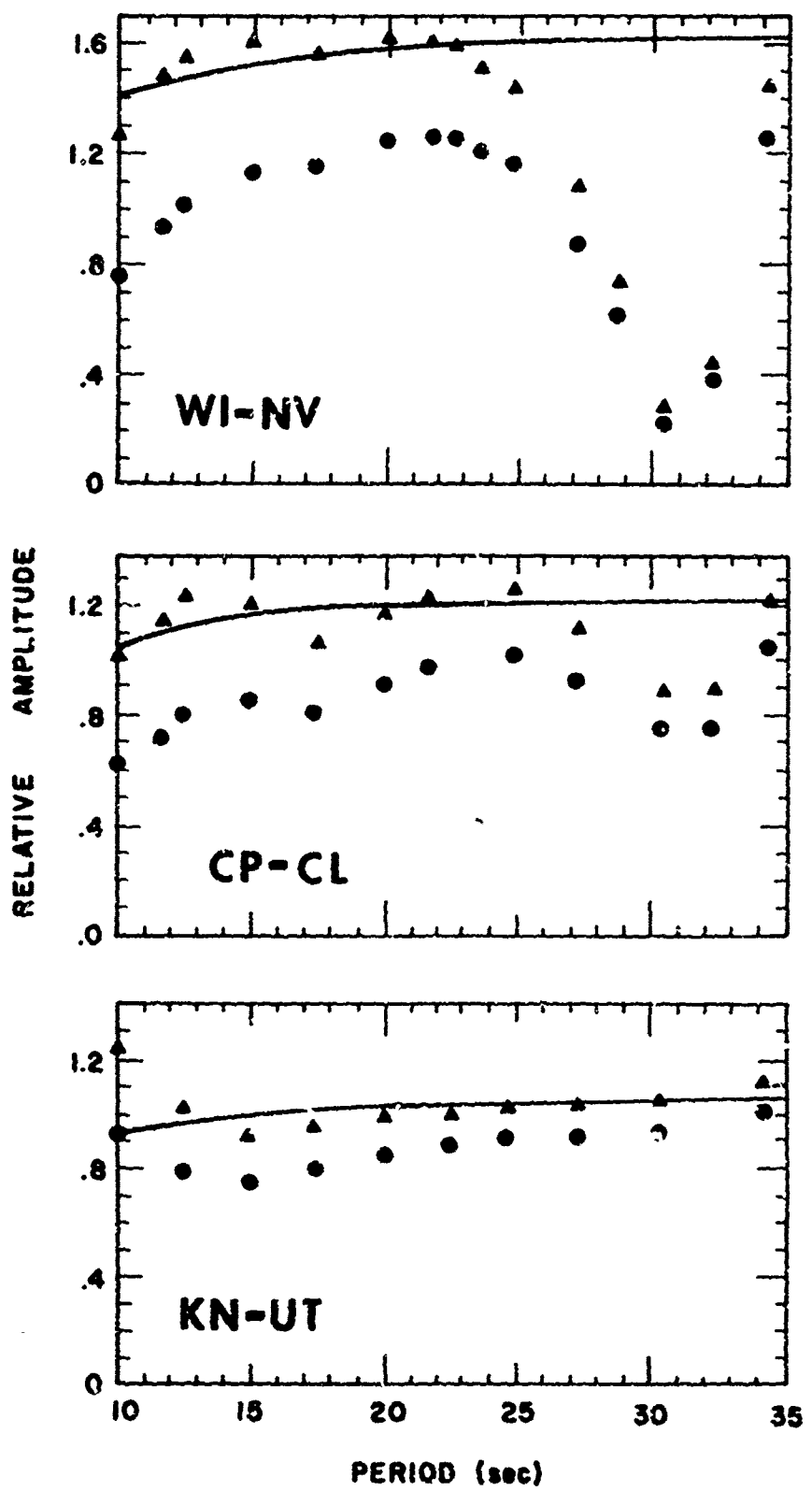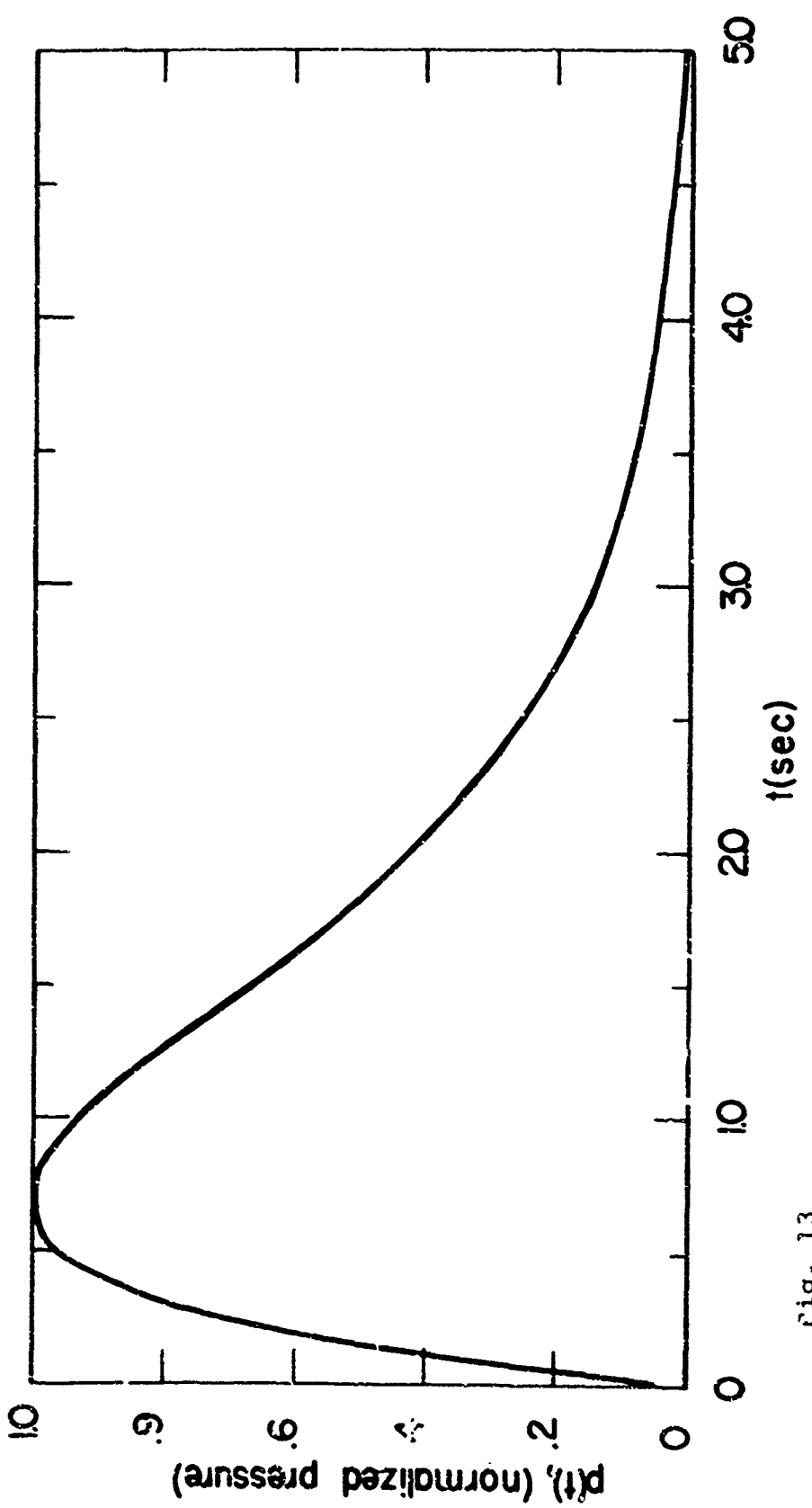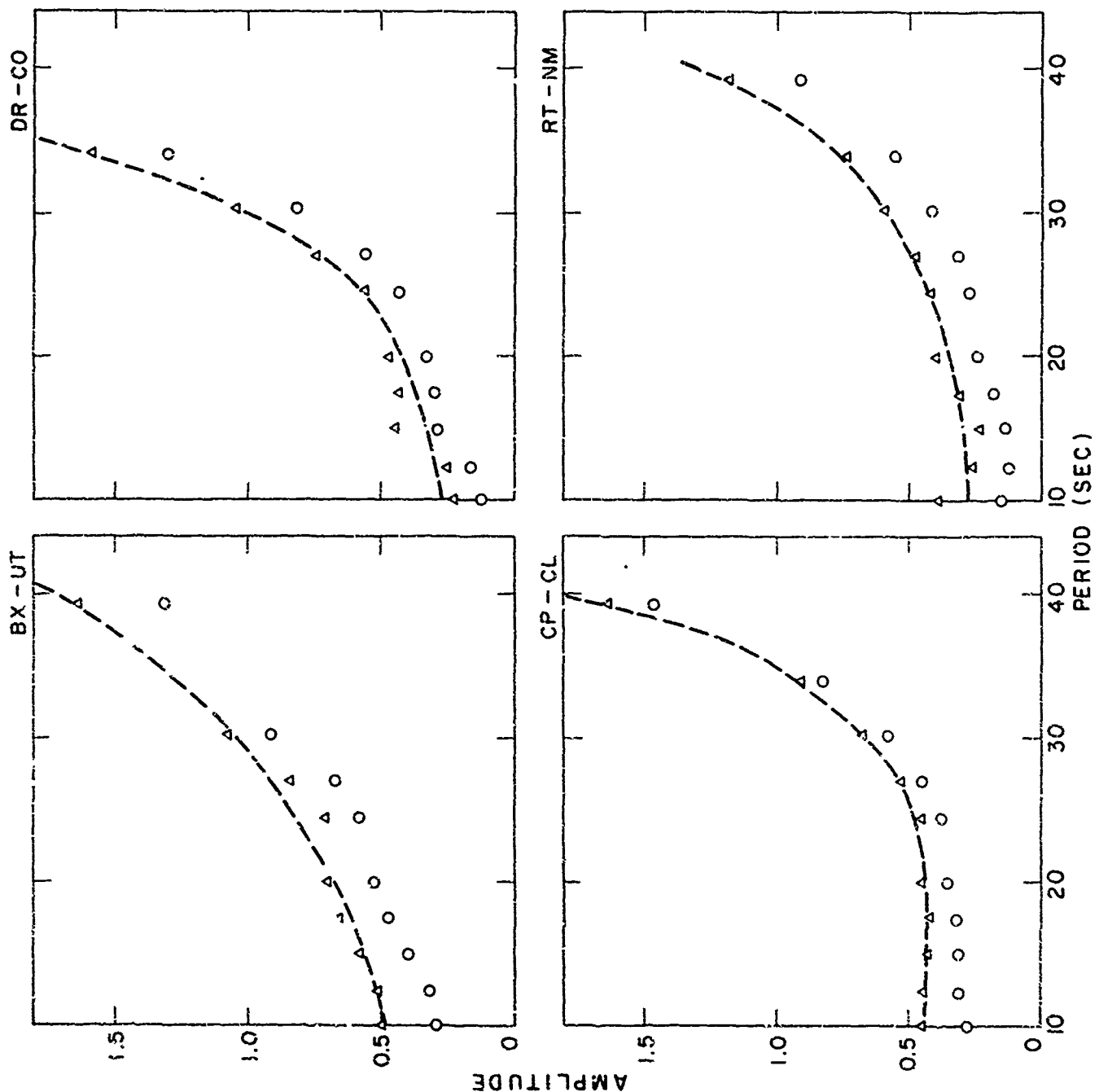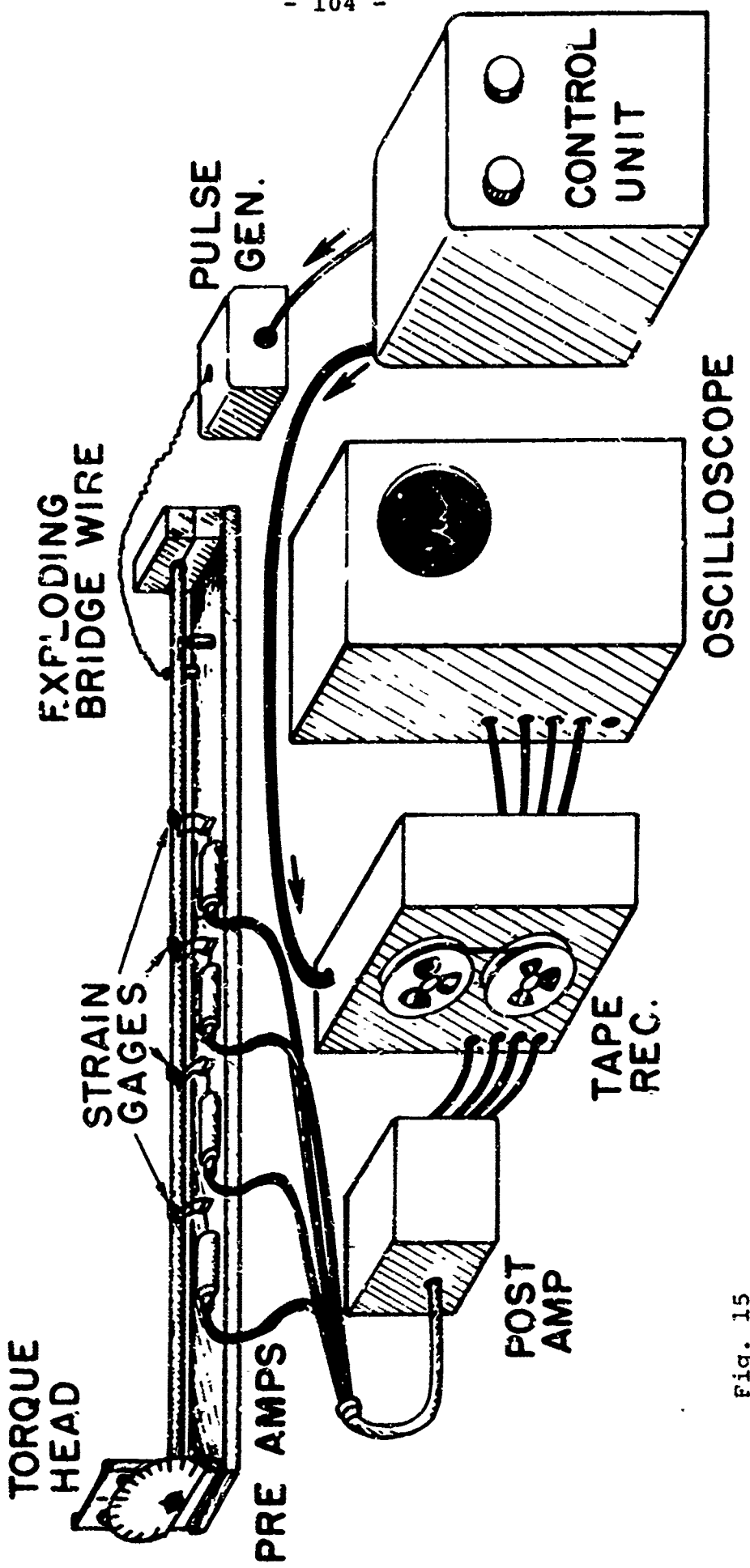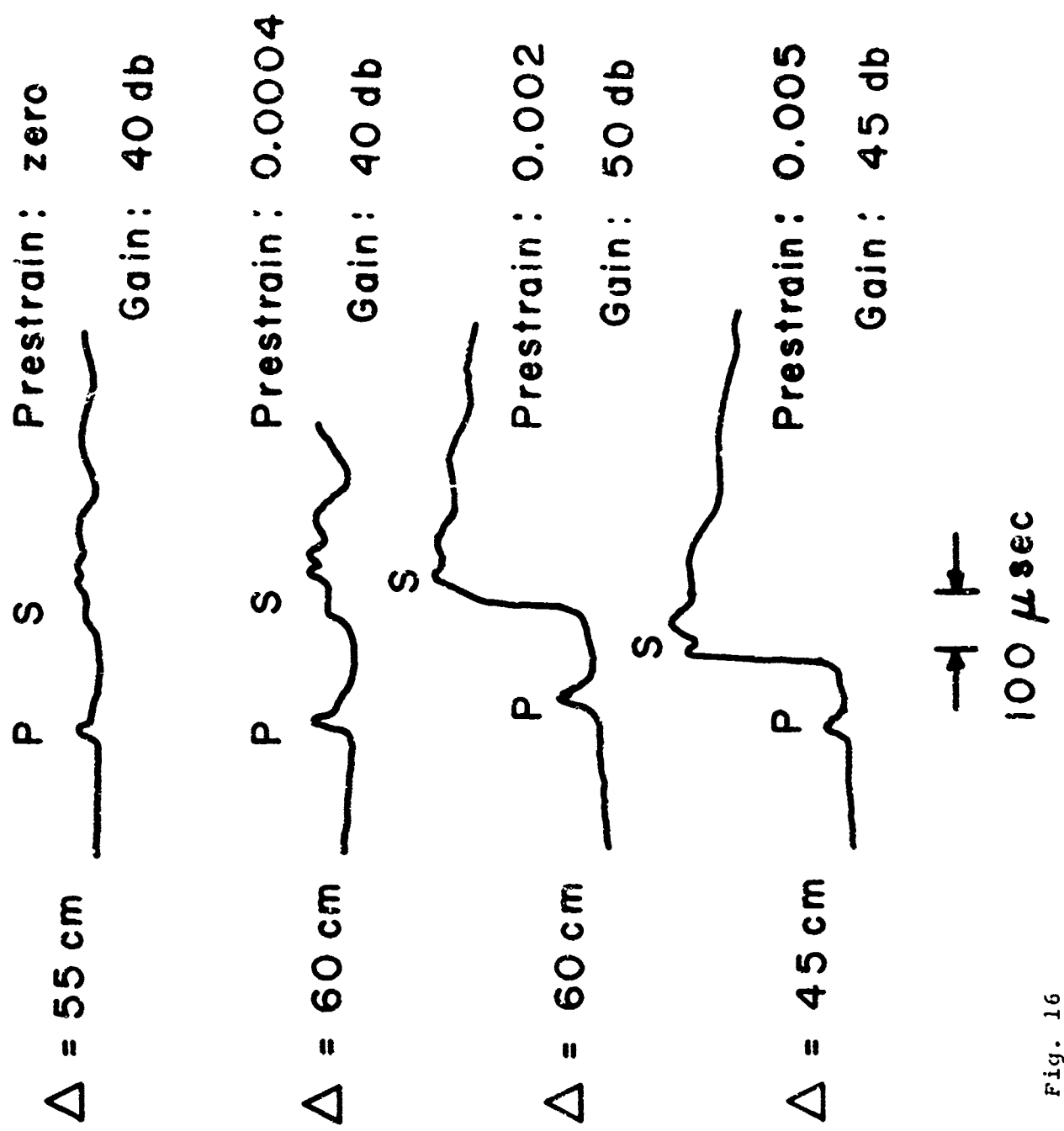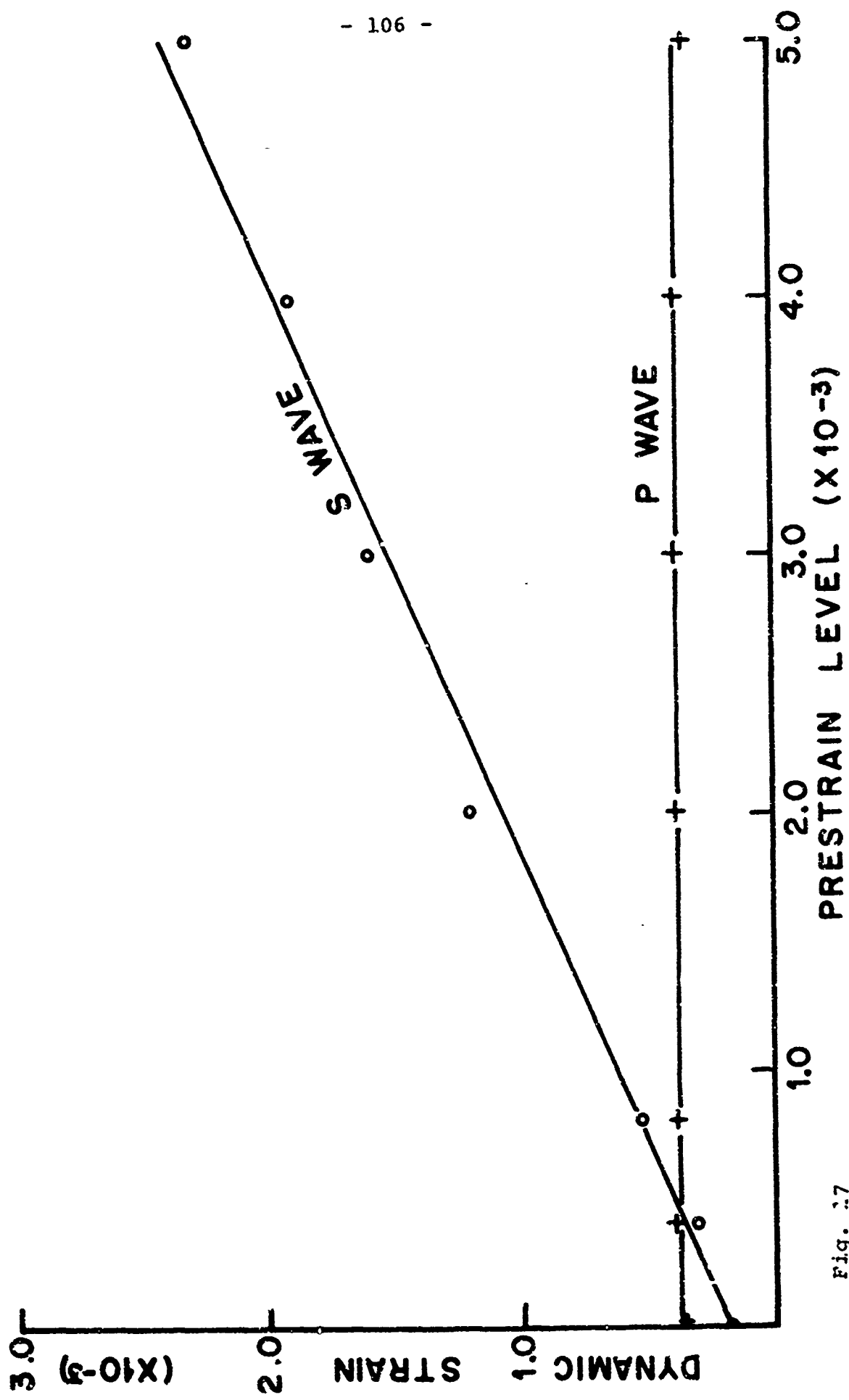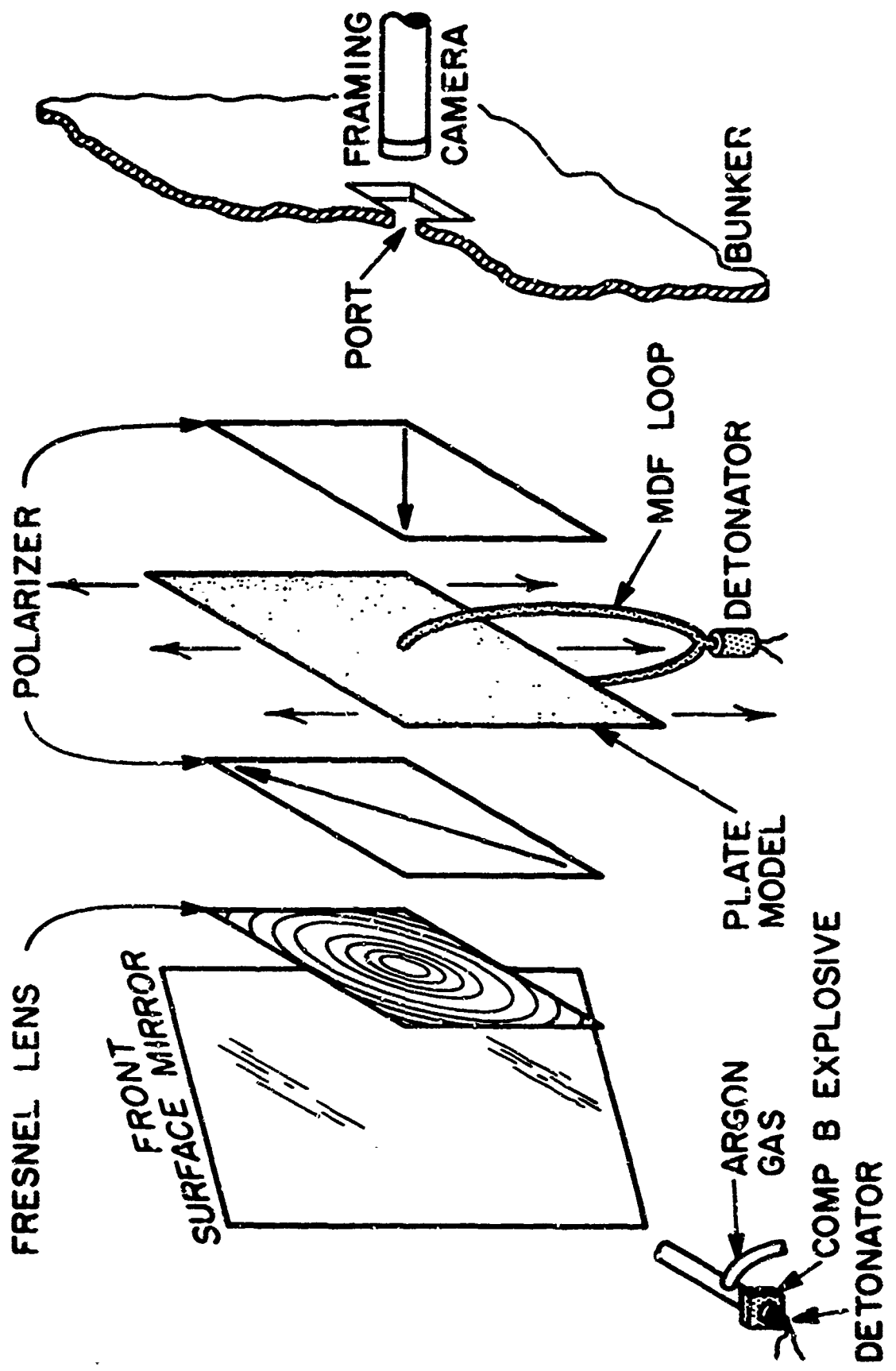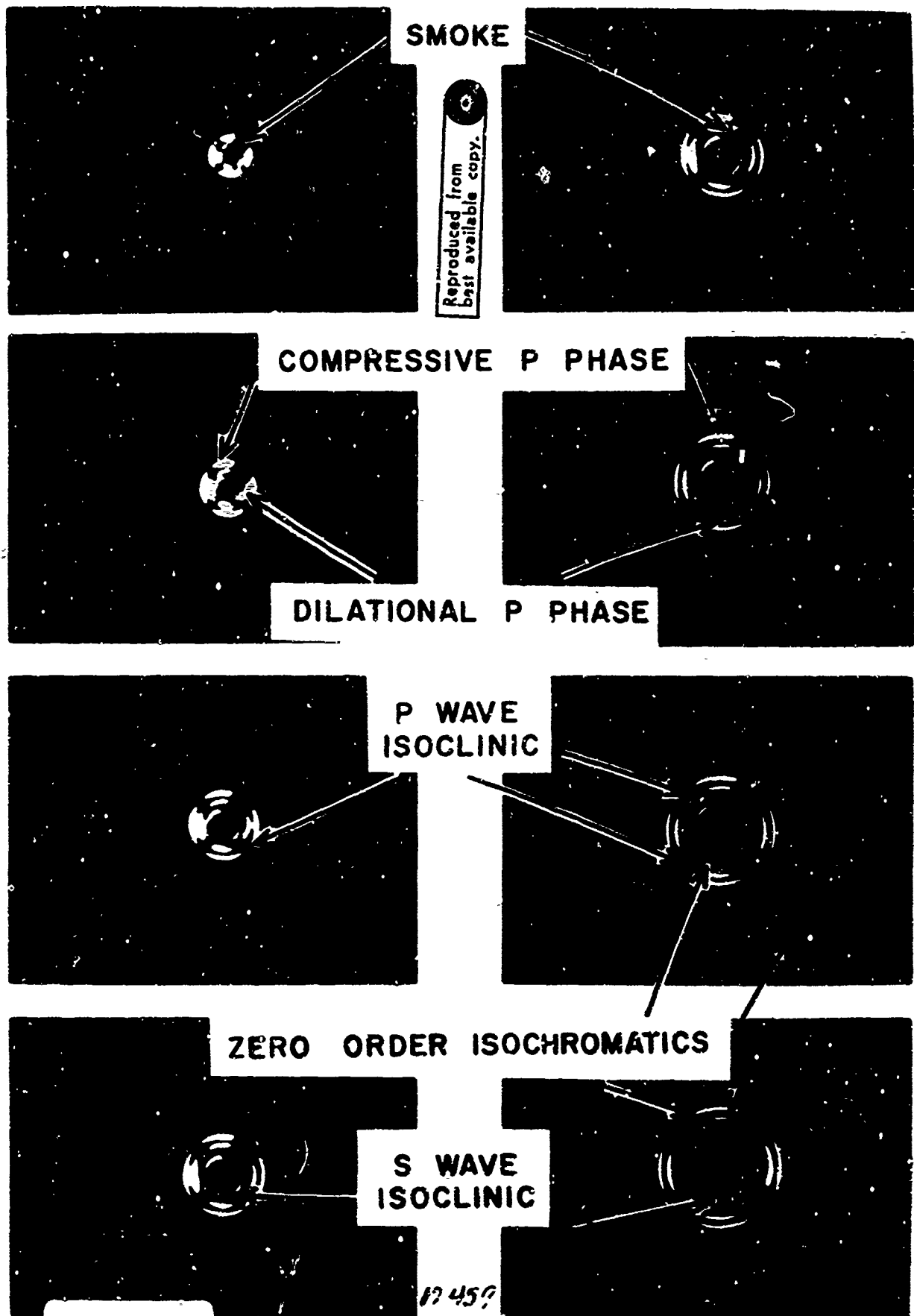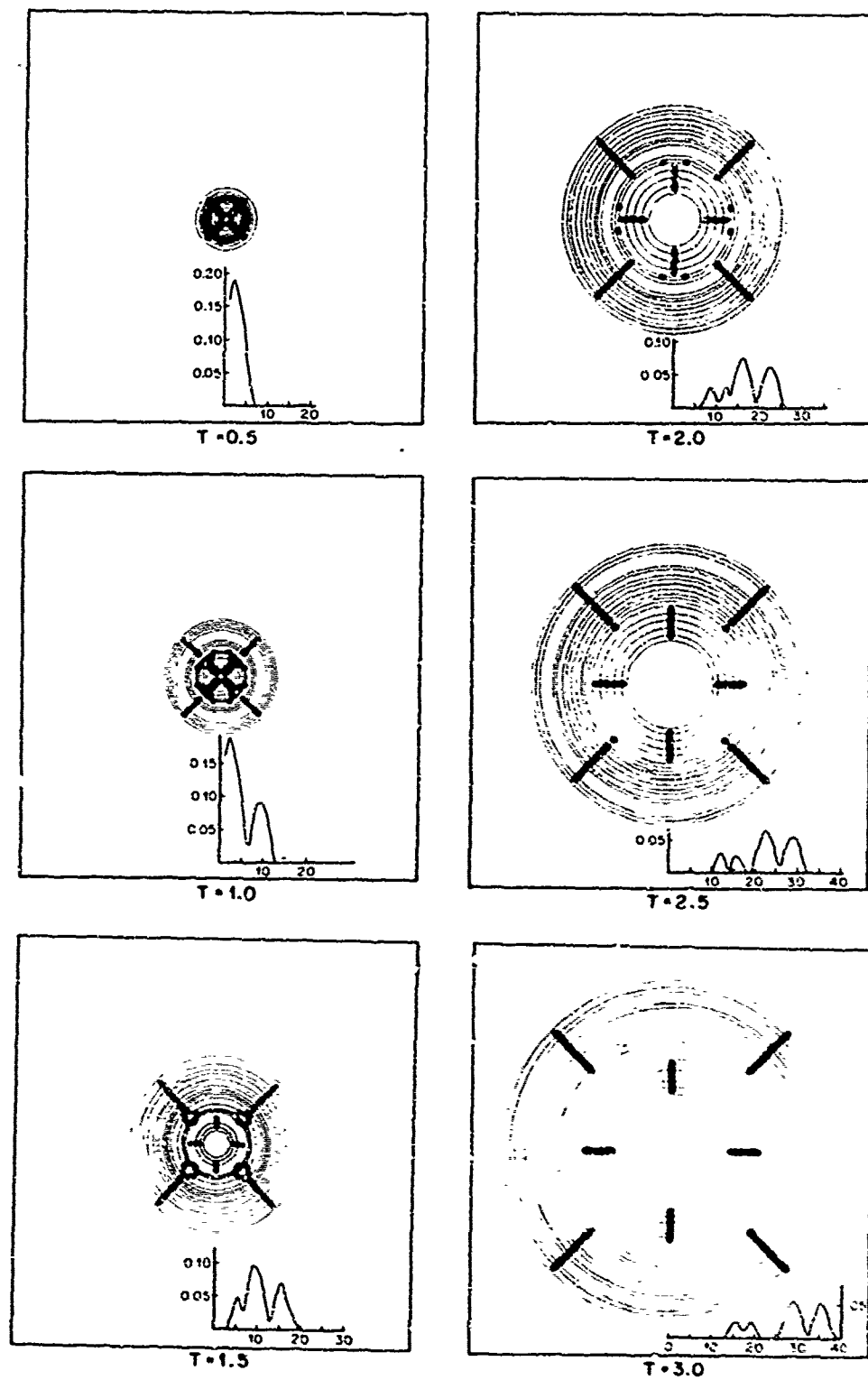
Fig. 20
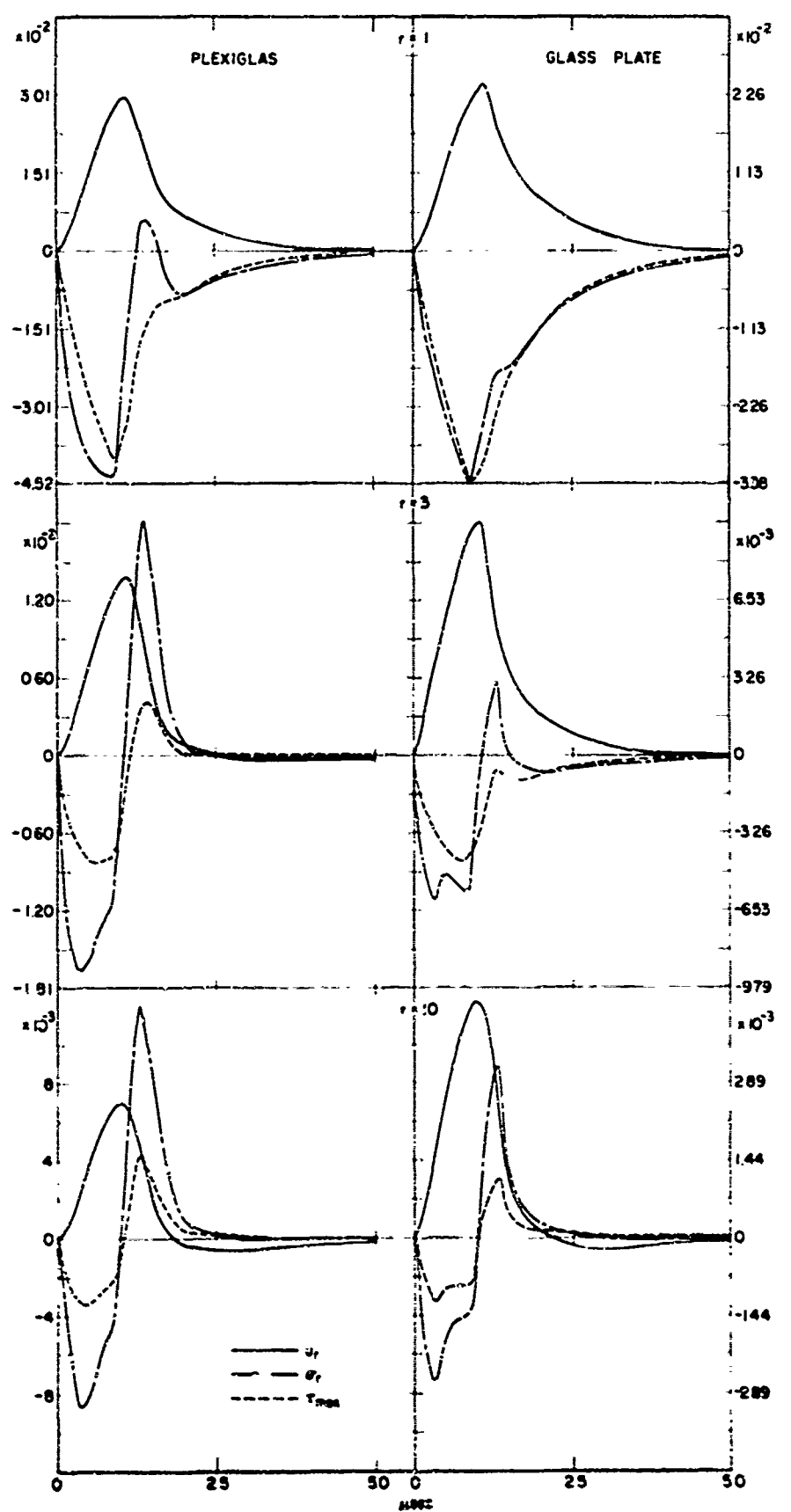
Fig. 21
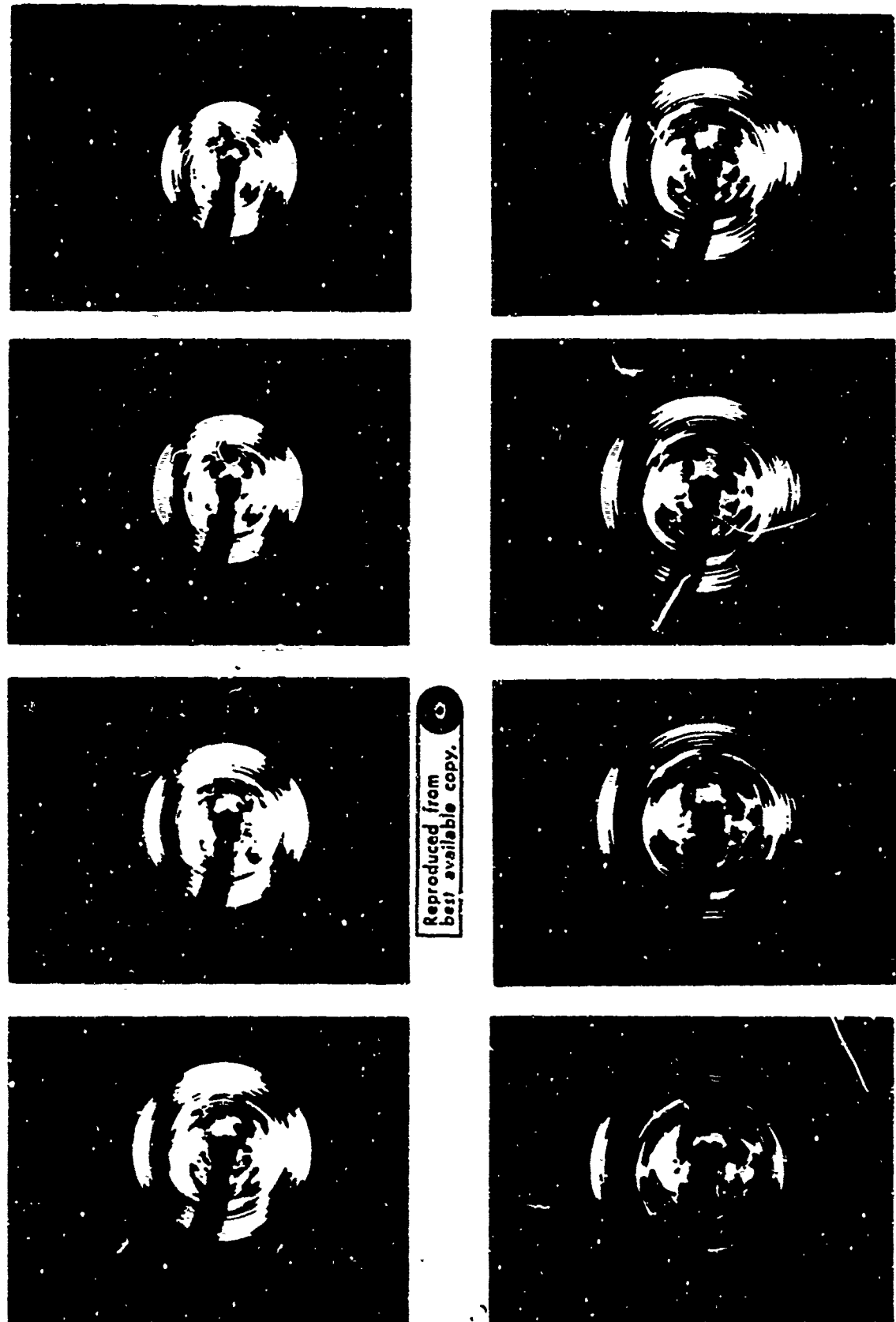
Fig. 22

Fig. 23

Fig. 24

$$\alpha = 1.852\beta$$

$C = .200\beta$ $C = .600\beta$

$\dfrac{(U_P)_I}{(U_P)_C} = 2.0$

$\dfrac{(U_P)_I}{(U_P)_C} = 1.0$
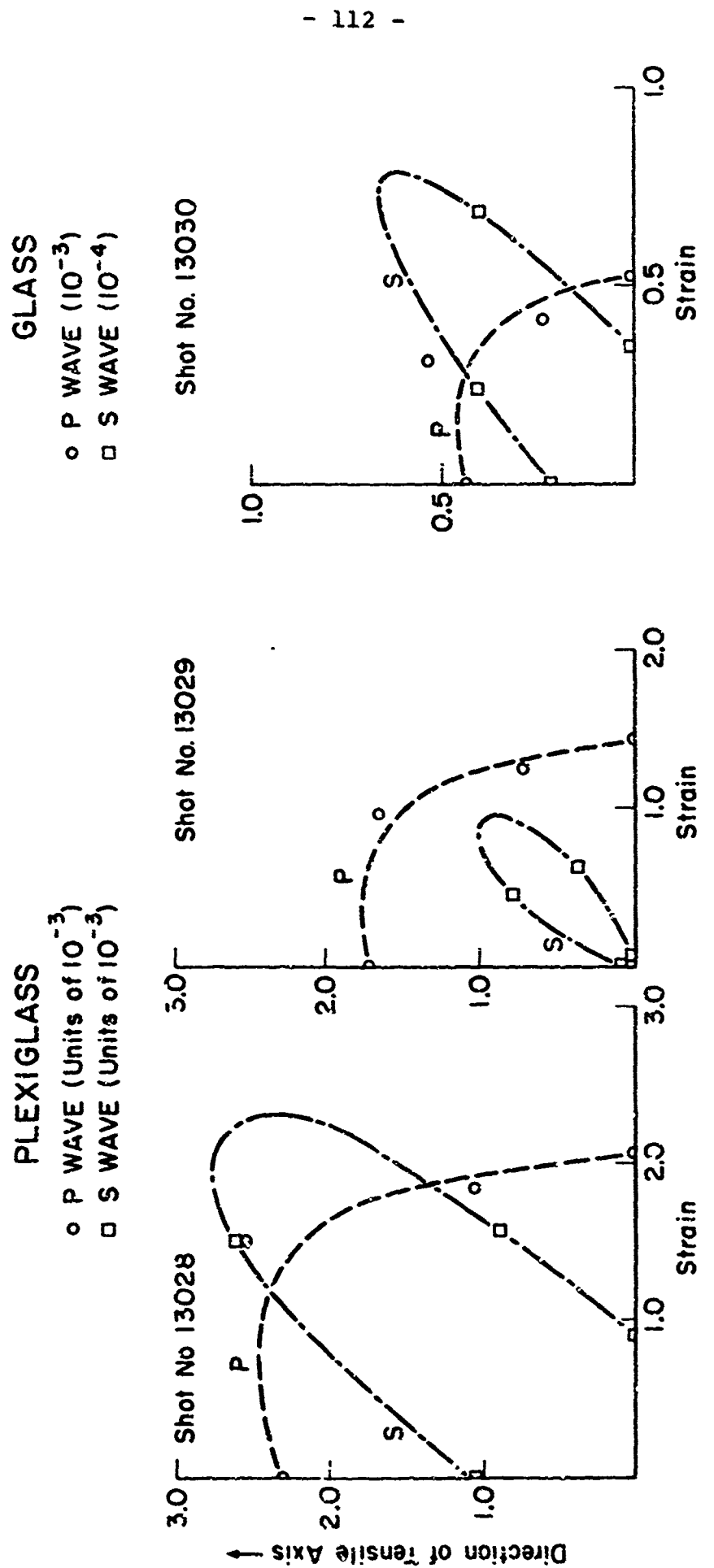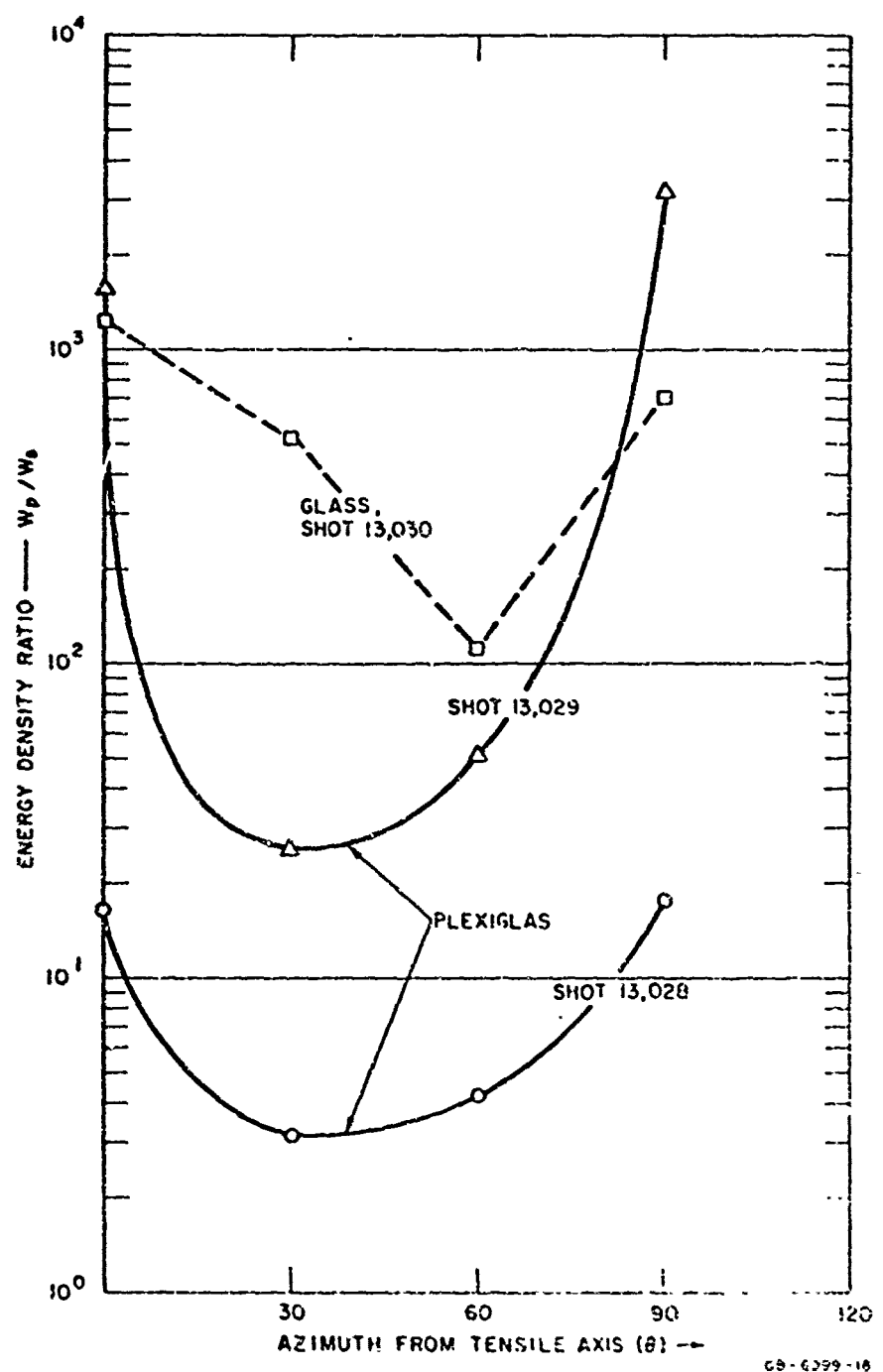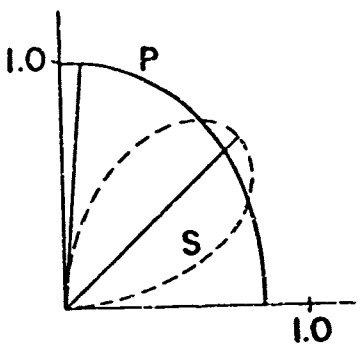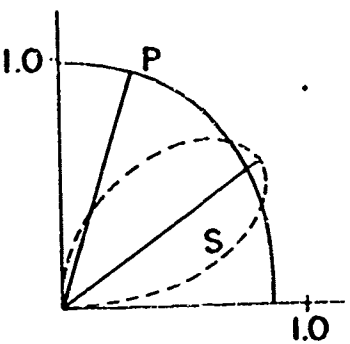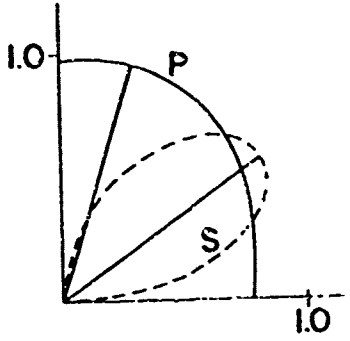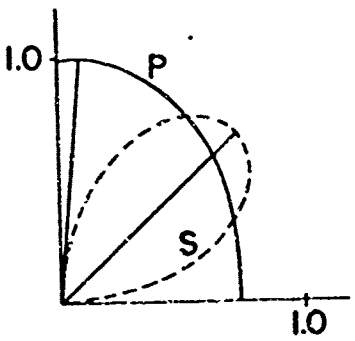
$\dfrac{(U_P)_I}{(U_P)_C} = 0.5$

TENSILE AXIS
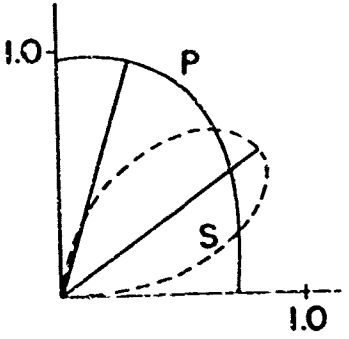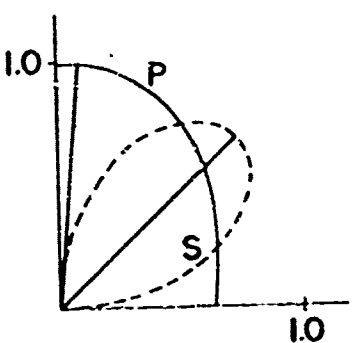
CRACK PROPAGATION

Fig. 25
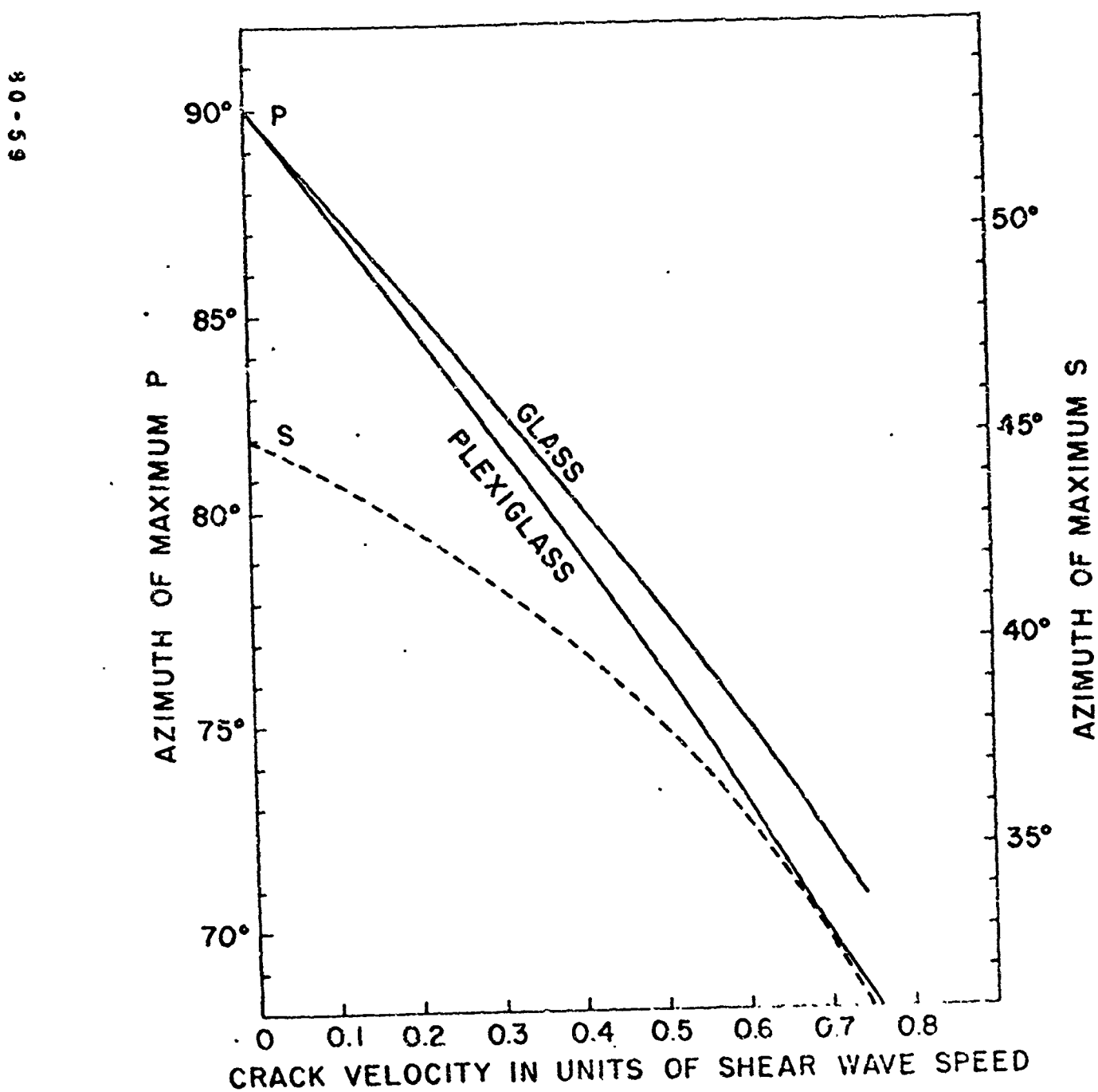
Fig. 26
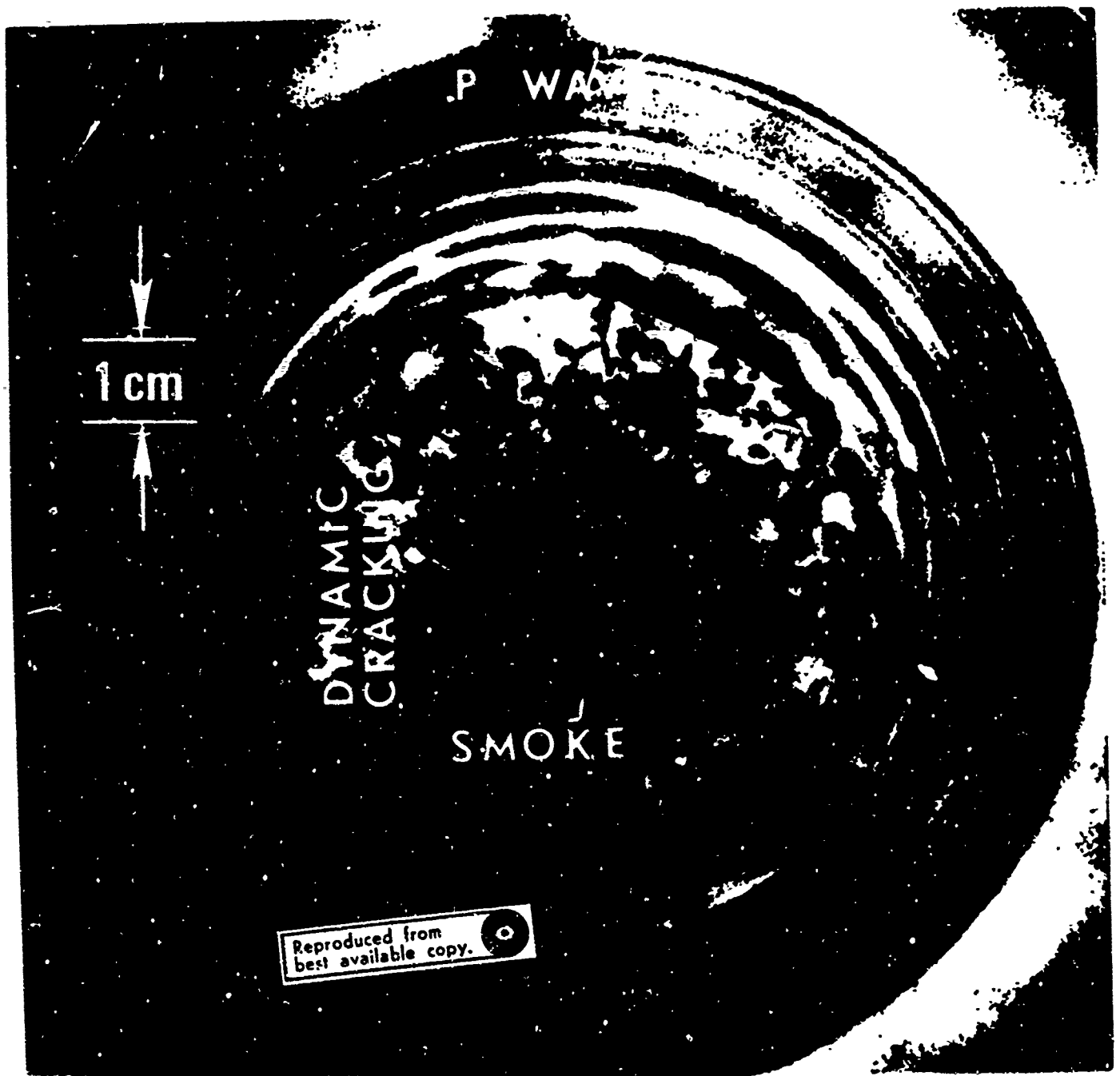
Fig. 27

INTENSE CRACKING

SMOKE FROM MDF

10 cm

A

Fig. 28a
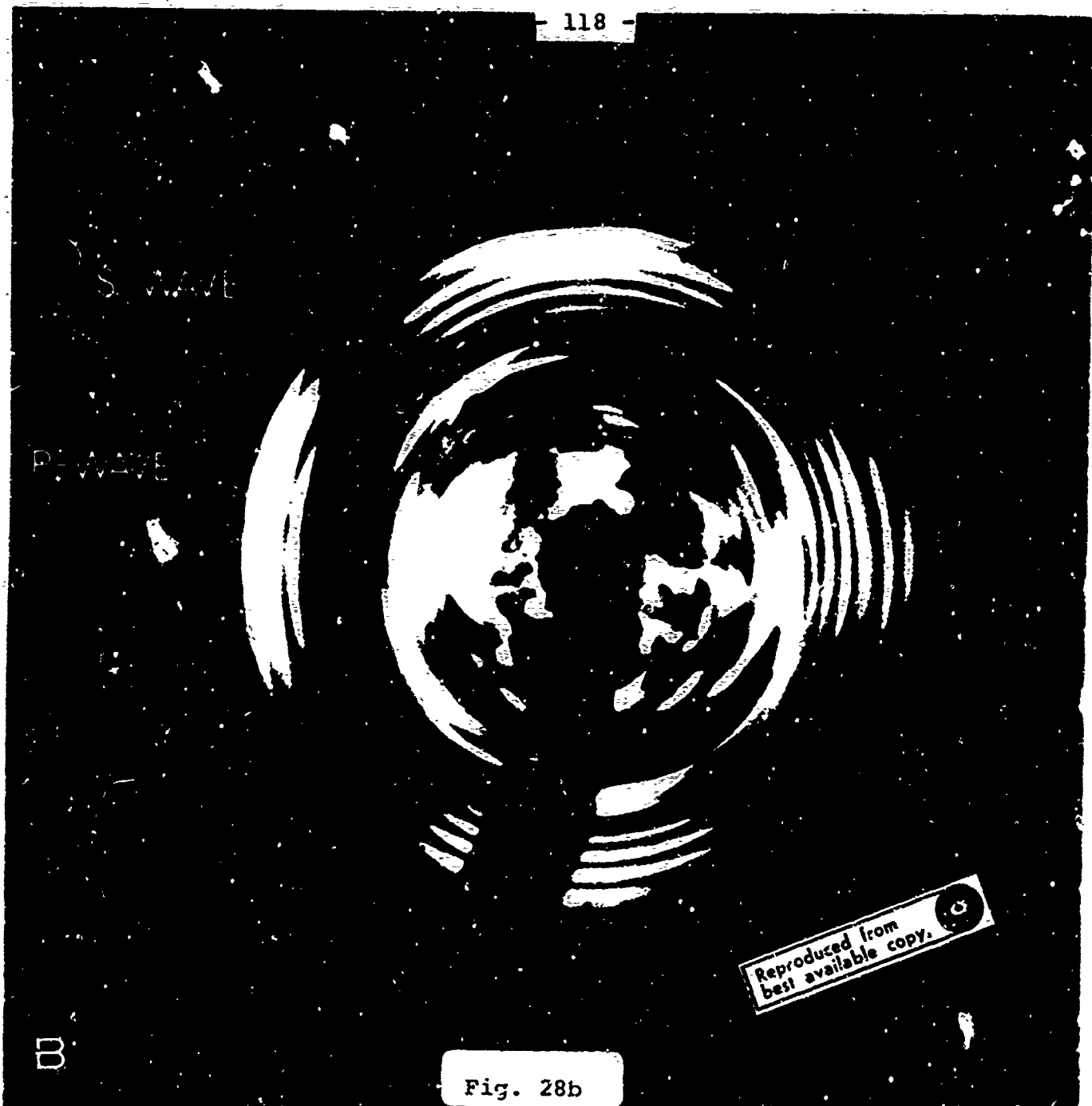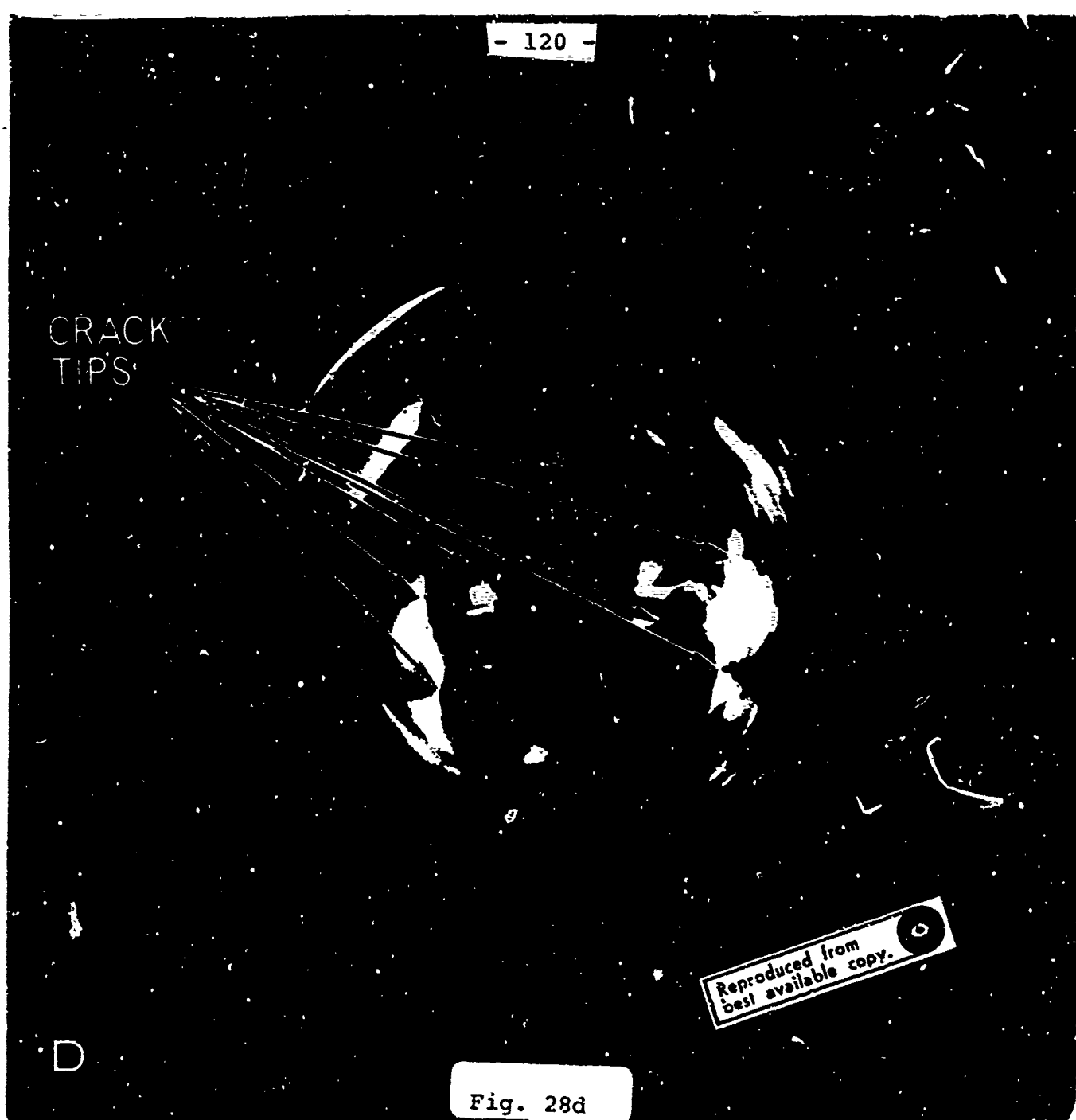
Fig. 28b

Fig. 28c

Fig. 28d
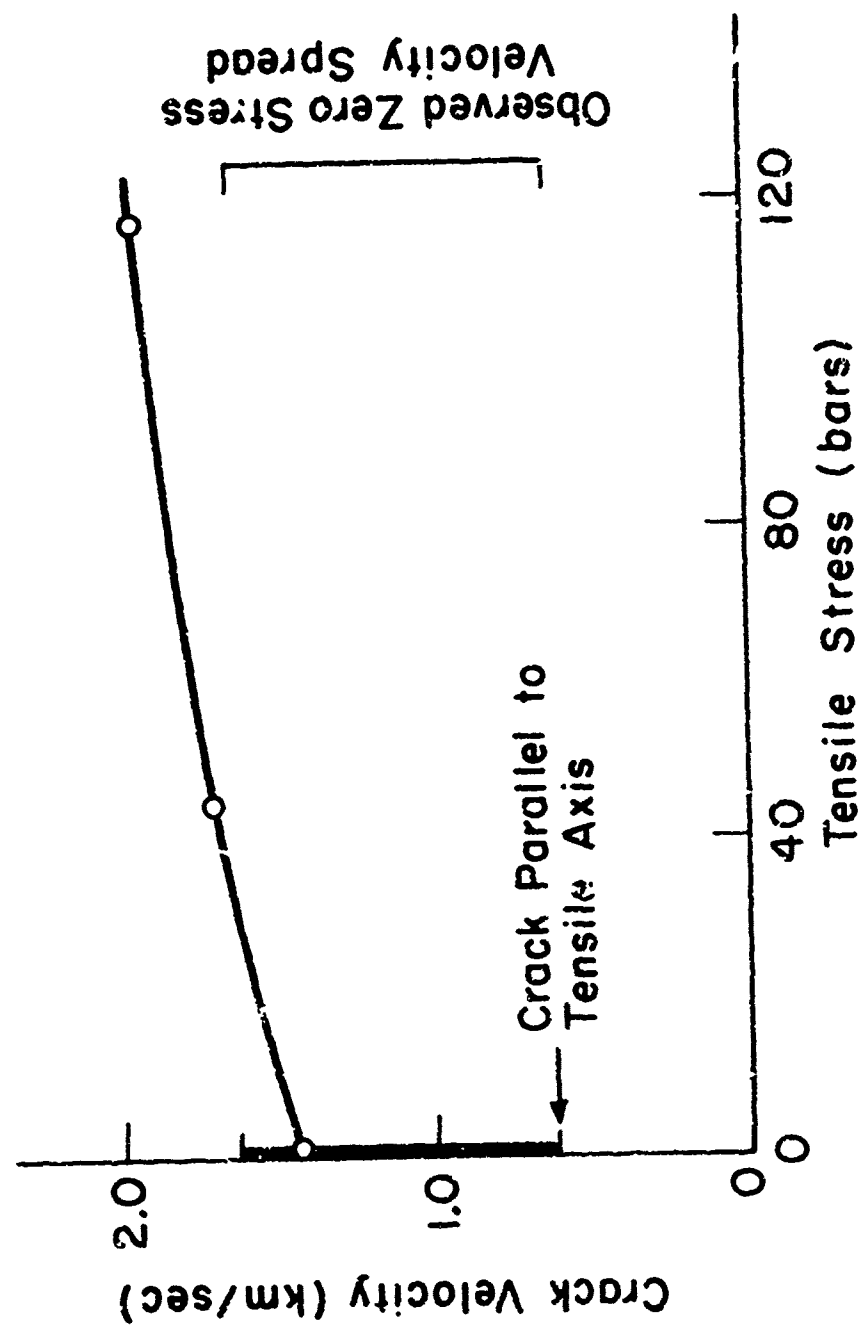
Fig. 29

III.   PILE DRIVER AND GREELEY: TECTONIC UTILITY AND DANGERS

OF NUCLEAR EXPLOSIONS

ABSTRACT

The tectonic strain energy released by several underground nuclear explosions has been calculated through an analysis of seismic surface waves. The proportionally great amount of energy released in the case of certain events suggests both the possible uses for as well as hazards of underground testing.

Seismic waves generated by underground nuclear explosions quite often indicate complications arising from the interaction of the explosive source with the surrounding inhomogeneous medium. The clearest evidence of such an interaction is the generation of horizontally polarized SH and Love waves by many explosions. The radiation patterns of these waves and the mechanisms of their generation have been a subject of a number of studies (1). It is generally agreed that an explosion detonated in a pre-stressed medium radiates some ambient strain energy because of relaxation around the cavity and extended cracks. The extent of this relaxation and the amount of energy released, however, have not been accurately determined.

The radius of the zone of relaxation and the amount of tectonic strain energy release are two characteristics of nuclear explosions which are of extreme importance. The first consideration which depends upon a knowledge of these characteristics is the feasibility of utilizing underground explosions for earthquake control. Explosions might be effective in periodically releasing accumulating tectonic strain energy in active areas, thus possibly preventing major earthquakes. The second consideration concerns the safety of large underground explosions. An explosion which releases very large amounts of strain energy would have the same effect as that of a large earthquake. If larger devices are tested in new locations where ambient stress patterns are not known, the strain release problem becomes more critical. As a third

point, the release of large amounts of pre-existing strain energy may affect some (but not all) of the seismic discrimination methods between earthquakes and explosions.

The cases that have been studied to date indicate that some strain energy was released by most nuclear explosions detonated in relatively hard media (2). However, the strain energy released was less than the equivalent seismic energy of the explosions themselves in all but one case. The exception was Hardhat, detonated in granite. The excessive strain energy release in this case was attributed to the possible triggering of an earthquake (3).

In this paper we will report on two other Nevada Test Site explosions (Pile Driver and Greeley) which generated large Love waves and released significant amounts of tectonic strain energy. Data from these events was obtained from LRSM (Long Range Seismic Measurements), WWSS (World Wide Standard Seismograph), and CSS (Canadian Standard Seismograph) system stations located throughout North America. The long period records were digitized and filtered. The two horizontal components at each station were rotated to radial and tangential directions with respect to the explosions in order to separate the Love waves. The resulting tangential component (Love waves) and the vertical component (Rayleigh waves) were then Fourier analyzed to obtain the amplitude spectra.

In Figure 1, long period seismograms of three explosions are illustrated. Tan, detonated near the other events, has

been included as an example of a typical explosion which did
not generate extensive Love waves. In this study both the
radiation patterns of Rayleigh waves and Love to Rayleigh
wave amplitude ratios were used to determine the strain
energy release.

An explosion with associated tectonic strain release can
be represented by a composite source consisting of an isotropic
explosion component and a double-couple strain release compo-
nent (4). Assuming that the time delay between the explosion
and the strain release as well as the differences between
Love and Rayleigh wave time functions are negligible, expres-
sions for Rayleigh and Love wave far field displacements from
such a composite source are given by

$$U_R(\omega) = C_R(\omega)[1 + F \sin 2\theta] \exp[i(\omega t - k_R r)]$$

$$(1)$$

$$U_L(\omega) = C_L(\omega) \cos 2\theta \exp[i(\omega t - k_L r)]$$

where C_R and C_L are functions of frequency, distance, and the
medium, ω is frequency, t is time, k_R and k_L are the Rayleigh
and Love wave numbers, and r is the radial distance from the
source. θ is the azimuthal orientation of the double-couple
and F, the parameter of greatest interest, is the strength of
the double-couple relative to the explosion.

If the differences between Love and Rayleigh wave attenua-
tion and source time functions are considered negligible, the

following expression is obtained for the Love over Rayleigh
wave amplitude ratio

$$\frac{|U_L|}{|U_R|} = \frac{C_{LR}(\omega) \ F \cos 2\theta}{1 + F \sin 2\theta} \quad \cdot \tag{2}$$

where C_{LR} is a function of frequency and the medium. An auto-
matic error scheme was applied to fit the observed data to
this formulation (5). A grid was formed between the two para-
meters F and θ, and the error between the data and the theore-
tical combinations of F and θ was contoured.

Figure 2 shows the best fitting Love over Rayleigh wave
radiation patterns for Pile Driver and Greeley along with the
observed data. The parameter F determined for these two events
was 3.2 and 1.6, respectively. In Figure 3a, the best fitting
Rayleigh wave pattern for Pile Driver is shown with the observed
data and some actual seismograms. In addition to amplitude,
phase (polarity) has been included. The polarity reversals
predicted by our best fitting theoretical model (since F >> 1)
are indeed observed when the Pile Driver data is compared to
that of Tan.

The Rayleigh wave radiation pattern for Greeley is shown
in Figure 3b. In this case, the strength of the strain release
component was close to that of the explosion, and the amplitudes
of the inverted lobes were therefore small. In spite of this,
a very clear phase reversal can be observed relative to the
Boxcar event as seen at LASA from the data of Filson (6).

The source model for the Hardhat event was studied by a similar technique and described in a previous publication (7). The results were almost identical to Pile Driver, and clear polarity reversals could be observed.

Since the radiation patterns of P waves are similar to those of Rayleigh waves, we investigated these body waves to determine any polarity reversals. The short period records, however, appeared to be dominated by the explosive component and near-source irregularities. Only on the long period components of 3 stations did P waves from Greeley appear reversed relative to Boxcar. In the case of Pile Driver, the long period P waves were far too small to be useful.

The source data for the three explosions of concern, Hardhat, Pile Driver, and Greeley, as well as that for some other events, are summarized in Table 1. In addition to double-couple strengths, we have computed the ratio of surface wave energy of the double-couple component, E_{tect} , to the energy of the explosion. This ratio (8) is closely approximated by

$$E_{tect} / E_{exp} = 4/3 \ F^2 .$$

Several conclusions can be derived from these data. Generally (in the Nevada Test Site), explosions in harder media such as granite release more tectonic strain energy than explosions in softer formations such as tuff or alluvium.

These latter media have low rigidities and cannot accumulate shear strain energy because of plastic deformation under stress. Salt is a very good example of such a plastic medium. None of the explosions in salt generated measurable Love waves. Not all explosions in a given medium, however, have proportionally the same strain release associated with them, as indicated by Shoal versus Pile Driver and Hardhat. Thus in addition to a rigid medium, high ambient tectonic stresses are important in determining the strain energy release by an explosion. The similarity of the Pile Driver and Hardhat results indicate that, 1) the regional tectonic framework controls the radiation pattern, 2) in a given medium and area, each explosion releases strain energy proportional to its own explosive energy, 3) the spontaneous energy release comes from the vicinity of the shot rather than from an earthquake triggered at a distance of ten kilometers or more. Strain adjustments at such distances appear to take place gradually as indicated by the spread of aftershock activity that follows some large explosions (9).

The implications of these results in terms of the utility of nuclear explosions for the release of tectonic stresses and earthquake control are encouraging. Since an explosion can release accumulated strain energy considerably greater than its own (more than ten times greater in the cases of Pile Driver and Hardhat) in the vicinity of the shot point, such events could be used to relax small regions. One

possible application would be to de-activate a site in a seis-
mically active region prior to the construction of some project
such as a nuclear power plant. However, at the present we do
not know how long it takes for the tectonic stress field to
build up to its initial level following an explosion. The
Hardhat and Pile Driver shot locations were only about a half
kilometer apart. Yet Pile Driver, detonated four years later,
radiated proportionately the same amount of strain energy.
This does not necessarily mean that strain energy reaccumulated
at the Hardhat site in only four years. Since the yield of
Pile Driver was 10 times greater than that of Hardhat, the
stress relaxation (primarily due to cracking) most likely ex-
tended beyond the relaxation zone of the Hardhat explosion.
Thus tectonic strain energy was released from a larger volume
in the case of Pile Driver. The use of explosions to release
tectonic strain energy in areas which are already developed,
however, is clearly not feasible.

For the same reasons that explosions could prove useful,
nuclear testing in regions of high ambient stresses might
have serious consequences. Since the medium properties and
not the shot yield control the proportion of energy release,
a large explosion could release large amounts of tectonic
strain energy. For example, with the energy factor of Pile
Driver or Hardhat, a one-megaton explosion could release energy
equivalent to that of a magnitude $M_S = 6.3$ earthquake. For
a ten megaton explosion this could be equivalent to a magnitude

$M_S = 7.2$ earthquake, indeed a potentially destructive earth-
quake. Thus in any testing program, these factors must be
taken into account, and hard media should be avoided unless
the ambient stress levels are known to be low.

M. Nafi Toksöz

Harold H. Kehrer

Department of Earth and

Planetary Sciences

Massachusetts Institute of

Technology

Cambridge, Massachusetts 02139

REFERENCES

1. M.N. Toksöz, D.G. Harkrider, and A. Ben-Menahem, *J. Geophys. Res.*, 70, 907 (1965); M.N. Toksöz, VESIAC Rep. no.7885-1-X, 65 (1967); P. Molnar et al., *Nature*, 24, 1268 (1969); Y.B. Tsai and K. Aki, submitted to *J. Geophys. Res.* (197`); H.H. Kehrer, M.S. Thesis, M.I.T. (1969).

2. M.N. Toksöz, K. Thomson, and T. Ahrens, submitted to *Bull. Seismol. Soc. Am.* (1971).

3. K. Aki, *J. Geophys. Res.*, 69. 1131 (1964); J.N. Brune and P.W. Pomeroy, *ibid.*, 68, 5005 (1963).

4. C.B. Archambeau, *Rev. Geophys.*, 6, 241 (1968); Toksöz et al., (1965) *op.cit.*

5. Kehrer, *op. cit.*

6. J. Filson and L. Lande, paper presented at Seismol. Soc. am. annual meeting (1971).

7. M.N. Toksöz, A. Ben-Menahem, and D.G. Harkrider, *J. Geophys. Res.*, 69, 4355 (1964).

8. Toksöz et al. (1965), *op. cit.*

9. R.M. Hamilton and J.H. Healy, *Bull. Seismol. Soc. Am.*, 59, 2271 (1969).

10. This research was supported by the United States Office of Aerospace Research and monitored by Air Force Cambridge Research Laboratories under Contract No. F19628-68-C-0043. The research was also supported by the Advanced Research Projects Agency and monitored by the Air Force Office of Scientific Research under contract AF 49(638)-1632.

Table 1. Tectonic strain release characteristics of a sampling of underground nuclear explosions. All events were at Nevada Test Site except for Shoal (Western Nevada) and Gnome (New Mexico). F is relative strength of tectonic strain release component.

Name	Yield (Kt)	Medium	F Value	Energy Ratio E_{tect} / E_{exp}
Pile Driver	58	Granite	3.20	13.65
Hardhat	6	Granite	3.00	12.00
Greeley	825	Zeolitized Tuff	1.60	3.41
Shoal	12.5	Granite	.90	1.05
Boxcar	1200	Rhyolite	.59	.46
Bilby	200	Tuff	.47	.29
Tan	Low-Intermediate	Tuff	.39	.20
Haymaker	56	Alluvium	.33	.14
Gnome	3.1	Salt	0	0

FIGURE CAPTIONS

Fig. 1. Long period filtered seismograms illustrating relative generation of Love waves by three N.T.S. explosions recorded at Weston, Massachusetts. Love waves appear on the tangential components (T) about two minutes earlier than the Rayleigh waves on the vertical components (Z). Note the large amplitude of Love waves relative to Rayleigh waves for Pile Driver and Greeley explosions.

Fig. 2. Love over Rayleigh wave amplitude radiation patterns for Pile Driver and Greeley. For theoretical curves (solid lines), the following parameters were used: orientation (θ) and strength of double couple (F), 340° from north and 3.2 respectively for Pile Driver, and 355° and 1.6 for Greeley. Data symbols: ■ WWSS stations; ▲ LRSM stations; ● CSS stations.

Fig. 3. Rayleigh wave radiation patterns for explosive component (circles), strain release component (broken curves), and composite source representing the theoretical models (solid curves, parameters those of Fig. 2). The polarity (phase) of Rayleigh waves in different quadrants of the radiation pattern is indicated by (+) and (-). (a) Pile Driver with seismograms compared to those of Tan. Pile Driver traces are below those of Tan. Dashed line traces have their polarities reversed. Note the perfect match of wave shapes, with polarities reversed

at JP-AT and BOZ as predicted by the model.   (b) Greeley with seismograms compared to those of Halfbeak (COL and OXF) and Boxcar (LASA). The lower traces are from Greeley. Polarity reversal is very clear at LASA. Data symbols: ▲ LRSM stations; △ LRSM stations where reversed polarity was observed; ▣ WWSS stations; ⊗ CSS stations.

Fig. 1

Fig. 2

Fig. 3